Numerical Prediction of Armor Stability and Movement under Irregular Wave Action

by

Nobuhisa Kobayashi and Andojo Wurjanto

Sponsored by
U.S. Army Coastal Engineering Research Center

Research Report No. CACR-90-04

October, 1990

Center for Applied Coastal Research
Department of Civil Engineering
University of Delaware
Newark, DE
19716

ABSTRACT

This report briefly summarizes the progress made since the computer program IBREAK and the user's manual were completed in the previous project sponsored by the Coastal Engineering Research Center.

Furthermore, the numerical model that was shown to be in fair agreement with six test runs of available data on the stability of rock units under irregular wave attack is used to examine the critical incident wave profile associated with the minimum rock stability for each run. The minimum rock stability computed for the runs with dominant plunging waves on gentle slopes is caused by the large wave with the maximum crest elevation during its uprush on the slope. The minimum rock stability computed for the runs with dominant surging waves on steeper slopes is caused by the downrushing water with high velocities resulted from a large zero-upcrossing wave with a high crest followed by a deep trough. These computed results may eventually allow one to quantify incident design wave conditions more specifically than the simple approach based on the representative wave height and period.

In addition, a simplified model is proposed to predict the eroded area due to the movement and dislodgement of rock units using the probability of armor movement computed by the numerical model. This model is shown to be in qualitative agreement with the empirical formula for the damage level proposed by Van der Meer (1988). The simplified model may be expanded to predict the change of the slope profile as a function of time since such a model is required for the design of berm and reef breakwaters.

ACKNOWLEDGEMENT

This is the first report resulting from research sponsored by the Coastal Engineering Research Center, U.S. Army Engineer Waterways Experiment Station under contract No. DACW 39-90-K-0006-P001. The authors would like to thank J. P. Ahrens and D. D. Davidson for their enthusiastic support of our continued efforts to improve the capabilities of numerical models for the design of coastal structures.

TABLE OF CONTENTS

NUMERICAL PREDICTION OF ARMOR STABILITY AND MOVEMENT UNDER IRREGULAR WAVE ACTION

PART I: INTRODUCTION

Background

Kobayashi and Wurjanto (1989a) synthesized their numerical models and presented a computer program called IBREAK, which may be used for the design of rough or smooth impermeable coastal structures of arbitrary geometry against normally incident waves. The capabilities of IBREAK are being expanded as summarized in the following.

Kobayashi and Wurjanto (1989c) showed that IBREAK could be calibrated and applied to predict the hydrodynamic forces and sliding motions of dolos units at the Crescent City breakwater in California. The calibrated numerical model was used to hindcast the response of the dolos units during a storm which occurred in 1987. The hindcast results were shown to be consistent with the measured results including the upslope movement of poorly interlocked dolos units and the importance of the static and wave forces with negligible impact forces. The numerical model was then used to predict the response of poorly and well interlocked dolos units under extreme wave conditions. The predicted results have suggested that the wave forces acting on these dolos units may possibly exceed the static forces, while the poorly interlocked dolos units may move considerably, resulting in possible impact forces.

Kobayashi, Cox and Wurjanto (1990) conducted three irregular wave test runs to obtain detailed data on irregular wave reflection and runup on a 1:3 rough impermeable slope. The test results were also used to evaluate the capabilities and limitations of IBREAK

for predicting the time series and spectral characteristics of the reflected wave and waterline oscillations on the slope. The numerical model was shown to predict the measured time series and spectra reasonably well, including the selective nature of wave reflection and dissipation as well as the appearance of low-frequency wave components in the waterline oscillations on the 1:3 slope.

On the other hand, Kobayashi and Wurjanto (1990) extended IBREAK to predict the flow and armor response on a rough permeable slope as well as the flow in a thin permeable underlayer for a normally incident wave train. In addition to the continuity and momentum equations used to compute the flow field, an equation of energy has been used to estimate the rate of energy dissipation due to wave breaking. Computation was made for six test runs to examine the accuracy and capability of the numerical model for simulating the fairly detailed hydrodynamics and armor response under the action of regular waves. The computed critical stability number for initiation of armor movement was compared with the measured stability number corresponding to the start of the damage under irregular wave action to quantify the limitations of the regular wave approximation. The computed wave runup, run-down and reflection coefficients were shown to be in qualitative agreement with available empirical formulas based on regular wave tests. Kobayashi and Wurjanto (1989b) applied the developed numerical model to hypothetical permeable slopes corresponding to available impermeable slope tests. The computed results with and without a permeable underlayer indicated that the permeability effects would increase the hydraulic stability of armor units noticeably and decrease wave runup and reflection slightly. The computed results were qualitatively consistent with available data although they were not extensive and limited to regular waves only.

Kobayashi, Wurjanto and Cox (1990) applied the extended numerical model to compute the irregular wave motion on a rough permeable slope. The normally-incident irregular wave

train characterized by its spectral density at the toe of the slope was generated numerically for six test runs. The computed critical stability number for initiation of armor movement under the computed irregular wave motion was shown to be in fair agreement with the measured stability number corresponding to the start of the damage. The comparison of the computed armor stability for the incident regular and irregular waves indicated that the armor stability would be reduced appreciably and vary less along the slope under the irregular wave action. On the other hand, the comparison between the computed reflected wave spectrum and the specified incident wave spectrum indicated the reflection of Fourier components with longer periods and the dissipation of Fourier components with shorter periods, while the average reflection coefficient increased with the increase of the surf similarity parameter. The computed waterline oscillations were examined using spectral and time series analyses. The computed spectra of the waterline oscillations showed the noticeable low-frequency components, which increased with the decrease of the surf similarity parameter. The statistical analysis of individual wave runup heights indicated that the computed runup distribution followed the Rayleigh distribution fairly well for some of the six test runs. The computed maximum wave run-up was in agreement with the empirical formula based on irregular wave runup tests.

The extended numerical model based on the assumption of a thin permeable underlayer was found to be inappropriate for additional three test runs conducted for a 1:3 rough permeable slope with a thick permeable underlayer. These three test runs corresponded to the three test runs for the 1:3 rough impermeable slope conducted by Kobayashi, Cox and Wurjanto (1990) except for the presence of the thick permeable underlayer. Kobayashi, Cox and Wurjanto (1991) compared the measurements of the permeable and impermeable slope tests. The permeability effects reduced the average reflection coefficient and significant runup as was observed by a number of researchers. The permeability effects on irregular

wave reflection were found to reduce the reflection coefficient fairly uniformly over the wind wave frequency range. The permeability effects on irregular wave runup were found to reduce the low frequency wave components significantly. The measured runup distribution for the impermeable and permeable slopes were represented by the Rayleigh distribution fairly well in the range of the exceedance probability greater than approximately 0.02.

Efforts are being made to develop a numerical model which is applicable to a rough permeable slope with a thick permeable underlayer. This numerical model will be compared with the permeable slope test results reported by Kobayashi, Cox and Wurjanto (1991).

Scope

In this report, the temporal and spatial variations of the stability of rock units computed by Kobayashi, Wurjanto and Cox (1990) using the numerical model of Kobayashi and Wurjanto (1990) are analyzed in detail to examine what wave conditions may cause the minimum stability of rock units. Gunbak and Bruun (1979) described the various sequences of waves which may cause severe conditions on breakwaters. Their descriptions were qualitative since it is very difficult to measure the flow and armor response simultaneously. This is an initial attempt to quantify incident design wave conditions more rationally than the simple approach based on the representative wave height and period such as the significant wave height and mean period (e.g., Van der Meer, 1988).

Furthermore, a simplified model is proposed to predict the eroded area due to the movement and dislodgement of rock units using the probability of armor movement computed by the numerical model. This model is shown to be in qualitative agreement with the empirical formula for the damage level proposed by Van der Meer (1988). This model is intended to be a first model for elucidating the mechanism of armor dislodgement and the resulting profile

change.

For brevity, this report makes the best use of the results presented in the papers of Kobayashi and Wurjanto (1990) and Kobayashi, Wurjanto and Cox (1990) which are attached in Appendices A and B, respectively. A concise version of this report will be published in the conference paper of Kobayashi, Wurjanto and Cox (1991).

PART II: ARMOR STABILITY

Comparison Between Measured and Computed Stability Numbers

In the following, the comparison made in the paper attached in Appendix B is summarized. The hydraulic stability condition against sliding or rolling of an armor unit on a rough permeable slope was expressed in the form

$$N_s = H'(s-1)^{-1}(\rho s/W')^{1/3} \leq N_R(t,x) \tag{1}$$

where N_s = stability number; H' = incident wave height used for the normalization of dimensional variables indicated by the prime; s = specific density of the armor unit; ρ = fluid density; W' = median mass of the armor units; and N_R = armor stability function. The dimensionless function N_R varies with the normalized time, $t = t'/T'$, and the normalized horizontal distance from the toe of the slope, $x = x'/[T'(gH')^{1/2}]$, where T' = incident wave period used for the normalization; and g = gravitational acceleration. The expression of N_R as a function of the normalized fluid velocity and acceleration was given in the paper attached in Appendix A where the input parameters for the computation of the armor stability were specified.

Computation was made for six test runs selected from the test results with the dimensionless damage level, S=2, and the number of incident waves, N = 1000, listed in Appendix II of the thesis of Van der Meer (1988). These runs corresponded to the start of damage. The incident irregular waves for the six runs were generated using the Pierson-Moskowitz spectrum. The significant wave height, H'_s, and the average period of the zero upcrossings, T'_m, of the incident wave train were used by Van der Meer to characterize the incident irregular waves. As a result, use was made of $H' = H'_s$ and $T' = T'_m$ for the normalization of the

Table 1: Six Test Runs Compared with Numerical Model

Run No.	$\cot\theta'$	H' (cm)	T' (sec)	ξ	Measured N_s	Computed N_{sc}	t_{sc}
R1	6	10.09	2.63	1.72	1.72	1.56	164.75
R2a	6	7.75	3.15	2.36	1.32	1.75	248.06
R2b	6	7.75	3.15	2.36	1.32	1.63	8.00
R3	4	8.16	3.22	3.52	1.39	1.15	156.38
R4	3	8.92	3.13	4.37	1.52	1.36	161.55
R5	2	7.98	2.69	5.95	1.36	1.01	176.53
R6	2	7.98	3.11	6.88	1.36	1.47	140.62

dimensional variables. The normalized incident wave train, $\eta_i(t) = \eta_i'/H'$, at the toe of the $1 : \cot\theta'$ slope required as input to the numerical model was generated numerically for the specified spectral density with assumed random phases. Since different sets of the random phases yield different temporal variations of $\eta_i(t)$, the incident irregular wave train specified for each run was not the same as that generated in a wave flume by Van der Meer (1988). In order to reduce the computation time, the duration of the computation was limited to $0 \leq t \leq 256$, corresponding to $N = 256$ instead of $N = 1000$.

Table 1 lists the values of $\cot\theta'$, $H' = H_s'$, $T' = T_m'$, $\xi = T'\tan\theta'/(2\pi H'/g)^{1/2}$ and N_s for each of the six test runs, where ξ =surf similarity parameter based on H_s' and T_m'. The six runs with $\xi = 1.72 - 6.88$ were selected to represent dominant breaker types of plunging, collapsing and surging waves on uniform slopes. Runs R2a and R2b corresponded to run R2 and were based on the same spectral density with given values of H_s' and T_m'. The time series $\eta_i(t)$ for runs R2a and R2b were generated numerically using different sets of the random phases.

Table 1 also lists the computed value of the critical stability number N_{sc} and the time t_{sc} of its occurrence for each run. The value of N_{sc} for each run was taken as the minimum

value of $N_R(t,x)$ for the range of $x \geq 0$ which occurred at time $t = t_{sc}$ during $8 \leq t \leq 256$ where the normalized horizontal coordinate x was taken to be positive landward with $x = 0$ at the toe of the slope and the duration $0 \leq t < 8$ was excluded to account for the initial transient waves in the computation starting from the initial conditions of no wave action in the region $x \geq 0$ at $t = 0$. The computed critical stability number N_{sc} and the measured stability number N_s are in fair agreement as shown in Table 1 where the values of N_{sc}/N_s are in the range 0.74–1.33. The small difference between the computed values of N_{sc} for runs R2a and R2b indicates the variability caused by the random phases, although a much larger number of simulated runs are required to perform a statistical analysis of the variability. The comparison between N_s and N_{sc} shown in Table 1 is not really rigorous because of the inherent differences between these stability numbers as discussed in Appendix B.

Wave Conditions for Critical Armor Stability

The wave conditions corresponding to the computed minimum stability of rock units for each run are examined herein to identify the wave conditions which are critical to the stability of rock units. In the following, runs R1 and R4 may be regarded as representative runs for dominant plunging and surging waves, respectively, whereas run R3 happens to include an exceptionally large wave.

The free surface displacement above the still water level (SWL) and the depth-averaged horizontal fluid velocity are normalized as $\eta = \eta'/H'$ and $u = u'/(gH')^{1/2}$, respectively, where u is taken to be positive landward. Figs. 1–3 show the computed variations of η, u and N_R with respect to x at the time, $t = t_{sc}$, when the minimum value of N_R in the range $x \geq 0$ corresponds to the critical stability number N_{sc}. The values of t_{sc} for runs R1, R3 and

R4 are 164.75, 156.38 and 161.55, respectively, as listed in Table 1. The shaded area shown in the figure for η corresponds to the permeable underlayer for each test where the numerical model is presently limited to the case of a thin permeable underlayer. Figs. 1–3 also show the computed variation of the local stability number N_{sx} with respect to x where N_{sx} was defined as the minimum value of $N_R(t,x)$ at the specified location during $8 \leq t \leq 256$. The minimum value of N_{sx} with respect to x equals the critical stability number N_{sc}.

The critical stability number for run R1 with $\xi = 1.72$ occurs slightly behind the steep front of the uprushing water with large upslope velocities and accelerations as shown in Fig. 1. The local stability number in the range $1.5 \leq x \leq 1.9$ is computed to occur when this steep front moves upslope. On the other hand, the critical stability number for run R4 with $\xi = 4.37$ is caused by the downrushing water with large downslope velocities as shown in Fig. 3. For the exceptional case of run R3 shown in Fig. 2, the downrushing water flows extremely deep below SWL and encounters the uprushing water. The corresponding incident wave profile for run R3 will be shown to exhibit a very high crest followed by a very deep trough. This is one of the dangerous wave conditions identified by Gunbak and Bruun (1979).

The incident wave profile associated with the critical stability number N_{sc} for each run is examined to identify the incident wave profiles which may cause the critical uprushing or downrushing flow on uniform slopes. Fig. 4 shows the incident wave profile $\eta_i(t)$ at the toe of the slope normalized by the zero-upcrossing significant wave height H_s' slightly before the time $t = t_{sc}$ when $N_R(t,x) = N_{sc}$ at the certain location on the slope. The crest elevation η_c above SWL associated with the critical incident wave profile is obtained. The trough elevations η_{td} and η_{tu} adjacent to the crest elevation η_c are then found using the zero-downcrossing and zero-upcrossing methods, respectively. The corresponding wave heights H_d and H_u are given by $H_d = (\eta_c - \eta_{td})$ and $H_u = (\eta_c - \eta_{tu})$.

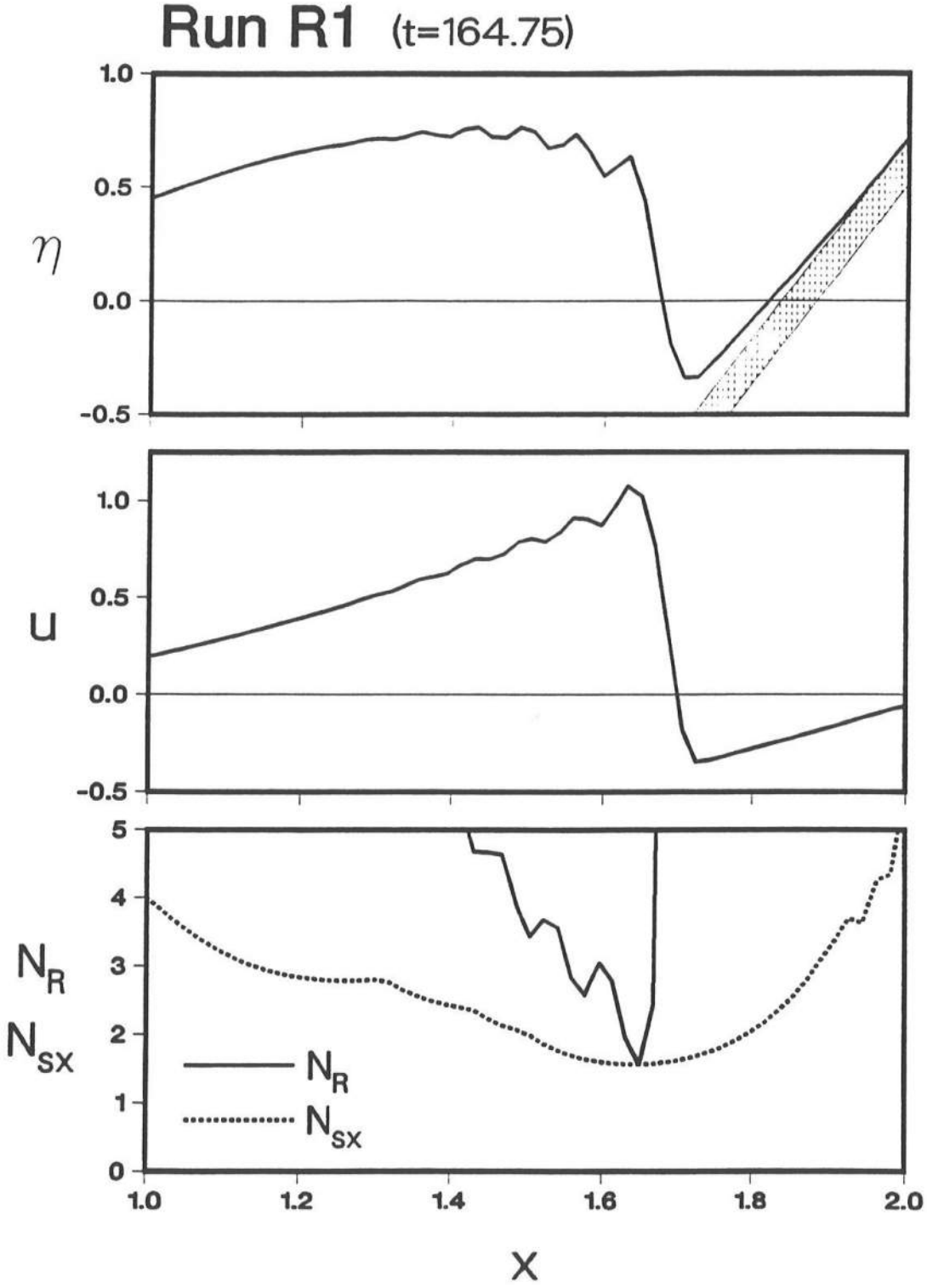

Figure 1: Variations of η, u and N_R with Respect to x at Time of Minimum Stability for Run 1

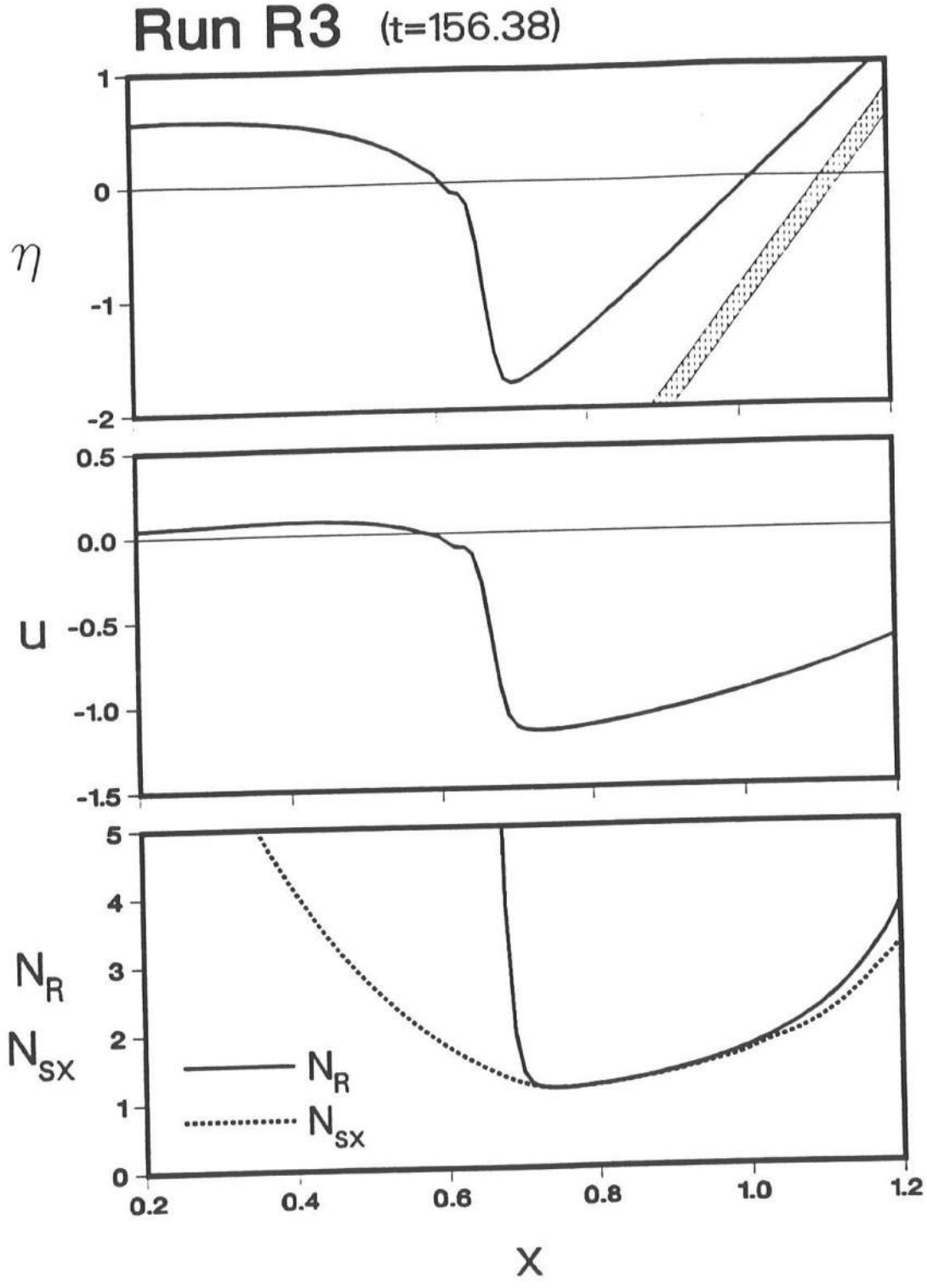

Figure 2: Variations of η, u and N_R with Respect to x at Time of Minimum Stability for Run 3

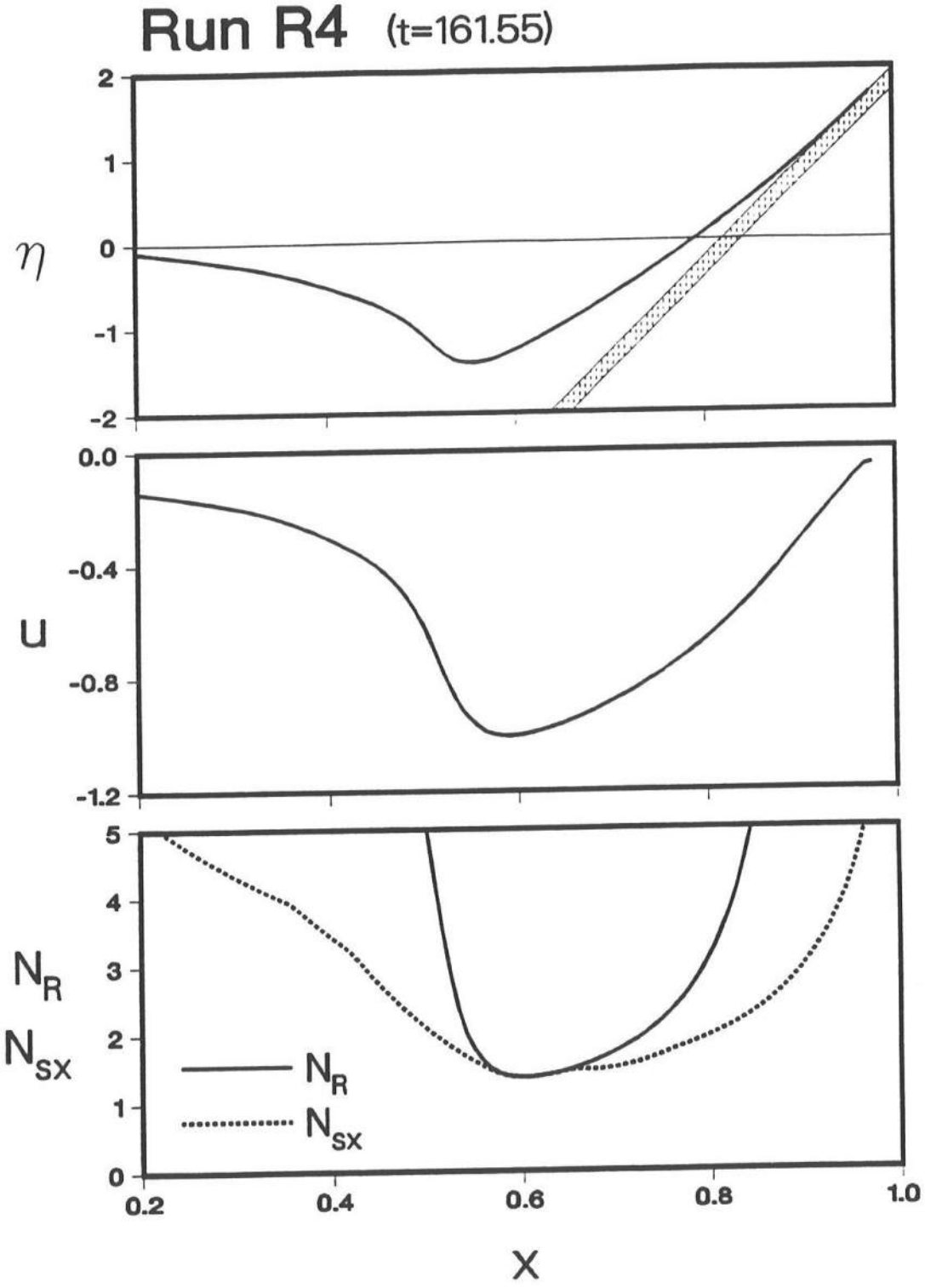

Figure 3: Variations of η, u and N_R with Respect to x at Time of Minimum Stability for Run 4

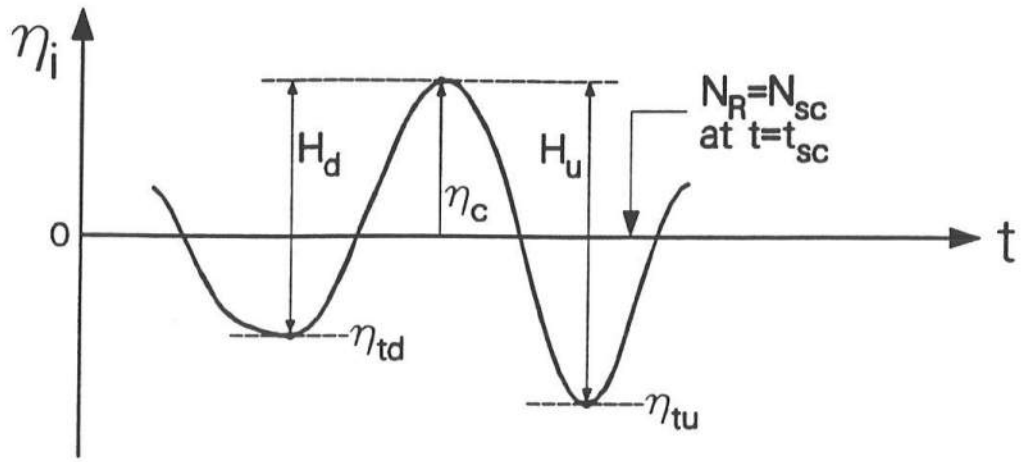

Figure 4: Definition Sketch of Critical Incident Wave Profile $\eta_i(t)$ Slightly before Time $t = t_{sc}$ when $N_R(t, x) = N_{sc}$ where η_c = Crest Elevation; η_{td} = Zero-Downcrossing Trough Elevation, η_{tu} = Zero-Upcrossing Trough Elevation; H_d = Zero-Downcrossing Wave Height; and H_u = Zero-Upcrossing Wave Height

The values of η_c, η_{td} and η_{tu} for each run are listed in Table 2. These values are compared with the maximum crest elevation η_{cm} and the minimum trough elevation η_{tm} for $\eta_i(t)$ during $0 \leq t \leq 256$. Table 2 shows that $\eta_c = \eta_{cm}$ for runs R1, R2a, R2b and R3 while $\eta_{tu} = \eta_{tm}$ for runs R3 and R4. For runs R5 and R6, η_c is somewhat smaller than η_{cm} and η_{tu} is somewhat larger than η_{tm}.

Table 3 lists the values of H_d, T_d, H_u and T_u for each run where T_d and T_u are the zero-downcrossing and zero-upcrossing periods, respectively, of the individual wave whose crest elevation is η_c. The wave periods are normalized by the average zero-upcrossing period T'_m. Table 3 also lists the ranks of H_d and H_u among the 256 zero-downcrossing and zero-upcrossing individual wave heights, respectively, which are ranked in the descending order. Table 3 suggests that the critical incident wave profile is more related to the zero-upcrossing wave than the zero- downcrossing wave for runs R4, R5 and R6. The zero-upcrossing wave with $\eta_c = 1.052$, $\eta_{tu} = -1.126$ and $H_u = 2.178$ for run R3 appears to be exceptional, although the computed critical stability number N_{sc} for run R3 listed in Table 1 is not exceptionally small.

Figs. 5-11 show the temporal variations of $\eta_i(t)$ and $Z_r(t)$ in the vicinity of $t = t_{sc}$ for each of the runs listed in Tables 1–3 where $Z_r = Z'_r/H'$ is the normalized waterline elevation on the slope above SWL corresponding to the instantaneous water depth $\delta'_r = 1cm$ as explained in Appendices A and B. Figs. 5-11 also show the zero-upcrossing and zero-downcrossing wave height distributions of the specified incident wave train $\eta_i(t)$ for each run as compared with the Rayleigh distribution given by $P = \exp[-2(H_p/H_s)^2]$ where P is the exceedance probability associated with the normalized wave height H_p and H_s is the normalized significant wave height.

Table 2: Crest and Trough Elevations of Critical Wave Profile

Run No.	Crest		Trough		
	η_c	η_{cm}	η_{td}	η_{tu}	η_{tm}
R1	0.905	0.905	-0.527	-0.669	-0.934
R2a	0.822	0.822	-0.602	-0.459	-0.833
R2b	0.969	0.969	-0.877	-0.648	-0.933
R3	1.052	1.052	-0.673	-1.126	-1.126
R4	0.605	0.873	-0.034	-0.783	-0.783
R5	0.720	0.787	-0.550	-0.686	-0.793
R6	0.772	0.940	-0.447	-0.712	-0.974

Table 3: Wave Heights and Periods of Critical Wave Profile

Run No.	Zero-Downcrossing			Zero-Upcrossing		
	H_d	Rank	T_d	H_u	Rank	T_u
R1	1.433	4	1.263	1.575	1	1.256
R2a	1.424	3	1.195	1.280	7	1.518
R2b	1.846	1	1.189	1.617	3	1.116
R3	1.726	2	1.134	2.178	1	1.014
R4	0.639	118	0.649	1.388	5	1.213
R5	1.270	5	0.951	1.407	2	0.904
R6	1.219	17	1.066	1.484	4	1.235

The value of P for give H_p is estimated by $P = n/(N_o + 1)$ where n = rank of H_p and N_o = number of individual waves, which is 256 for these runs. Since the zero-upcrossing significant wave height H_s' is used for the normalization, $H_s = 1$ for the zero-upcrossing wave height distribution. The values of H_s for the zero-downcrossing wave height distribution are found to be essentially unity for all runs. Figs. 5-11 also point out the exceedance probability P for H_u and H_d for each of the runs to indicate the values of H_u and H_d as compared with the rest of the individual wave heights.

Figs. 5-11 together with Figs. 1-4 and Tables 1-3 elucidate the critical wave conditions corresponding to the minimum stability of rock units for each run. For run R1 with $\cot\theta' = 6$ and $\xi = 1.72$, the critical stability number occurs at the time t_{sc} when the large wave with the maximum crest elevation $\eta_c = \eta_{cm}$ uprushes on the slope and encounters the trough of the waterline oscillation on the slope as shown in Fig. 5. The computed results shown in Figs. 6 and 7 for runs R2a and R2b with $\cot\theta' = 6$ and $\xi = 2.36$ are very similar to those for run R1. Additional runs are required to determine whether these critical wave conditions are limited to relatively gentle slopes such as $\cot\theta' = 6$ or can occur for steeper slopes as long as the surf similarity parameter is roughly two. For run R3 with $\cot\theta' = 4$ and $\xi = 3.52$, the critical stability number occurs at the time t_{sc} when the extremely large wave with the maximum crest elevation $\eta_c = \eta_{cm}$ and the minimum trough elevation $\eta_{tu} = \eta_{tm}$ causes the downrushing water with large velocities following large runup as shown in Fig. 8. For run R4 with $\cot\theta' = 3$ and $\xi = 4.37$, the critical stability number occurs at the time t_{sc} when the relatively large zero-upcrossing wave with the high crest followed by the deep trough causes the downrushing water with large velocities with the waterline on the slope being near SWL as shown in Fig. 9. The computed results shown in Figs. 10 and 11 for run R5 with $\cot\theta' = 2$ and $\xi = 5.95$ and run R6 with $\cot\theta' = 2$ and $\xi = 6.88$ are similar to those for run R4.

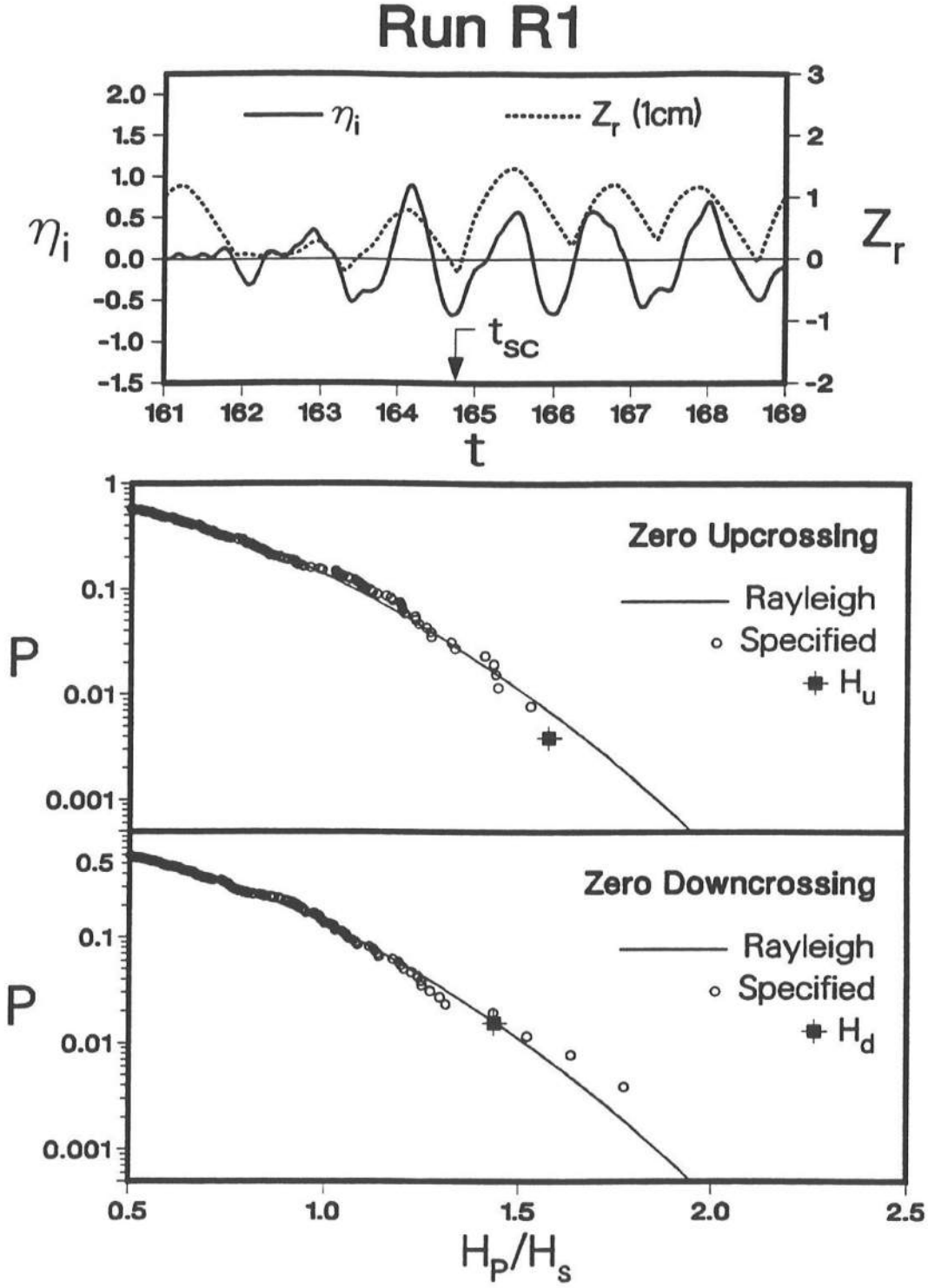

Figure 5: Analysis of Critical Incident Wave Profile for Run R1

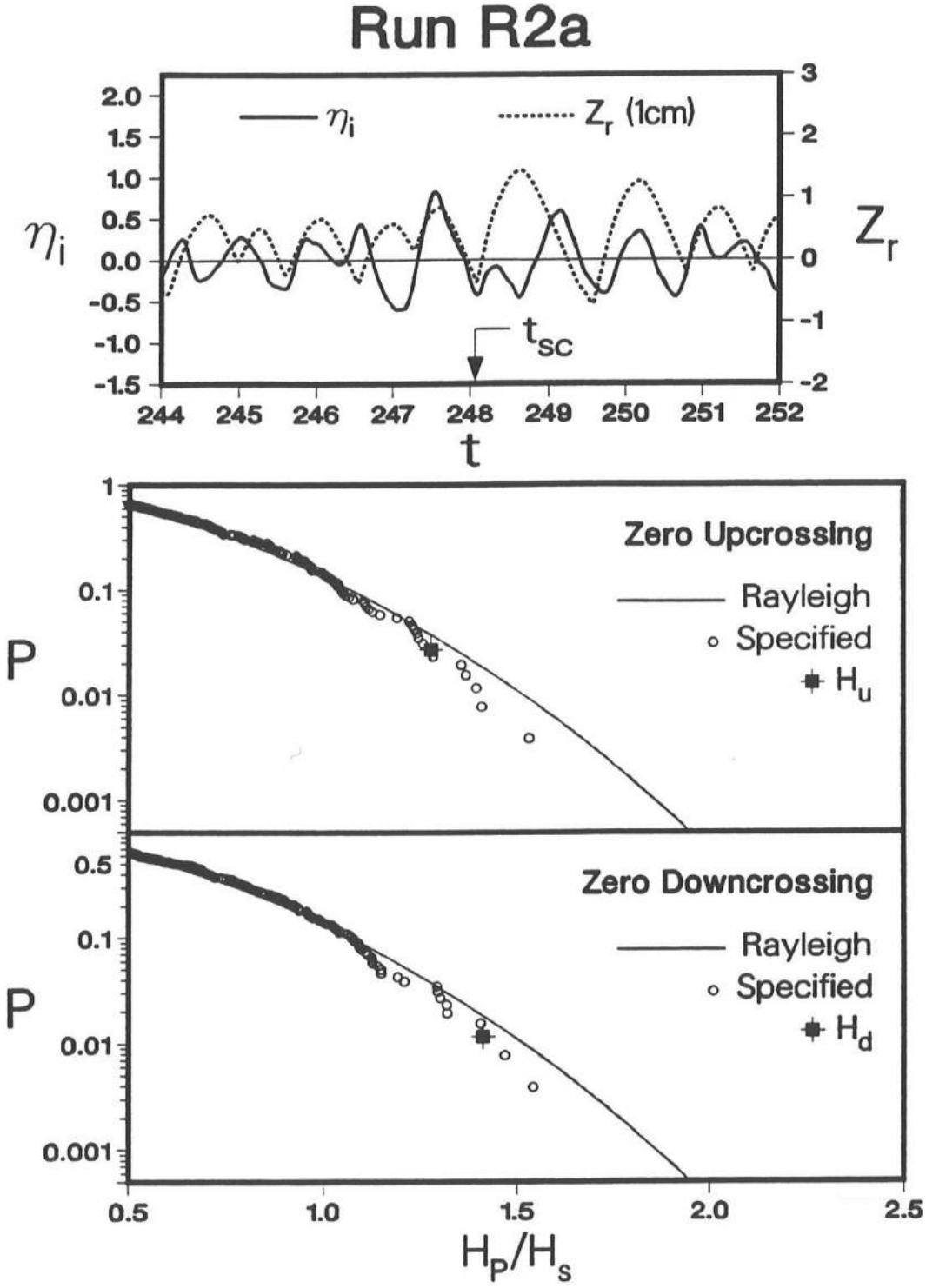

Figure 6: Analysis of Critical Incident Wave Profile for Run R2a

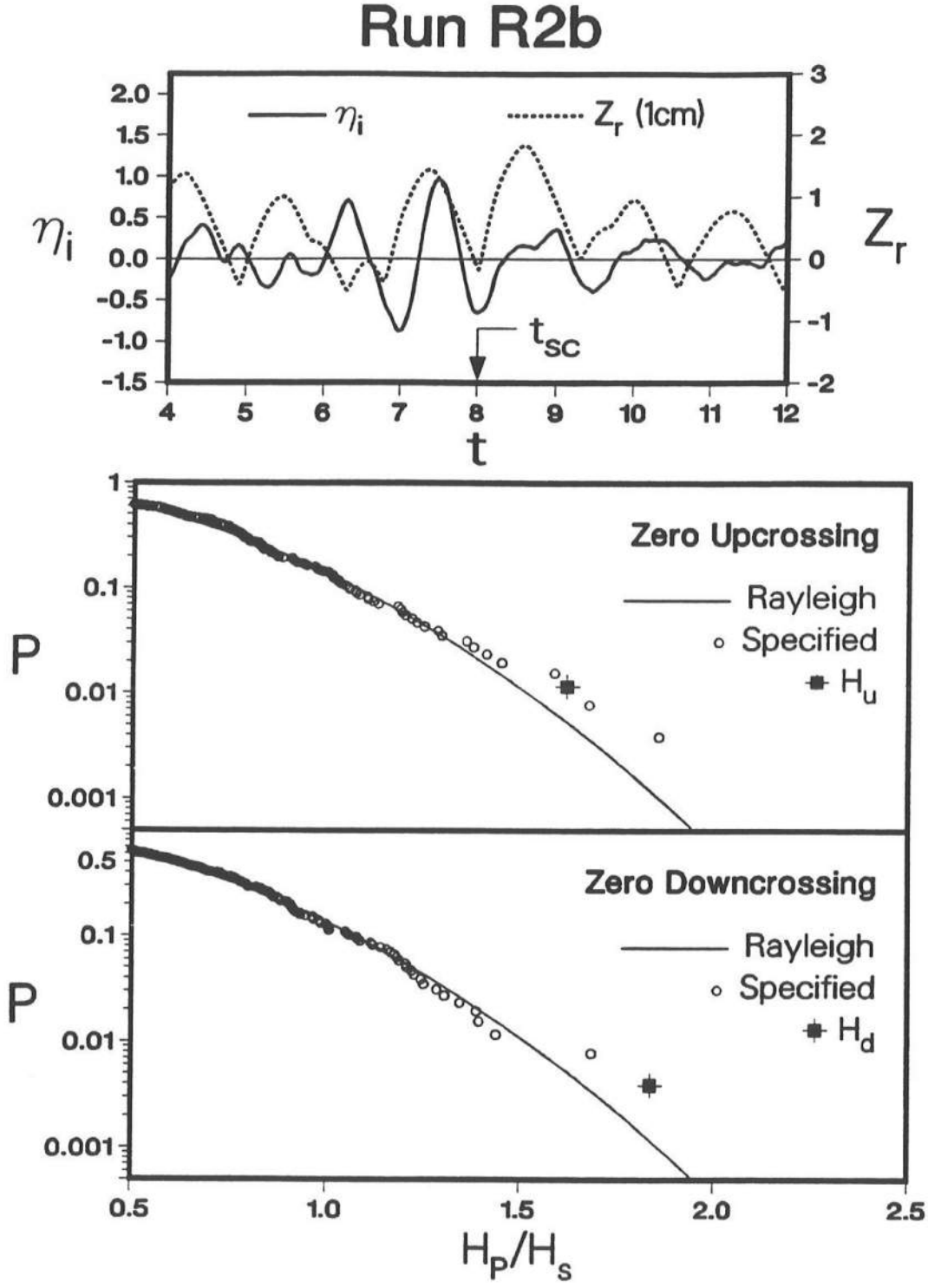

Figure 7: Analysis of Critical Incident Wave Profile for Run R2b

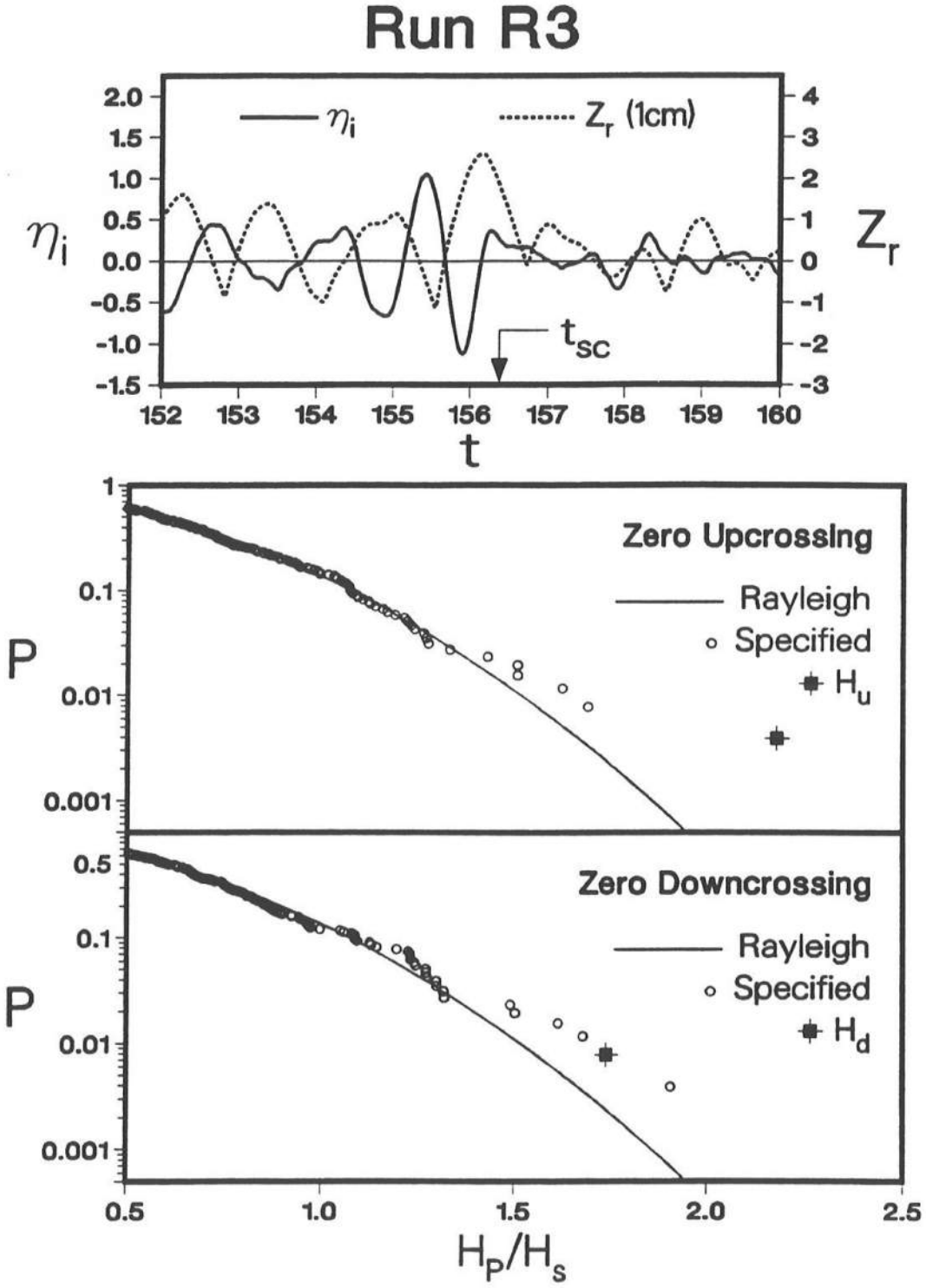

Figure 8: Analysis of Critical Incident Wave Profile for Run R3

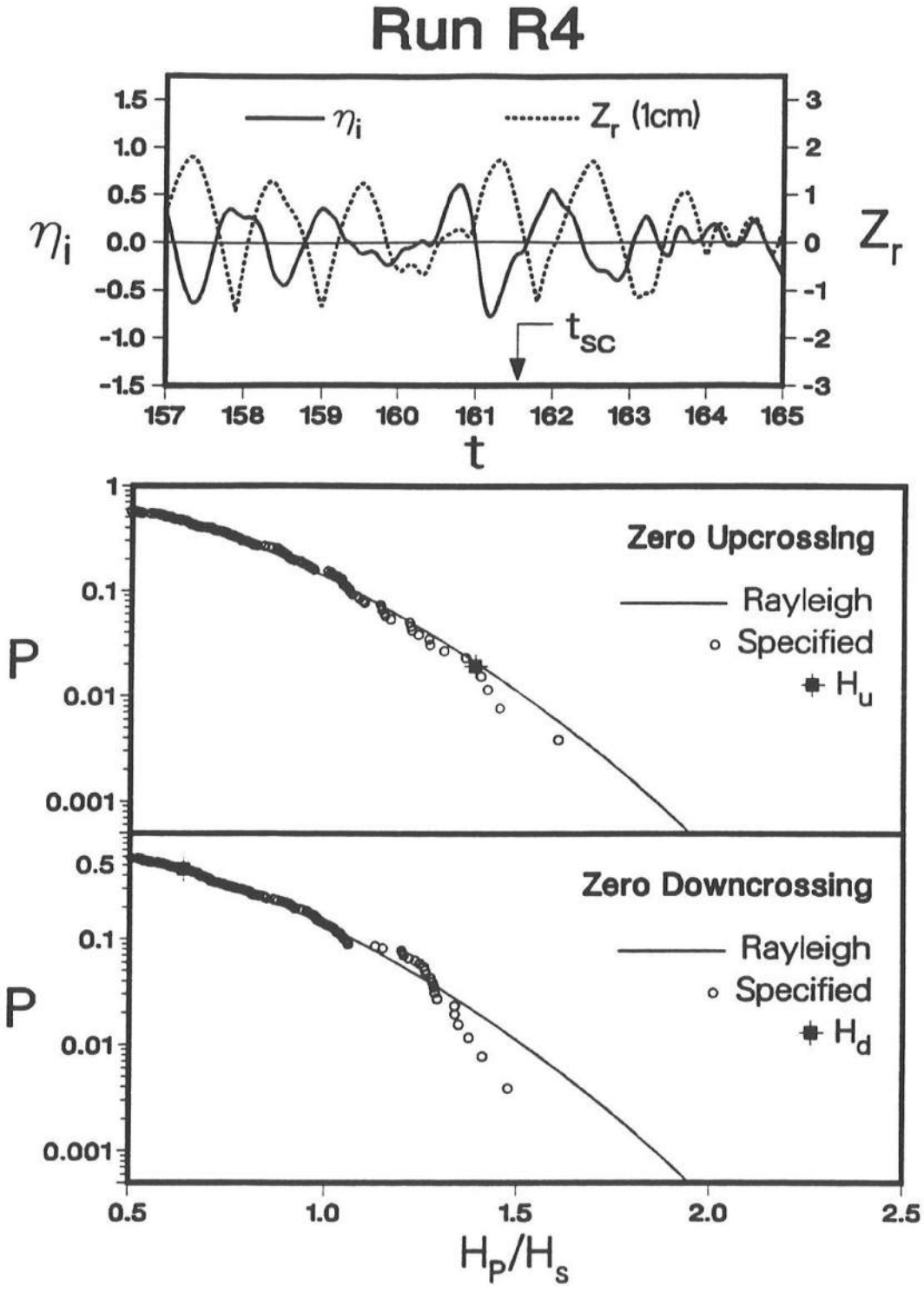

Figure 9: Analysis of Critical Incident Wave Profile for Run R4

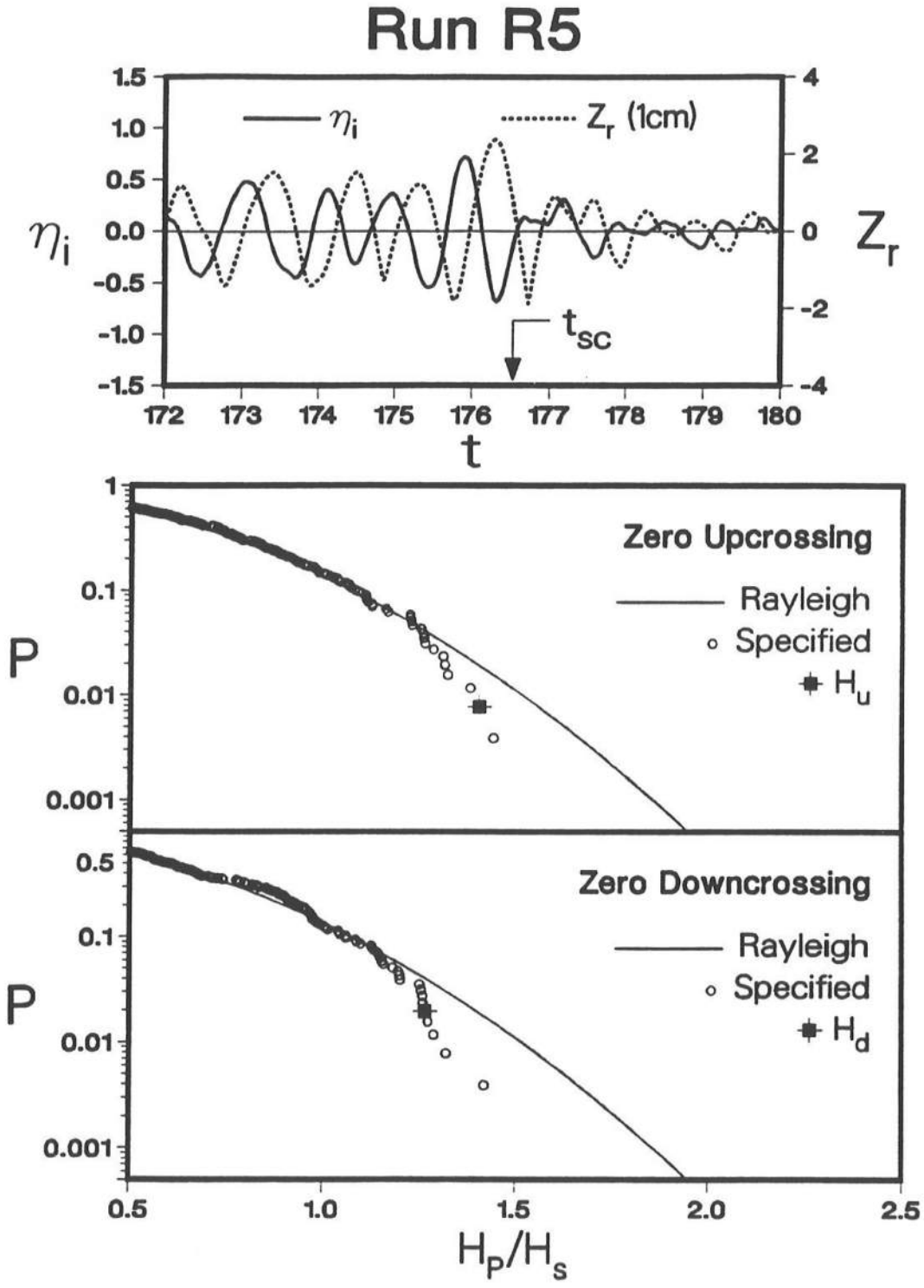

Figure 10: Analysis of Critical Incident Wave Profile for Run R5

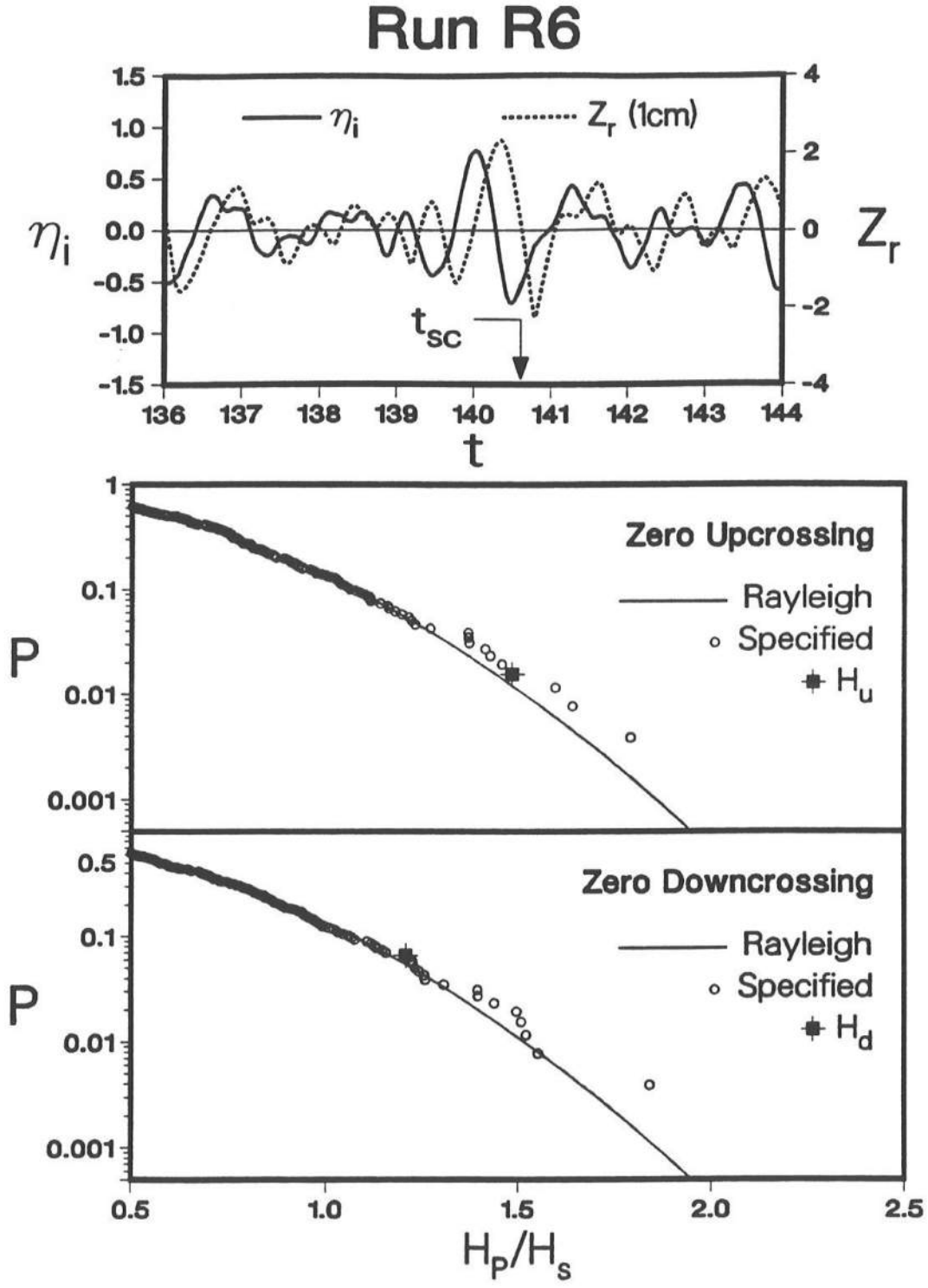

Figure 11: Analysis of Critical Incident Wave Profile for Run R6

PART III: ARMOR MOVEMENT AND DISLODGEMENT

Probability of Armor Movement

The critical incident wave profile and resulting critical stability number N_{sc} is useful for the design of armor units in which $N_s < N_{sc}$ so that armor units will not move under the action of design waves. If the mass of armor units is reduced such that $N_s > N_{sc}$, the degree of armor movement and resulting profile change will need to be predicted.

The computed armor stability function $N_R(t, x)$ depends on the normalized incident wave train $\eta_i(t)$ and the slope and armor characteristics specified as input to the numerical model. In the numerical model, the constant friction factor f' is used to account for the roughness effects of the primary cover layer on the flow over the rough permeable slope, while the effects of the permeable underlayer are taken into account by the volume and momentum fluxes into or out of the permeable underlayer. Since the computed flow field is not very sensitive to the assumed value of f', the computed temporal and spatial variations of $N_R(t, x)$ for each run in Table 1 may be assumed to remain essentially the same even if the stability number N_s defined in Eq. 1 is increased somewhat by decreasing only the median mass W' of the armor units.

In the following, the probability of armor movement based on the movement duration, P_t, and the probability of armor movement per unit normalized time, P_m, are predicted as a function of the stability number $N_s > N_{sc}$ and the location x of the armor unit along the uniform slope. For given N_s and x, armor movement will occur during the time when $N_s > N_R$. The duration of each event of armor movement is denoted by t_j with $j = 1, 2, \ldots, J$ where J = number of armor movement events during the specified duration $t_{min} \leq t \leq t_{max}$. In this paper $t_{min} = 8$ and $t_{max} = 256$. From the computed armor movement statistics, the

probabilities P_t and P_m may be defined as

$$P_t = (t_{max} - t_{min})^{-1} \sum_{j=1}^{J} t_j \;\; ; \;\; P_m = \frac{J}{(t_{max} - t_{min})} \tag{2}$$

For example, Fig. 12 shows the computed probabilities P_t and P_m for $N_s/N_{sc} = 1.1$, 1.3 and 1.5 for run R1 where the normalized elevation, $z = z'/H'$, of the armor unit on the slope relative to SWL located at $z = 0$ is used instead of x. The computed probabilities of the armor movement occurring mostly below SWL increase with the increase of N_s. For run R1, the computed value of N_{sc} is 1.56 and the measured value of N_s corresponding to the start of the damage was 1.72 as listed in Table 1. This implies that the numerical model predicts the movement of the armor units with $N_s = 1.72$, that is, $N_s/N_{sc} = 1.10$. However, the predicted probabilities for $N_s/N_{sc} = 1.1$ are very small as shown in Fig. 12.

Prediction of Damage Level

The probability of armor dislodgement per unit normalized time, P_d, is expected to be less than P_m. As a first attempt, it is simply assumed that $P_d = C_d P_m$ where C_d = empirical parameter. The rate of vertical erosion of the primary cover layer may be given by

$$\frac{\partial \eta_e'}{\partial t'} = \frac{C_3 (d')^3}{1 - n_a} \frac{1 - n_a}{C_2 (d')^2} \frac{P_d}{T'} = \frac{C_3 d' P_d}{C_2 T'} \tag{3}$$

where η_e' = vertical erosion depth of the primary cover layer taken positive downward; t' = time associated with the profile change; d' = characteristic length of the armor unit; C_3 = armor volume coefficient; C_2 = armor area coefficient; n_a = porosity of the primary cover layer; and (P_d/T') = probability of dislodgement of a single unit per unit time. In Eq. 3, $C_3(d')^3/(1 - n_a)$ is the volume occupied by a single unit, while $(1 - n_a)/C_2(d')^2$ is the number of armor units per unit area along the slope. Eq. 3 predicts the erosion only since the dislodged armor units are assumed to be deposited in the region where P_d is essentially zero.

In the following, the profile change is assumed to be so small that P_d may be assumed to be independent of t'. Then, Eq. 3 yields $\eta'_e = (C_3 d' P_d t)/C_2$ where $\eta'_e = 0$ at $t' = 0$ and $t = t'/T'$ is the normalized time which is equal to the number of individual waves. Integration of η'_e along the slope in the region $\eta'_e > 0$ yields the eroded area A'_e. Van der Meer (1988) defined the damage level S by $S = A'_e/(W'/\rho s)^{2/3}$. The present analysis can be shown to yield

$$S = \frac{C_d C_3^{2/3}(s-1)N_s t}{C_2 \sin\theta'} \int P_m dz \tag{4}$$

where the stability number N_s is defined in Eq. 1 and the integration of P_m with respect to z can be performed for given $N_s > N_{sc}$ using the computed variation of P_m such as those shown in Fig. 6. For the runs listed in Table 1, use was made of $C_3 = 0.66$, $C_2 = 0.90$ and $s = 2.63$ in Appendix A. In the following computation, the number of individual waves is taken to be $t = 1000$ and the value of N_s is varied such that $N_s/N_{sc} = 1.1,\ 1.2, \ldots,\ 2.0$.

Figs. 13-19 show the computed damage level S as a function of N_s for each of the runs listed in Table 1. The empirical parameter C_d is taken as $C_d = 0.005,\ 0.01$ and 0.02 so that the computed values of S are of the order of the values of S based on the empirical formula of Van der Meer (1988) which is also plotted for each run. The computed variations of S with respect to N_s for all runs are in qualitative agreement with the empirical formula. Eq. 4 will overestimate the value of S if S becomes so large that the profile change will result in the decrease in P_m and P_d. The major difference between Eq. 4 and the empirical formula is that the probability of armor movement P_m in Eq. 4 is computed for the specified incident wave train $\eta_i(t)$ for each run. It is hence possible to examine the sensitivity of P_m to various incident wave trains and explain some of the scatter of data points associated with the empirical formula of Van der Meer (1988) as discussed in Appendix B.

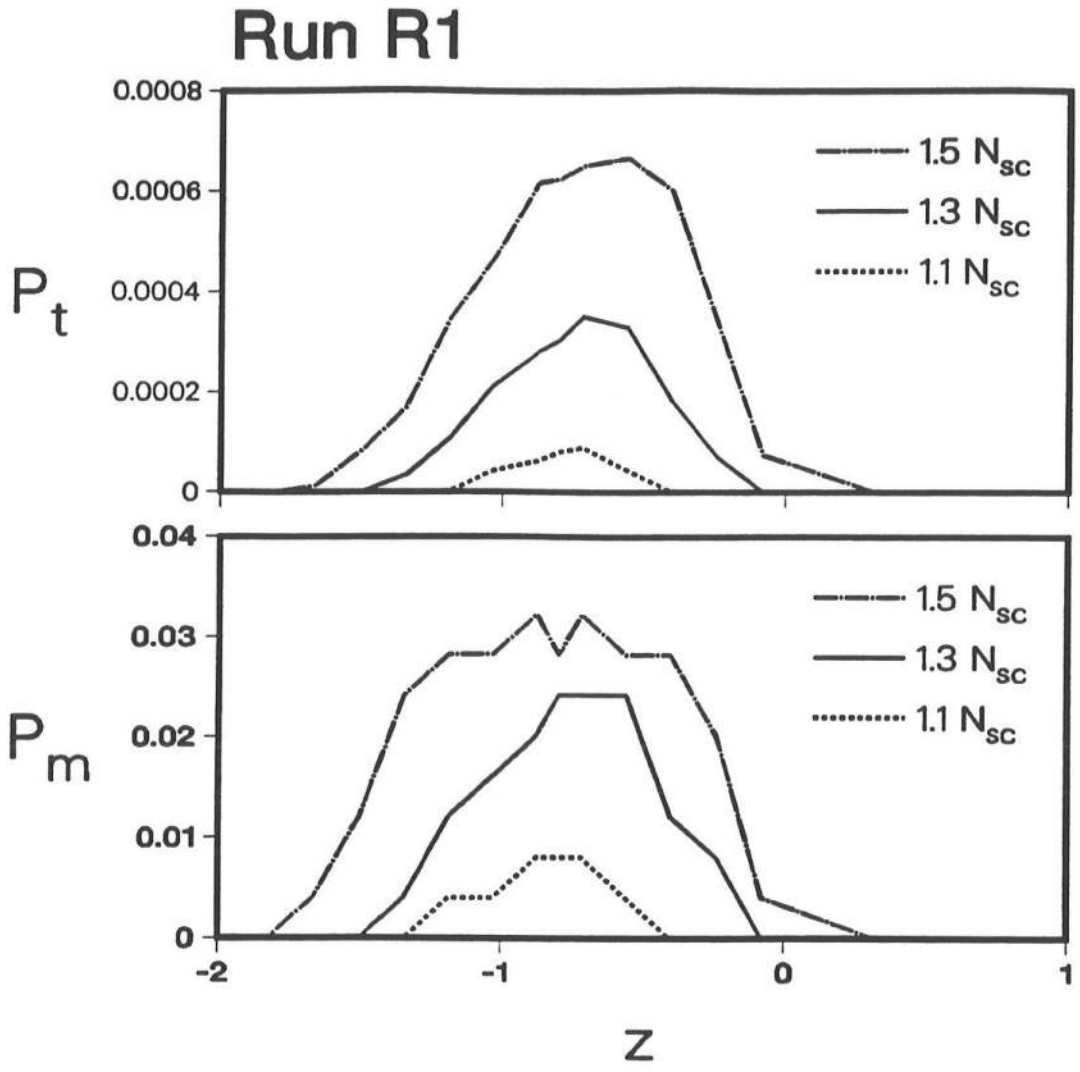

Figure 12: Computed Probabilities P_t and P_m of Rock Movement as a Function of Normalized Elevation z for $N_s/N_{sc} = 1.1, 1.3$ and 1.5 for run R1

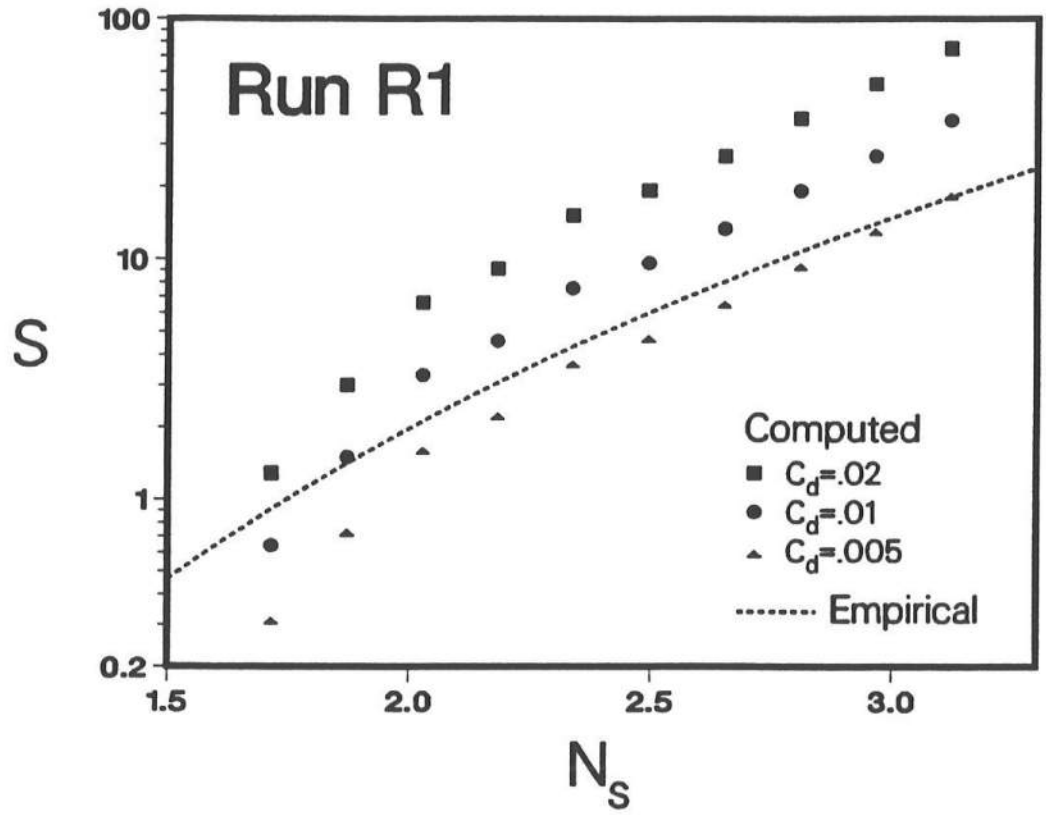

Figure 13: Computed Damage Level S as a Function of N_s for $C_d = 0.005,\ 0.01$ and 0.02 as Compared with Empirical Formula for Run R1

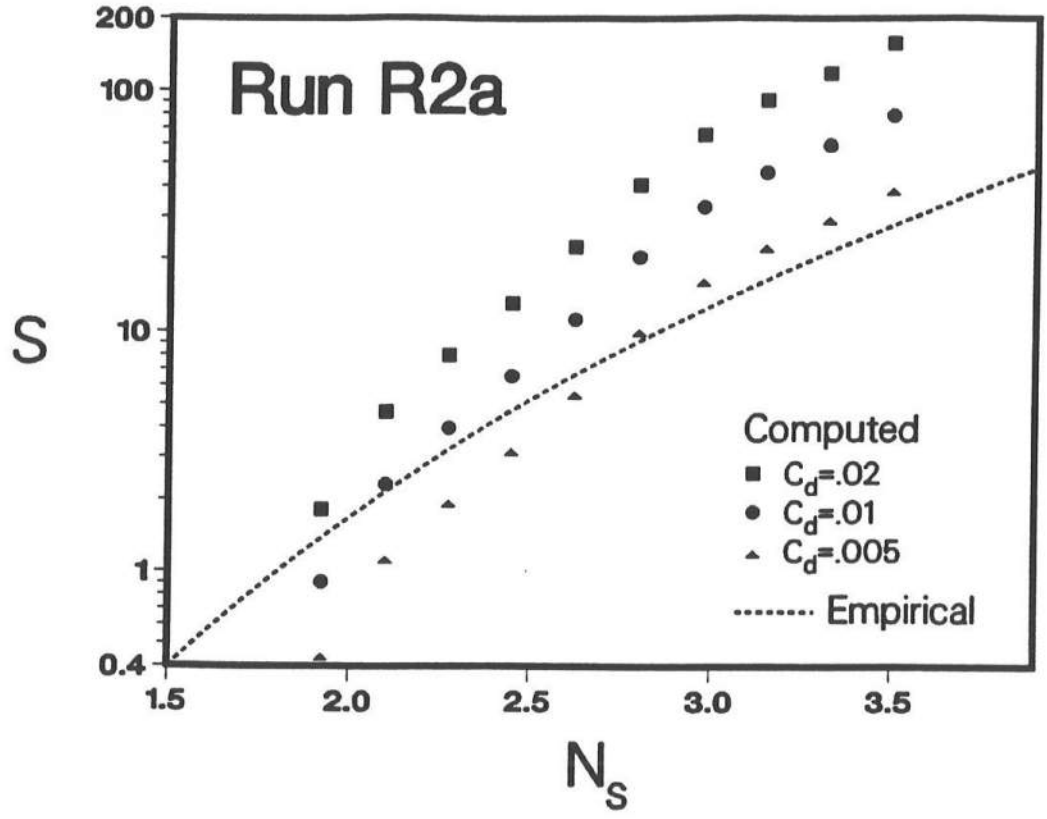

Figure 14: Computed Damage Level S as a Function of N_s for $C_d = 0.005$, 0.01 and 0.02 as Compared with Empirical Formula for Run R2a

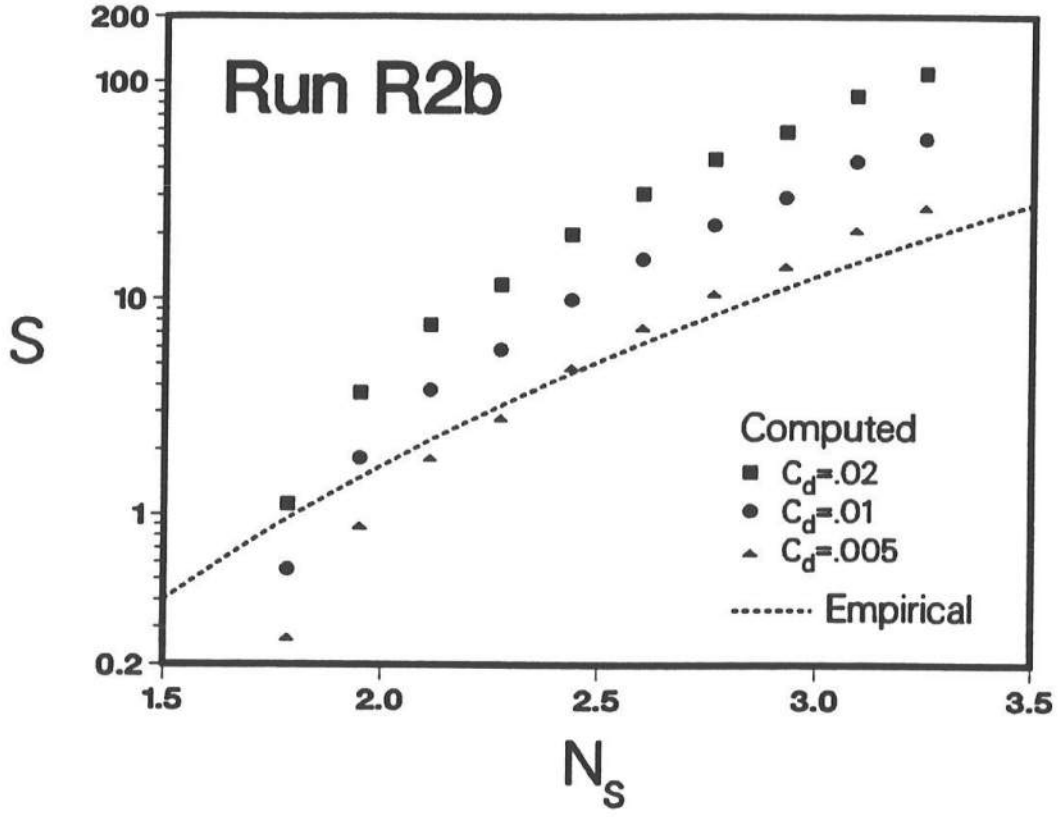

Figure 15: Computed Damage Level S as a Function of N_s for $C_d = 0.005$, 0.01 and 0.02 as Compared with Empirical Formula for Run R2b

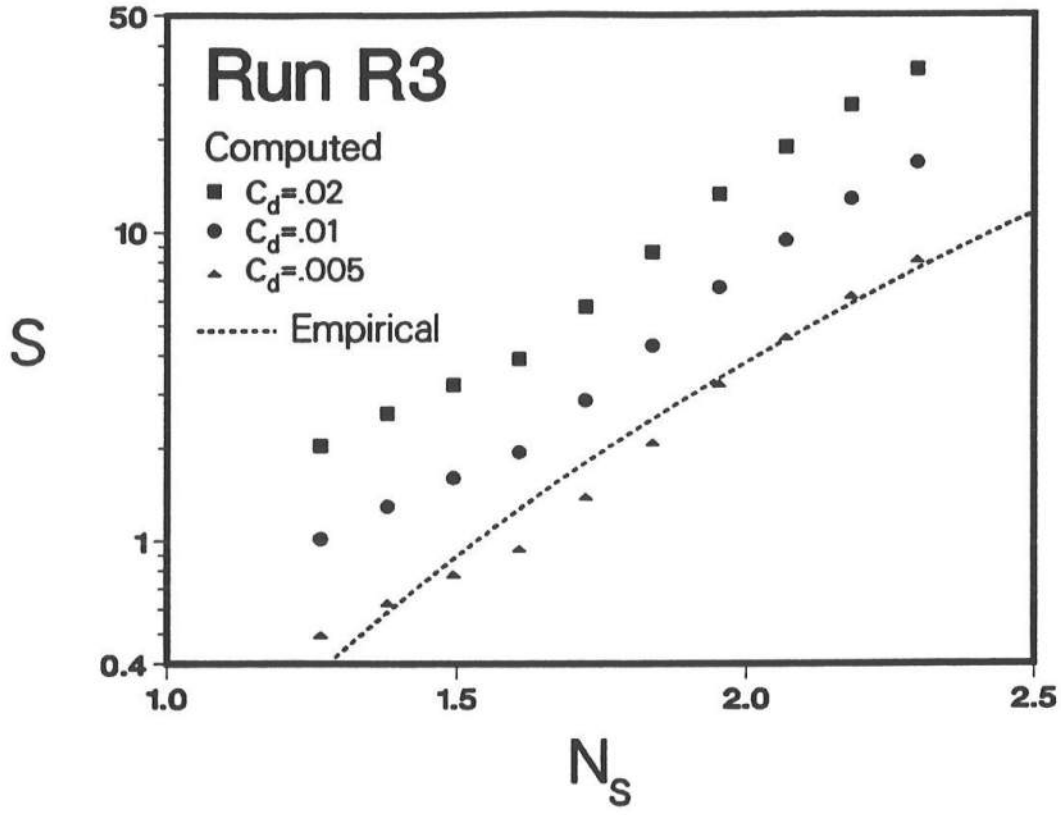

Figure 16: Computed Damage Level S as a Function of N_s for $C_d = 0.005$, 0.01 and 0.02 as Compared with Empirical Formula for Run R3

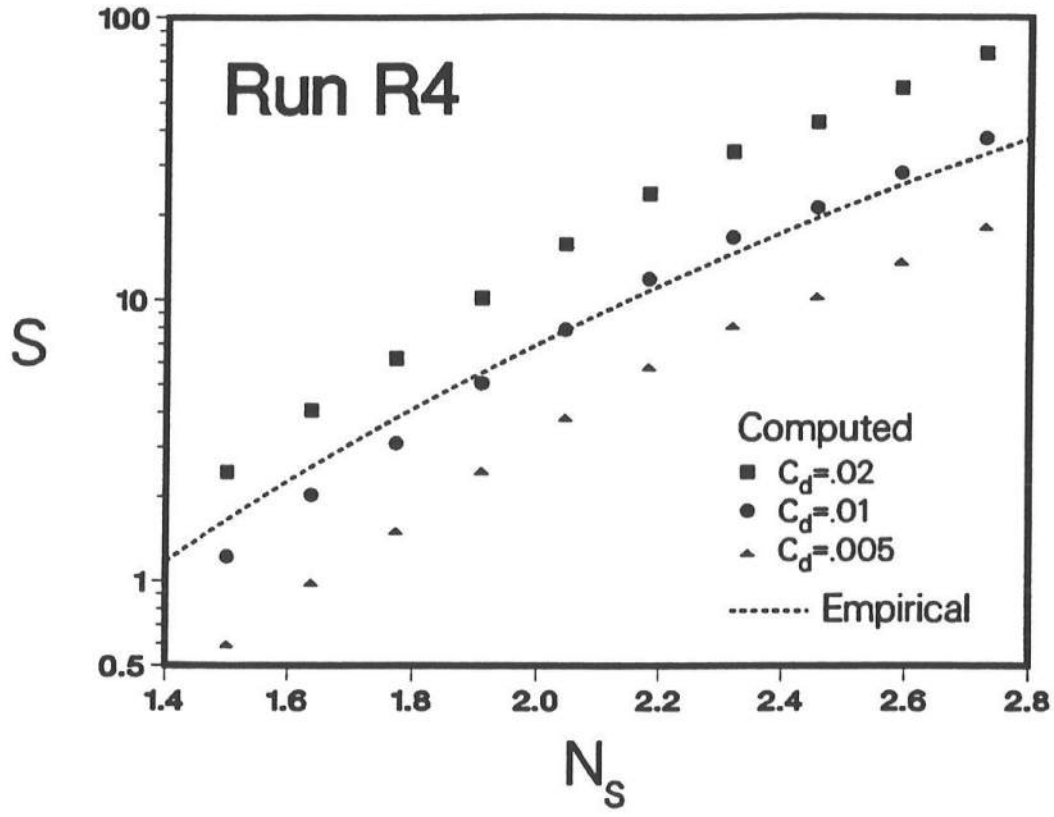

Figure 17: Computed Damage Level S as a Function of N_s for $C_d = 0.005,\ 0.01$ and 0.02 as Compared with Empirical Formula for Run R4

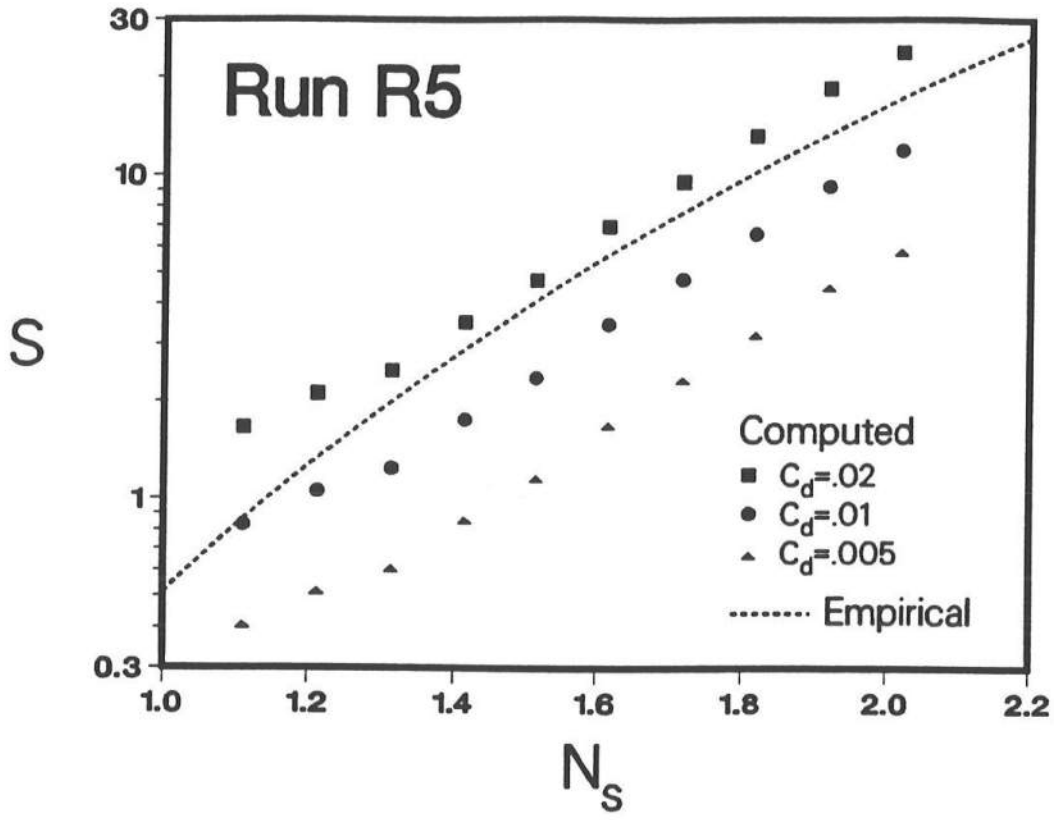

Figure 18: Computed Damage Level S as a Function of N_s for $C_d = 0.005$, 0.01 and 0.02 as Compared with Empirical Formula for Run R5

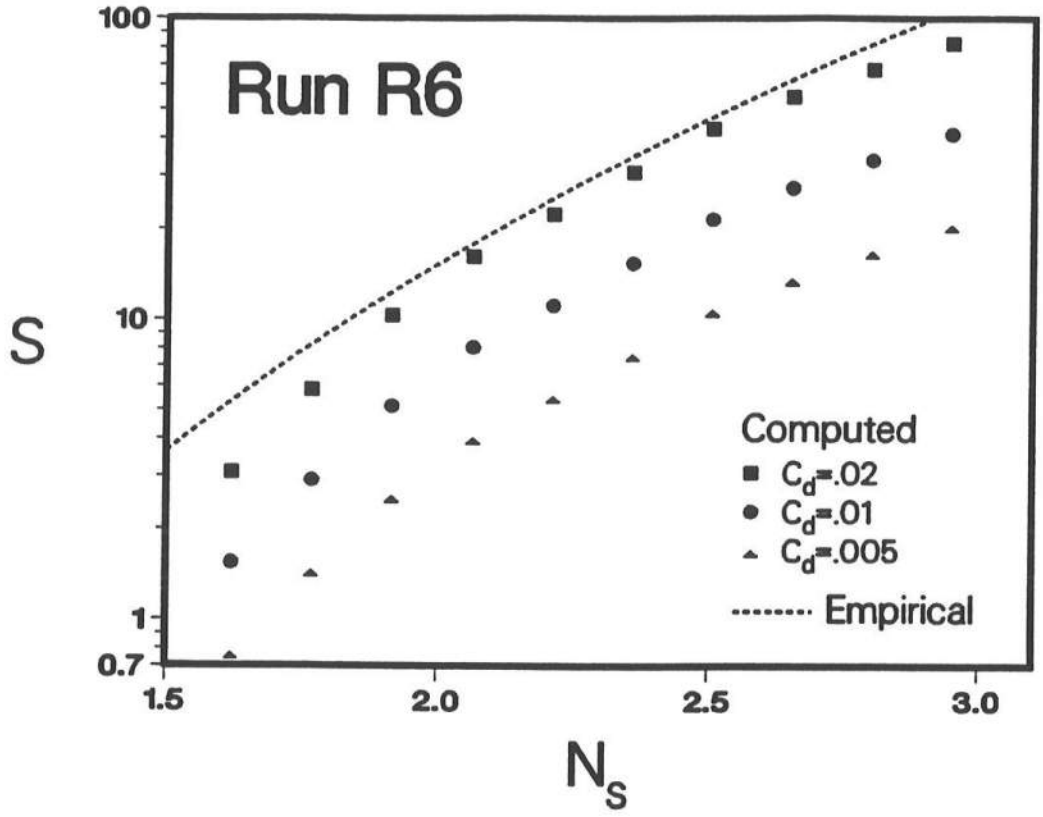

Figure 19: Computed Damage Level S as a Function of N_s for $C_d = 0.005,\ 0.01$ and 0.02 as Compared with Empirical Formula for Run R6

PART IV: CONCLUSIONS AND FUTURE WORK

The computed results presented herein is not extensive and need to be verified. The numerical model is used to examine the detailed armor response to the specified incident wave trains since the detailed quantitative understanding is essential for improving the design of rock slopes for specified design waves as well as determining the design wave conditions more specifically than those based on the representative wave height and period. Generally, the scatter of data points about an empirical curve used for the design of a coastal structure against irregular waves is fairly large. Some of the scatter appears to be caused by the use of the representative wave height and period.

The computer program called RBREAK and detailed user's manual are being written by synthesizing the results obtained so far. RBREAK can be used for the design of essentially impermeable coastal structures against normally incident random waves as well as for the prediction of swash oscillations caused by normally incident random waves on essentially impermeable beaches.

Furthermore, a more general numerical model is being developed to eliminate the limitations of a thin permeable underlayer and examine the effects of a thick underlayer on the flow and armor response on the rough permeable slope. Such a numerical model is required to predict the behavior of a berm breakwater with a thick layer of graded stone (Baird and Hall, 1984).

REFERENCES

Baird, W.R. and Hall, K.R. (1984), "The design of breakwaters using quarried stones," *Proc. 19th Coast. Engrg. Conf.*, ASCE, 1024-1031.

Gunbak, A. R. and Bruun, P. M. (1979), "Wave mechanics principles on the design of rubble-mound breakwaters." *Proc. P.O.A.C.*, Norwegian Inst. of Tech., Trondheim, Norway, 1301-1318.

Kobayashi, N. and Wurjanto, A. (1989a), "Numerical model for design of impermeable coastal structures." *Res. Rept. No. CE-89-75*, Department of Civil Engineering, University of Delaware, Newark, DE 19716.

Kobayashi, N. and Wurjanto, A. (1989b), "Armor stability on rough permeable slopes of marine structures." *Proc. 23rd I.A.H.R. Congress*, Ottawa, Canada, C, 407-414.

Kobayashi, N. and Wurjanto, A. (1989c), "Numerical prediction of hydrodynamic forces and sliding motion of dolos units." *Proc. Stresses in Concrete Armor Units*, ASCE, 355-378.

Kobayashi, N. and Wurjanto, A. (1990), "Numerical model for waves on rough permeable slopes." *J. Coast, Res.*, Special Issue No. 7 on Rational Design of Mound Structures, 149-166.

Kobayashi, N., Wurjanto, A. and Cox, D.T. (1990), "Irregular waves on rough permeable slopes." *J. Coast. Res.*, Special Issue No. 7 on Rational Design of Mound Structures, 167-184.

Kobayashi, N., Cox, D.T. and Wurjanto, A. (1990), "Irregular wave reflection and runup on rough impermeable slopes." *J. Wtrway. Port Coast. and Oc. Engrg.*, ASCE, 116(6)

(in press).

Kobayashi, N., Cox, D.T. and Wurjanto, A. (1991), "Permeability effects on irregular wave runup and reflection." *J. Coast. Res.*, 7(1), (in press).

Kobayashi, N., Wurjanto, A. and Cox, D.T. (1991), "Rock slopes under irregular wave attack." *Proc. 22nd Coast. Engrg. Conf*, ASCE, (in press).

Van der Meer, J. W. (1988), "Rock slopes and gravel beaches under wave attack." Delft Univ. of Tech., Delft, The Netherlands, Doctoral Thesis.

APPENDIX A

NUMERICAL MODEL FOR WAVES ON ROUGH PERMEABLE SLOPES

Nobuhisa Kobayashi and Andojo Wurjanto

Journal of Coastal Research
Special Issue No. 7, pp. 149-166

Spring, 1990

Journal of Coastal Research	SI	7	149–166	Fort Lauderdale, Florida	Spring 1990

Numerical Model for Waves on Rough Permeable Slopes

Nobuhisa Kobayashi and Andojo Wurjanto

Department of Civil Engineering
University of Delaware
Newark, DE 19716, U.S.A.

ABSTRACT

KOBAYASHI, N. and WURJANTO, A., 1990. Numerical model for waves on rough slopes. *Journal of Coastal Research*, SI#7, 149–166. Fort Lauderdale (Florida). ISSN 0749-0208.

A numerical model is presented for predicting the flow and armor response on a rough permeable slope as well as the flow in a permeable underlayer for a normally incident wave train. In addition to the continuity and momentum equations used to compute the flow field, an equation of energy is used to estimate the rate of energy dissipation due to wave breaking. Computation is made for six test runs to examine the accuracy and capability of the numerical model for simulating the fairly detailed hydrodynamics and armor response under the action of regular waves. The computed critical stability number for initiation of armor movement is compared with the measured stability number corresponding to the start of the damage under irregular wave action to quantify the limitations of the regular wave approximation. The computed wave run-up, run-down and reflection coefficients are shown to be in qualitative agreement with available empirical formulas based on regular wave tests.

ADDITIONAL INDEX WORDS: *Waves, reflection, run-up, armor units, breakwaters.*

INTRODUCTION

Design of coastal structures protected with armor units is presently based on empirical formulas and hydraulic model tests. The detailed hydrodynamics and armor response are not measured in most model tests because of the difficulties of instrumentation. Numerical models may hence be used to improve our understanding of the detailed mechanics as well as to interpret the model test results. Furthermore, a hybrid approach based on empirical formulas, numerical models and hydraulic model tests will improve the efficiency and reliability of the design procedure.

The numerical model developed by KOBA YASHI *et al.* (1987) for predicting the regular wave motion on the rough primary cover layer of a rubble structure is expanded herein to include a permeable underlayer below the primary cover layer. The boundary below the permeable underlayer is assumed to be impermeable. The continuity and momentum equations for the flow on the rough permeable slope and the flow in the permeable underlayer are solved numerically in the time domain. A conservation equation of energy is derived and used to estimate the spatial variation of the rate of energy dissipation due to wave breaking from the computed spatial variations of the wave energy flux on the slope, the energy dissipation rate due to bottom friction and the energy flux into the permeable underlayer. Moreover, the hydraulic stability of armor units in the primary cover layer is computed using the armor stability model of KOBAYA SHI and OTTA (1987) in which the drag, lift and inertia forces acting on an armor unit are estimated using the computed fluid velocity and acceleration on the rough permeable slope.

Computation is made for six test runs selected from the extensive random wave test data on the stability and damage of rock slopes tabulated by VAN DER MEER (1988b). The selected six runs corresponded to the start of the damage and covered a wide range of the surf similarity parameter. The incident irregular wave train characterized by its significant wave height and average wave period is approximated by the regular wave train with the same height and period in this paper. This is because randomness makes it difficult to examine the accuracy and capability of the expanded numerical model for simulating the flow and armor response on the rough permeable slope as well as the flow in the permeable underlayer. The computation using the incident irregular wave

90035 received June 1989; accepted in revision September 1989.

train generated numerically is performed and presented in the accompanying paper by KOBAYASHI *et al.* (1990). The comparison of the computed critical stability number for initiation of armor movement and the measured stability number corresponding to the start of the damage under the irregular wave action indicates that the regular wave approximation will result in the appreciable overestimation of the armor stability. The computed wave run-up, run-down and reflection coefficients are also compared with available empirical formulas based on regular wave tests.

FLOW ON ROUGH PERMEABLE SLOPE

The wave motion on a rough permeable slope is computed for the normally incident wave train specified at the toe of the slope as shown in Figure 1 where the prime indicates the dimensional variables. The symbols shown in Figure 1 are as follows: x' = horizontal coordinate taken to be positive landward with $x' = 0$ at the toe of the slope; z' = vertical coordinate taken to be positive upward with $z' = 0$ at the still water level (SWL); d'_t = water depth below SWL at the toe of the slope; θ' = local angle of the slope which may vary along the slope; η' = free surface elevation above SWL; h' = water depth above the rough permeable slope; u' = depth-averaged horizontal velocity above the rough permeable slope; h'_p = thickness of the permeable underlayer below the primary cover layer which may vary along the slope; u'_p = vertically-averaged horizontal discharge velocity in the permeable underlayer; and q'_b = volume influx per unit horizontal area into the permeable underlayer. The numerical flow model developed by KOBAYASHI *et al.* (1987) assumed a rough impermeable slope, corresponding to $h'_p = 0$ and $q'_b = 0$.

For the flow over the rough permeable slope, the vertically-integrated equations for mass and x'-momentum may be expressed as (KOBAYASKI, 1986)

$$\frac{\partial h'}{\partial t'} + \frac{\partial}{\partial x'}(h'u') = -q_b' \tag{1}$$

$$\frac{\partial}{\partial t'}(h'u') + \frac{\partial}{\partial x'}(h'u'^2) = -gh'\frac{\partial \eta'}{\partial x'} - \frac{1}{2}f'|u'|u' - u_b' q_b' \tag{2}$$

where t' = time; g = gravitational acceleration; f' = constant friction factor related to the shear stress on the rough primary cover layer; and u'_b = horizontal fluid velocity between the primary cover layer and the permeable underlayer. In this simplified analysis, the friction factor f' accounts for the roughness effects of the primary cover layer on the flow over the rough permeable slope, while the effects of the permeable underlayer are taken into account by the volume influx, q'_b, and the momentum influx, $u'_b q'_b$, per unit horizontal area into the permeable underlayer. Admittedly, the assumed separation between the roughness and permeability effects is somewhat artificial. Moreover, the theoretical bed level for the flow over the rough permeable slope is difficult to pinpoint as is the case with oscillatory rough turbulent boundary layers (JONSSON, 1980).

For the flow in the permeable underlayer in the region seaward of the instantaneous waterline on the rough permeable slope where the water depth h' is essentially zero, the vertically-integrated equations of mass and x'-momentum may be expressed as (KOBAYASHI, 1986)

$$\frac{\partial}{\partial x'}(h_p'u_p') = q_b' \tag{3}$$

$$\frac{\partial}{\partial t'}(h_p'u_p') + \frac{1}{n_p}\frac{\partial}{\partial x'}(h_p'u_p'^2) - u_b'q_b' = -gn_p h_p'\frac{\partial \eta'}{\partial x'} - n_p h'_p(\alpha' + \beta'|u_p'|)u_p' \tag{4}$$

where n_p = porosity of the permeable underlayer; α' = coefficient expressing the laminar flow resistance; and β' = coefficient expressing the turbulent flow resistance. Eqs. 3 and 4 are based on the assumption of the impermeable boundary below the permeable homogeneous underlayer. The coefficients α' and β' may empirically be expressed as (MADSEN and WHITE, 1975)

$$\alpha' = \frac{\alpha_0(1-n_p)^3\nu}{(n_p d_p')^2}\ ;\ \beta' = \frac{\beta_0(1-n_p)}{n_p^3 d_p'} \tag{5}$$

where d'_p = representative diameter of the stone in the permeable underlayer; ν = kinematic viscosity of the fluid; α_o = dimensionless constant in the range $780 \leq \alpha_o \leq 1500$; and β_o = dimensionless constant in the range $1.8 \leq \beta_o \leq 3.6$.

In order to compute the variations of h', u',

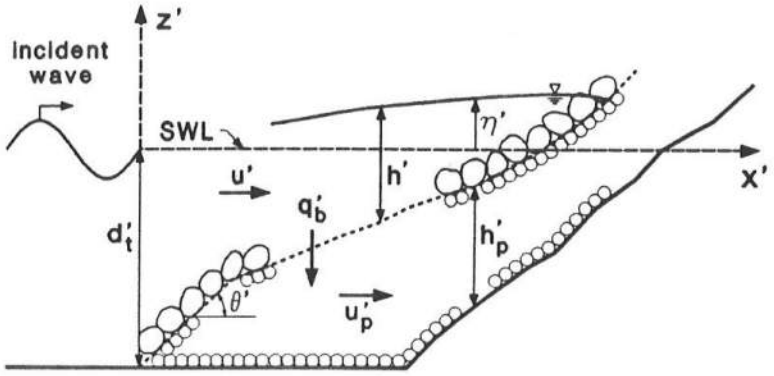

Figure 1. Flow over rough slope and in permeable underlayer.

q'_b and u'_p with respect to t' and x' using Eqs. 1–5, u'_b in Eqs. 2 and 4 may be given by $u'_b = u'$ for $q'_b \geq 0$ and $u'_b = u'_p/n_p$ for $q'_b < 0$ in which u'_p/n_p is the actual horizontal fluid velocity in the permeable underlayer. This assumption may cause a sudden change of u'_b but is necessary since the vertical variation of the fluid velocity is not analyzed herein.

The following dimensionless variables and parameters are introduced to normalize Eqs. 1 and 2:

$$t = t'/T' \; ; \; x = x'/[T'(gH')^{1/2}] \; ; \quad (6)$$
$$u = u'/(gH')^{1/2} \; ; \; u_b = u_b'/(gH')^{1/2} \; ;$$

$$z = z'/H' \; ; \; h = h'/H' \; ; \quad (7)$$
$$\eta = \eta'/H' \; ; \; d_t = d_t'/H' \; ;$$

$$q_b = q_b'/(pH'/T') \; ; \; \sigma = T'(g/H')^{1/2} \; ;$$
$$\theta = \sigma \tan\theta' \; ; \; f = \sigma f'/2 \quad (8)$$

where T' = representative wave period; H' = representative wave height; p = dimensionless parameter expressing the degree of the permeability effects on the flow over the rough permeable slope; σ = dimensionless parameter related to wave steepness; θ = dimensionless gradient of the slope; and f = normalized friction factor. The representative wave period and height used for the normalization can be taken as the period and height used to characterize the incident wave at the toe of the slope. Substitution of Eqs. 6–8 into Eqs. 1 and 2 yields.

$$\frac{\partial h}{\partial t} + \frac{\partial}{\partial x}(hu) = -pq_b \quad (9)$$

$$\frac{\partial}{\partial t}(hu) + \frac{\partial}{\partial x}\left(hu^2 + \frac{1}{2}h^2\right) = -\theta h - f|u|u - pu_b q_b \quad (10)$$

where θ, f and p express the effects of the slope, friction and permeability, respectively. For a uniform slope, θ in Eq. 10 can be replaced by the surf similarity parameter, $\xi = \theta/(2\pi)^{1/2}$. The expression of p is obtained in relation to the normalization of Eqs. 3 and 4 performed below.

The following dimensionless variables and parameters are introduced to normalize Eqs. 3 and 4:

$$h_p = h_p'/h_c' \; ; \; u_p = u_p'/[p_u \, n_p (gH')^{1/2}] \quad (11)$$

$$p_u = \left[\frac{n_p d_p'}{\beta_0(1 - n_p)T'(gH')^{1/2}}\right]^{1/2}$$
$$p = \frac{p_u n_p h_c'}{H'} \quad (12)$$
$$\mu = \frac{\alpha_0(1 - n_p)^2 \nu}{\beta_0 p_u d_p'(gH')^{1/2}}$$

where h'_c = characteristic thickness of the permeable underlayer used to normalize h'_p such that h_p is on the order of unity; p_u = dimensionless parameter expressing the order of magnitude of the terms on the left hand side of Eq. 4 as compared to the terms on the right hand side; and μ = dimensionless parameter expressing the order of magnitude of the laminar flow resistance as compared to the turbulent flow resistance in Eq. 4. Substitution of Eqs. 11 and 12 together with Eqs. 5–7 into Eqs. 3 and 4 yields

$$\frac{\partial}{\partial x}(h_p u_p) = q_b \tag{13}$$

$$p_u\left[\frac{\partial}{\partial t}(h_p u_p) + p_u \frac{\partial}{\partial x}(h_p u_p^2) - u_b q_b\right] = -h_p \frac{\partial \eta}{\partial x} - h_p(\mu + |u_p|)\, u_p \tag{14}$$

Furthermore, u_b in Eqs. 10 and 14 is given by

$$u_b = u \quad \text{for } q_b \geq 0 \tag{15a}$$

$$u_b = p_u u_p \text{ for } q_b < 0 \tag{15b}$$

For most applications, the parameter p_u defined in Eq. 12 is expected to be much less than unity since the diameter d'_p of the underlayer material is normally much less than the horizontal length scale $T'(gH')^{1/2}$. For the case of $p_u << 1$, Eq. 14 may be simplified by neglecting the terms on its left hand side. This simplified equation can be solved to obtain u_p for given $\partial\eta/\partial x$

$$u_p \simeq \frac{i_p}{2}\left[\left(\mu^2 + 4\left|\frac{\partial \eta}{\partial x}\right|\right)^{1/2} - \mu\right] \quad \text{for } p_u << 1 \tag{16}$$

where $i_p = -1$ and $u_p < 0$ for $\partial\eta/\partial x > 0$, whereas $i_p = 1$ and $u_p > 0$ for $\partial\eta/\partial x < 0$. Eq. 16 implies that the horizontal variation of the hydrostatic pressure in the permeable underlayer determined by the instantaneous free surface elevation η drives the flow against the resistance in the permeable underlayer. The parameter μ defined in Eq. 12 accounts for the viscous effect and may be used to evaluate the increased viscous effect in small-scale hydraulic model tests. For the case of $p_u << 1$, the parameter p defined in Eq. 12 may be assumed to be much less than unity as long as the value of $n_p h'_c/H'$ is on the order of unity or less. Since Eqs. 3 and 4 are based on the assumption of the impermeable boundary below the permeable underlayer, practical applications of the present numerical model will be limited to the case where the void thickness $n_p h'_c$ of the permeable underlayer is on the order of the representative incident wave height H′ or less.

NUMERICAL METHOD

A numerical method is developed to solve Eqs. 9, 10. 13, 15 and 16 for the case of $p_u << 1$ and $p << 1$. The variations of h, u, q_b, u_p and u_b with respect to t and x are computed using a finite difference grid of constant space size Δx in the computation domain $x \geq 0$ and constant time step Δt starting from the initial time $t = 0$.

The initial time $t = 0$ for the computation marching forward in time is taken to be the time when the specified incident wave train arrives at the seaward boundary located at $x = 0$ as shown in Figure 1. The initial conditions for the computation are thus given by $\eta = 0$, $u = 0$, $q_b = 0$, $u_p = 0$ and $u_b = 0$ at $t = 0$ in the region $x \geq 0$. It is noted that h and η are uniquely related for given slope geometry.

The seaward boundary is located at $x = 0$ where the normalized water depth below SWL is d_t. In order to derive an appropriate seaward boundary condition, Eqs. 9 and 10 are expressed in the following characteristic forms

$$\frac{\partial \alpha}{\partial t} + (u+c)\frac{\partial \alpha}{\partial x} = -\theta - \frac{f|u|u}{h} + \frac{pq_b(u-c-u_b)}{h}; \quad \frac{dx}{dt} = u + c \tag{17}$$

$$\frac{\partial \beta}{\partial t} + (u-c)\frac{\partial \beta}{\partial x} = \theta + \frac{f|u|u}{h} - \frac{pq_b(u+c-u_b)}{h}; \quad \frac{dx}{dt} = u - c \tag{18}$$

$$\text{with } c = h^{1/2};\ \alpha = u + 2c;\ \beta = -u + 2c \tag{19}$$

Assuming that $u < c$ in the vicinity of the seaward boundary, α and β represent the characteristics advancing landward and seaward, respectively, in the vicinity of the seaward boundary. Following the procedure developed by KOBAYASHI *et al.* (1987), the total water depth at the seaward boundary is expressed in the form

$$h = d_t + \eta_i(t) + \eta_r(t) \text{ at } x = 0 \tag{20}$$

where η_i and η_r are the free surface variations normalized by H′ at $x = 0$ due to the incident and reflected waves, respectively. The incident wave train is specified by prescribing the variation of η_i with respect to $t \geq 0$. The normalized reflected wave train η_r is approximately expressed in terms of the seaward advancing characteristic β at $x = 0$

$$\eta_r(t) \simeq \frac{1}{2} d_t^{1/2}\, \beta(t) - d_t \text{ at } x = 0 \tag{21}$$

where β is given by Eq. 18.

The landward boundary on the slope is located at the moving waterline where the water depth is essentially zero. In reality, it is

difficult to pinpoint the exact location of the moving waterline on the rough permeable slope. For the computation, the waterline is defined as the location where the normalized water depth h equals a small value δ. Use is made of $\delta = 10^{-3}$ in the following computation. The procedure of the waterline computation is explained in detail in relation to the numerical method used to solve Eqs. 9 and 10. It should be mentioned that Eqs. 13 and 16 are applicable only to the region seaward of the moving waterline. The approximation of Eq. 14 by Eq. 16 for the case of $p_u << 1$ allows us to limit the computation domain seaward of the moving waterline. However, this implicitly assumes that the waterline movement is not affected by the flow in the permeable underlayer landward of the waterline. This implicit assumption may be appropriate if the thickness of the permeable underlayer is small enough to satisfy the condition of $p<<1$.

For the known values of h, u, q_b, u_p and u_b at the time level, $t=(n-1)\Delta t$, with n being a positive integer, the values of these variables at the next time level, $t=n\Delta t$, are computed in the following manner.

First, Eqs. 9 and 10 are used to compute the values of h and u at $t=n\Delta t$ excluding those at the seaward and landward boundaries. The finite difference method used to solve Eqs. 9 and 10 is an extension of the explicit dissipative Lax-Wendroff method used by KOBAYASHI *et al.* (1987) for the case of $p=0$ as explained in Appendix A. The values of h and u at the seaward boundary are computed using Eqs. 18–21. The value of $\eta_r(t)$ at $t=n\Delta t$ is calculated using Eq. 21 where the value of $\beta(t)$ at $x=0$ is computed using Eq. 18 with $f=0$ and $p=0$ which is discretized using a simple first-order finite difference. It is noted that the friction and permeability effects are normally negligible at the seaward boundary. Eq. 20 yields the value of h at $t=n\Delta t$ while the value of u at $t=n\Delta t$ is given by $u = (2h^{1/2}-\beta)$ at $x=0$. On the other hand, the values of h and u at $t=n\Delta t$ in the vicinity of the moving waterline are computed using the predictor-corrector-smoothing procedure which is explained in detail in Appendix B since numerical difficulties tend to occur at the moving waterline (*e.g.*, SYNOLAKIS, 1989).

Second, the values of u_p, q_b and u_b at $t=n\Delta t$ are computed using the computed values of h and u at $t=n\Delta t$. The value of u_p at $t=n\Delta t$ is computed using Eq. 16 in which $\partial\eta/\partial x$ is discretized using a central finite difference. The value of q_b at $t=n\Delta t$ is then computed using Eq. 13 which is approximated by a spatial central finite difference. The value of u_b at $t=n\Delta t$ is obtained from Eq. 15.

WAVE ENERGY BALANCE

The wave energy balance is examined for the flow on the rough permeable slope computed using the continuity and momentum equations given by Eqs. 9 and 10. The normalized equation of energy corresponding to Eqs. 9 and 10 may be expressed as

$$\frac{\partial E}{\partial t} + \frac{\partial}{\partial x}(E_F) = - D_f - D_p - D_B \qquad (22)$$

with

$$E = \frac{1}{2}(hu^2 + \eta^2) \qquad \text{for } h > \eta$$
$$E = \frac{1}{2}[hu^2 + \eta^2 - (h-\eta)^2] \quad \text{for } h < \eta \qquad (23)$$

$$E_F = uh\left(\frac{1}{2}u^2 + \eta\right); \; D_f = f|u|u^2 \qquad (24)$$

$$D_p = pq_b\left(\frac{1}{2}u_b^2 + \eta\right)$$

where E = normalized specific energy defined as the sum of kinetic and potential energy per unit horizontal area; E_F = normalized energy flux per unit width; D_f = normalized rate of energy dissipation per unit horizontal are due to bottom friction; D_p = normalized energy flux per unit horizontal area into the permeable underlayer; and D_B = normalized rate of energy dissipation per unit horizontal area due to wave breaking. It should be noted that the normalized potential energy included in the specific energy E given by Eq. 23 is taken to be relative to the normalized potential energy at $t=0$ when the incident wave train arrives at $x=0$ as shown in Figure 1. Eq. 22 may be used to estimate D_B invoking the analogy between the present analysis and that used for a hydraulic jump. The dimensional rate D'_B of energy dissipation due to wave breaking is given by $D'_B = (\rho g H'^2/T')D_B$ where ρ = fluid density, which is assumed to be constant.

Since the wave energy balance is normally

analyzed in terms of the time-averaged quantities, the time-averaged dissipation rate, $\overline{D_B}$, due to wave breaking is computed using the following time-averaged energy equation obtained from Eq. 22:

$$\overline{D_B} = -\frac{d}{dx}(\overline{E_F}) - \overline{D_f} - \overline{D_p} \qquad (25)$$

where the overbar indicates the time averaging. The present numerical model needs to predict that $\overline{D_B}$ is positive or zero depending on whether wave breaking occurs or not. The energy flux $\overline{E_F}$ should decrease with the increase of x, while $\overline{D_f} > 0$ since D_f defined in Eq. 24 is positive or zero. The time-averaged energy flux, $\overline{D_p}$, into the permeable underlayer should be positive and correspond to the energy dissipation inside the permeable underlayer.

The specific energy $\overline{E}$ and the energy flux $\overline{E_F}$ at the seaward boundary where $\eta = (\eta_i + \eta_r)$ at $x = 0$ from Eq. 20 may approximately be given by (KOBAYASHI and WURJANTO, 1989a)

$$\overline{E} \simeq \overline{\eta_i^2} + \overline{\eta_r^2} \qquad \text{at } x = 0 \qquad (26)$$

$$\overline{E_F} \simeq (d_t)^{1/2}\left(\overline{\eta_i^2} - \overline{\eta_r^2}\right) \qquad \text{at } x = 0 \qquad (27)$$

where $\overline{\eta_i^2}$ and $\overline{\eta_r^2}$ are the normalized wave energy per unit horizontal area associated with the incident and reflected waves, respectively, and $(d_t)^{1/2}$ is the normalized group velocity based on linear long wave theory at $x = 0$. The wave reflection coefficient r based on the incident and reflected wave energy may be defined as

$$r = \left[\frac{\overline{(\eta_r - \overline{\eta_r})^2}}{\left(\overline{\eta_i^2}\right)}\right]^{1/2} \qquad (28)$$

where $\overline{\eta_r}$ is the difference between the still water level and the mean water level at $x = 0$. The incident wave train $\eta_i(t)$ in the subsequent computations is specified such that $\overline{\eta_i} = 0$. The wave reflection coefficient may also be computed using Eq. 28 without the term $\overline{\eta_r}$ or the difference between the maximum and minimum values of the periodic reflected wave train $\eta_r(t)$ (KOBAYASHI and WURJANTO, 1989a). Eq. 28 appears to be more general than the other methods since it may be applied to random waves in shallow water where $\overline{\eta_r}$ may not be negligible. The method used to compute the reflection coefficient should be consistent with the method used to determine the reflection coefficient in experiments.

HYDRAULIC STABILITY OF ARMOR UNITS

The hydraulic stability of armor units is analyzed using the computed flow field over the rough permeable slope. The mass and momentum exchanges between the flow over the rough slope and the flow in the permeable underlayer affect the computed variations of u and h with respect to t and x over the rough permeable slope. In the following, the direct effects of these mass and momentum exchanges on the hydraulic stability of armor units are assumed to be negligible for the case where the permeability parameter p introduced in Eqs. 9 and 10 is much less than unity. It should be mentioned that the complicated flow inside the primary cover layer is not analyzed herein except that the friction factor f′ is used in Eq. 2 to account for its effects on the flow over the rough permeable slope.

For the case of $p << 1$, the drag, lift and inertia forces acting on individual armor units in the primary cover layer may be expressed in terms of the fluid velocity and acceleration on the rough permeable slope. Use may then be made of the results of the stability analysis of KOBAYASHI and OTTA (1987) for rough impermeable slopes except that the normalized fluid velocity u and the normalized fluid acceleration du/dt in the present analysis include the permeability effects of the underlayer. The normalized fluid acceleration obtained from Eqs. 9 and 10 is given by

$$\frac{du}{dt} = \frac{\partial u}{\partial t} + u\frac{\partial u}{\partial x} = -\frac{\partial h}{\partial x} - \theta - \frac{f|u|u}{h} + \frac{pq_b(u - u_b)}{h} \qquad (29)$$

KOBAYASHI and OTTA (1987) expressed the stability condition against the sliding or rolling of an armor unit for the case of $C_D > C_L \tan\phi$ in the following form:

$$N_s \leq N_R(t,x) = Au^{-2}\left\{\cos\theta' \tan\phi - \frac{u}{|u|}\left[\frac{C_M}{(s-1)\sigma}\frac{du}{dt} - \sin\theta'\right]\right\} \qquad (30)$$

with

Table 1. *Six test runs compared with numerical model.*

Run No.	cotθ	H′ (cm)	T′ (sec)	ξ	p	P_u	μ
1	6	10.09	2.63	1.72	0.0022	0.027	0.698
2	6	7.75	3.15	2.36	0.0028	0.027	0.816
3	4	8.16	3.22	3.52	0.0026	0.026	0.814
4	3	8.92	3.13	4.37	0.0025	0.026	0.785
5	2	7.98	2.69	5.95	0.0032	0.029	0.748
6	2	7.98	3.11	6.88	0.0030	0.027	0.805

$$N_s = H'(s - 1)^{-1} \left[\frac{W'}{\rho s}\right]^{-1/3} \tag{31}$$

$$A = 2C_3^{2/3} [C_2(C_D + C_L \tan\phi)]^{-1} \tag{32}$$

where N_s = stability number; N_R = dimensionless function expressing the degree of the armor unit stability as a function of t and x; and θ′ = local slope angle as shown in Figure 1. The characteristics of the armor unit are expressed by the following parameters: W′ = median mass; s = specific density; C_2 = area coefficient; C_3 = volume coefficient; and φ = frictional angle. The hydrodynamic forces acting on the armor unit are separated into the drag, lift and inertia forces whose coefficients are denoted by C_D, C_L and C_M, respectively. KOBAYASHI and OTTA (1987) imposed the upper and lower bounds of the fluid acceleration so that the inertia force alone would not cause the initiation of armor movement

$$a_{min}\,\sigma \leq du/dt \leq a_{max}\,\sigma \tag{33}$$

with

$$a_{min} \geq -\frac{s - 1}{C_M}\frac{\sin(\phi - \theta')}{\cos\phi}; \quad a_{max} \leq \frac{s - 1}{C_M}\frac{\sin(\phi + \theta')}{\cos\phi} \tag{34}$$

In the following, the temporal and spatial variations of the stability of armor units on the rough permeable slope are computed using Eq. 30 together with Eqs. 32–34 and compared with available data on the stability number N_s.

COMPARISON WITH AVAILABLE DATA

VAN DER MEER (1987, 1988a, 1988b) conducted extensive hydraulic model tests for the hydraulic stability of uniform slopes protected with rock. The numerical model is compared with the test results for the structure with an impermeable core in water depth d'_t = 80 cm with no wave overtopping since the model is based on the assumption of the impermeable boundary below the permeable underlayer as illustrated in Figure 1. Furthermore, the following comparison is limited to the test results with S = 2 and N = 1000 where S = dimensionless damage level based on the measured erosion area and N = number of individual waves attacking the tested structure. This is because the test results with S = 2 and N = 1000 approximately correspond to the initiation of armor movement predicted by the present numerical model. The numerical model will need to be improved to predict the slope profile change with time if it is to be compared with the test results with larger values of S and N.

Six runs are selected from the test results with S = 2 and N = 1000 listed in Appendix II of the thesis of VAN DER MEER (1988b). Table 1 summarizes the selected six test runs compared with the numerical model. Run 1, 2, 3, 4, 5 and 6 in this paper correspond to No. 181, 187, 146, 94, 41 and 45 in Appendix II, respectively. The six runs include the uniform slopes with cotθ′ = 2, 3, 4 and 6. The incident irregular waves for the six runs were generated using the Pierson-Moskowitz spectrum. The significant wave height, H'_s, and the average period of the zero upcrossings, T'_m, of the incident wave train were used by VAN DER MEER (1987, 1988a, 1988b) to characterize the incident irregular waves. As a result, the representative wave height and period used for the normalization of Eqs. 1 and 2 are taken as H′ = H'_s and T′ = T'_m herein. The surf similarity parameter, ξ = $T' \tan\theta'(2\pi H'/g)^{-1/2}$, for the six runs listed in Table 1 is in the range ξ = 1.72–6.88, corresponding to plunging, collapsing and surging waves on uniform slopes.

The primary cover layer for the six runs listed in Table 1 consisted of the riprap with the nominal diameter based on the median mass, $(W'/\rho s)^{1/3}$ = 3.6 cm, and the specific density, s = 2.63, and the grading, D_{85}/D_{15} = 2.25, based on the 85 and 15 percent diameters of the sieve analysis of the riprap. The thickness of the primary cover layer normal to the slope was 8 cm. The following input parameters required for the numerical model are taken to be the same as those used by KOBAYASHI and OTTA (1987) for the comparison with the large-scale riprap tests by AHRENS and MCCARTNEY (1975)

since VAN DER MEER (1989b) found his small-scale tests to be consistent with his large-scale tests: $f' = 0.3$, $\phi = 50°$, $C_2 = 0.90$, $C_3 = 0.66$, $C_D = 0.5$, $C_L = 0.4$, $C_M = 1.5$, $a_{max} = 1.0$ and $a_{min} = -0.8$ except for $a_{min} = -0.6$ for runs 5 and 6 to satisfy the condition for a_{min} given in Eq. 34. It should be mentioned that KOBAYASHI and OTTA (1987) varied the lift coefficient in the range $C_L = 0.18$–0.4 and used $C_L = 0.18$ for $\cot\theta' = 2.5$ and $C_L = 0.4$ for $\cot\theta' = 3.5$ and 5. The uncertainty of C_L will be discussed when the computed and measured stability numbers of the riprap are compared.

The permeable underlayer consisted of the gravel with its nominal diameter of 0.8 cm which is taken to be the representative diameter d'_p of the underlayer stone used in Eq. 5. The thickness of the permeable underlayer normal to the slope was 2 cm. Consequently, the characteristic thickness h'_c used in Eq. 11 to normalize the vertical thickness of the permeable underlayer, h'_p, as defined in Figure 1 is taken as $h'_c = 2\sec\theta'$ cm. The variation of h'_p with respect to x' is given by $h'_p = x'\tan\theta'$ for $0 \leq x' \leq h'_c\cot\theta'$ and $h'_p = h'_c$ for $x' \geq h'_c\cot\theta'$. The additional input parameters required to express the flow resistance coefficients defined in Eq. 5 are taken as follows: $n_p = 0.4$, $\alpha_o = 1140$, $\beta_o = 2.7$ and $\nu = 10^{-2}$ cm^2/s. Table 1 lists the dimensionless parameters p, p_u and μ defined in Eq. 12. The selected six runs satisfy the conditions of $p << 1$ and $p_u << 1$ assumed in the present numerical model. The parameter μ is on the order of unity for these small-scale test runs for which the viscous effects in the permeable underlayer are not negligible. This will cause only minor scale effects if the effects of the permeable underlayer on the flow over the primary cover layer are not significant.

The incident wave train, $\eta_i(t)$, normalized by the significant wave height H′ and the average period T′ needs to be specified for each of the six runs. As a first approximation, the irregular wave train generated in the tests of VAN DER MEER (1989b) is assumed to be represented by the regular wave train whose height and period are H′ and T′, respectively. The computed results based n this assumption are used to quantify the limitations of the regular wave approximation as well as to evaluate the accuracy and capability of the numerical model including the permeability effects. For the six runs, $d_t = 7.9$–10.3, $L = 8.5$–10.7 and $U_r = 7.6$–12.0 at the seaward boundary located at $x = 0$ where $d_t = d'_t/H'$ with $d'_t = 80$ cm; $L = L'/d'_t$ with L' being the wavelength based on linear wave theory; and U_r = Ursell parameter defined as $U_r = L^2/d_t$. It should be noted that the selected six runs correspond to relatively large values of L since d'_t = 80 cm used by VAN DER MEER (1989b) appears to be too deep for breakwaters, which are generally located in relatively shallow water during storms. The normalized incident wave profile $\eta_i(t)$ with unit wave height and period for $t \geq 0$ may be specified using Stokes second-order wave theory (KOBAYASHI and WURJANTO, 1989b). For the six runs, $a_1 = 0.5$ and $a_2 = 0.050$–0.072 where a_1 and a_2 are the normalized amplitudes of the first and second-order harmonics. The nonlinear effects are relatively small at $x = 0$ for these runs with $d_t = 7.9$–10.3.

In the following, the computed results based on the monochromatic wave approximation are denoted by run M1 to M6 for the six runs listed in Table 1. The computed results based on the random wave train generated numerically will be denoted by run R1 to R6 in the accompanying paper (KOBAYASHI *et al.*, 1990). The computation for run M1 to M6 is made for the duration $0 \leq t \leq 256$ used for run R1 to R6, although the computed flow field and armor response for run M1 to M6 become periodic before $t = 4$. This is because the accuracy of the numerical model including the permeability effects is not completely certain for the long computation time, while the errors of the computed results for incident random waves are harder to detect.

First, the computed results for run M3 are presented in detail as a typical run. Figure 2 shows the computed reflected wave train $\eta_r(t)$ at $x = 0$ during $0 \leq t \leq 256$. The computed temporal variation of η_r becomes periodic very quickly and remains periodic without spurious long-period oscillations, which would have occurred if the seaward boundary of the numerical model had become partially reflecting. The computed periodic oscillations of $\eta_i(t)$ and $\eta_r(t)$ are used to compute the wave reflection coefficient r defined by Eq. 28. The computed reflection coefficient is $r = 0.35$. Eq. 28 with $\overline{\eta_r} = 0$ yields essentially the same value of r since the time-average value, $\overline{\eta_r}$, is computed to be essentially zero for the six runs with large values of d_t. Furthermore, the wave reflection coefficient defined as the normalized height of the periodic reflected wave

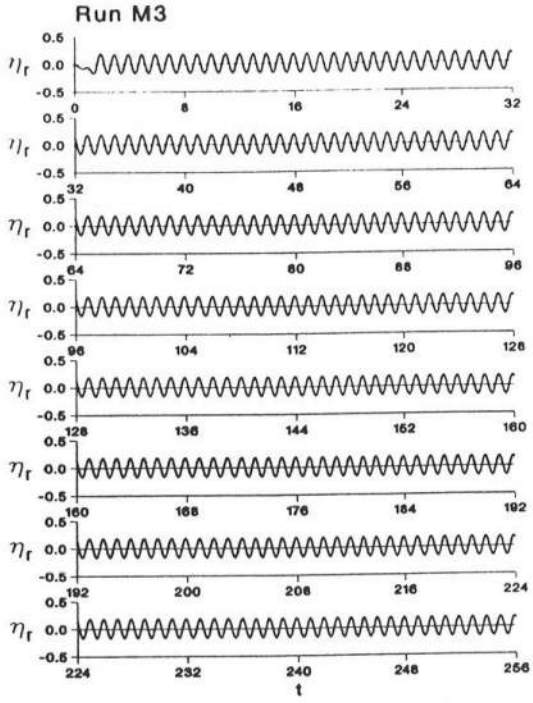

Figure 2. Computed reflected wave train at x = 0 during $0 \leq t \leq 256$ for run M3.

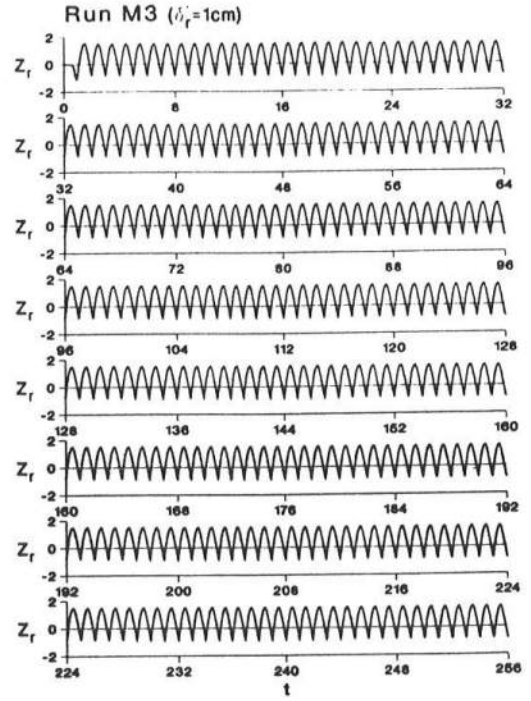

Figure 3. Computed oscillation of 1-cm water depth on rough permeable slope during $0 \leq t \leq 256$ for run M3.

train is found to be essentially the same as that based on Eq. 28 for the six runs. This is related to the approximately sinusoidal variation of the computed reflected wave train as shown in Figure 2.

Figure 3 shows the computed temporal oscillation of the waterline elevation above SWL normalized by the wave height H′ for run M3. The normalized waterline elevation Z_r is defined as the location where the instantaneous water depth $h = \delta_r$ with $\delta_r = \delta'_r/H'$. The temporal oscillation of Z_r shown in Figure 3 corresponds to $\delta'_r = 1$ cm. The oscillations of Z_r with $\delta'_r = 0.1$, 0.5 and 1.0 cm are computed to examine the sensitivity of Z_r to the dimensional water depth δ'_r. It should be stated that it is extremely difficult to pinpoint the waterline location on the rough permeable slope in experiments while the present numerical model accounts for the presence of the primary cover layer through the friction factor f′ only. Consequently, the measured and computed waterline elevations are difficult to compare if they are sensitive to the water depth δ'_r. Figure 3 shows that the computed waterline oscillation becomes periodic very quickly and remains periodic without spurious long-period oscillations. This requirement has been used to check appropriateness of the numerical procedure of the waterline computation given in Appendix B. The maximum and minimum values of the periodic oscillation of Z_r are taken as the normalized run-up R and run-down R_d, respectively. For run M3, R = 1.56, 1.51 and 1.50 for $\delta'_r = 0.1$, 0.5 and 1.0 cm, indicating that R is not sensitive to δ'_r. On the contrary, R_d is very sensitive to δ'_r since $R_d = 0.50$, -0.39 and -0.84 for $\delta'_r = 0.1$, 0.5 and 1.0 cm. This is because a thin layer of water remains on the slope during wave downrush as shown in Figure 4.

Figure 4 shows the computed spatial variations of the normalized free surface elevation η and the normalized horizontal velocity u over the rough slope at t = 255, 255.25, 255.5, 255.75 and 256 for run M3 with $\xi = 3.52$. The computed spatial variations at t = 255 and 256 are the same because of the periodicity. The shaded

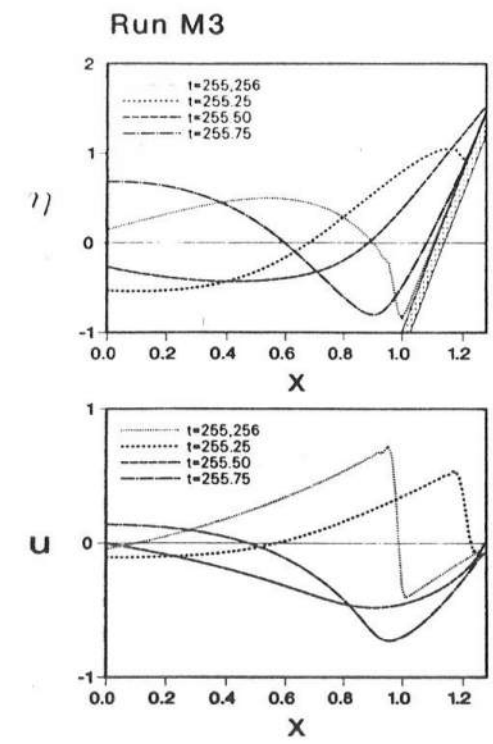

Figure 4. Computed spatial variations of η and u at t = 255, 255.25, 255.5, 255.75 and 256 for run M3.

area shown in the figure for η corresponds to the permeable underlayer.

Figure 5 shows the computed spatial variations of the normalized horizontal discharge velocity u_p in the permeable underlayer and the normalized volume influx q_b per unit horizontal area into the permeable underlayer at t = 255, 255.25, 255.5, 255.75 and 256 for run M3. The spatial variation of u_p at given time computed using Eq. 16 with $\mu = 0.814$ for run M3 is determined by the slope of the free surface, $\partial\eta/\partial x$, at the same time. The positive or negative slope of the free surface causes the negative or positive flow in the permeable underlayer, respectively, where the x-coordinate and the flow direction are positive landward. The spatial variations of u_p at t = 255 and 255.25 shown in Figure 5 indicate the convergence of the landward and seaward flows in the permeable underlayer at the wave front shown in Figure 4 where η decreases rapidly and then increases in the landward direction. It should be noted that the numerical high-frequency oscillations on the seaward side of the wave front which may not be discernible in Figure 4 become more apparent in Figure 5 on the seaward side of the converging flow in the permeable underlayer.

The spatial variations of q_b shown in Figure 5 are computed using $q_b = \partial(h_p u_p)/\partial x$ from Eq. 13 where $h_p = 34.9x$ for $0 \leq x \leq 0.0286$ and $h_p = 1$ for $x \geq 0.0286$ for run M3. Since $q_b = \partial u_p/\partial x$ for $x \geq 0.0286$ in Figure 5, the large negative value of q_b occurs where u_p decreases rapidly in the positive x-direction. Since q_b is taken to be positive into the permeable underlayer, the noticeable outflux from the permeable underlayer occurs where the landward and seaward flows in the permeable underlayer converge under the wave front of the free surface variation. It should be noted that the permeability effects in Eqs. 9 and 10 for the flow on the rough permeable slope appear in the terms pq_b and pu_bq_b where the value of u_b computed using Eq. 15 is on the order of unity or less. As a result, the absolute value of q_b may become large under the wave front but the absolute value of pq_b is less than unity where $p = 0.0026$, $\theta = 8.82$ and $f = 5.30$ in Eqs. 9 and 10 for run M3. The simplified stability analysis of armor units in this paper does not account for the direct effect of outflux from the permeable underlayer which may increase the lift force acting on an armor unit under the wave front. However, the simplified analysis may be sufficient in view of the uncertainty of the lift coefficient C_L where KOBAYASHI and OTTA (1987) varied C_L in the range $C_L = 0.18$–0.4. Considering the possibility of the increase of the lift force due to the outflux from the permeable underlayer, use is made of the upper-bound value of $C_L = 0.4$ in this simplified computation of the stability of armor units.

Figure 6 shows the computed spatial variations of the normalized time-averaged quantities $\overline{E}$, $\overline{E_F}$, $\overline{D_f}$, $\overline{D_p}$ and $\overline{D_B}$ for runs M3 and M1 where $\overline{E}$ is the wave energy per unit horizontal area and $\overline{E_F}$ is the energy flux per unit width, while $\overline{D_f}$, $\overline{D_p}$ and $\overline{D_B}$ are the rates of energy dissipation per unit horizontal area due to bottom friction, permeability and wave breaking, respectively. $\overline{E}$, $\overline{E_F}$, $\overline{D_f}$ and $\overline{D_p}$ are computed using Eqs. 23 and 24, whereas $\overline{D_B}$ is computed from the time-averaged energy equation given by Eq. 25. The wave energy flux $\overline{E_F}$ decreases slowly and then rapidly near the still water level on the slope where Figure 4 shows the

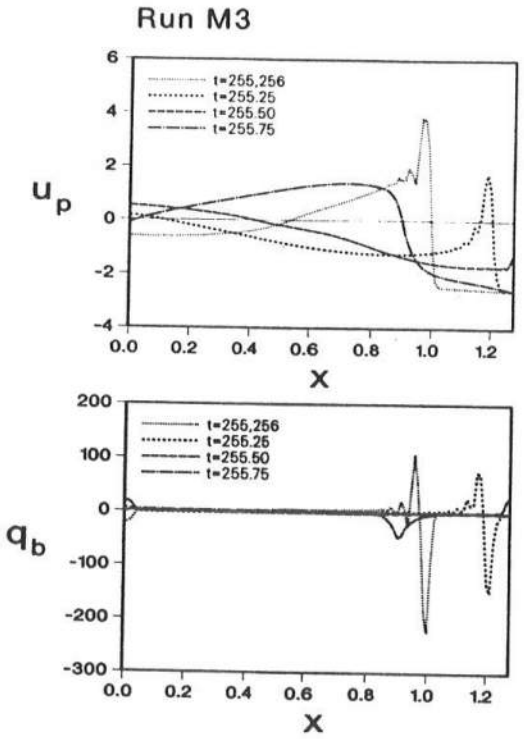

Figure 5. Computed spatial variations of u_p and q_b at t = 255, 255.25, 255.5, 255.75 and 256 for run M3.

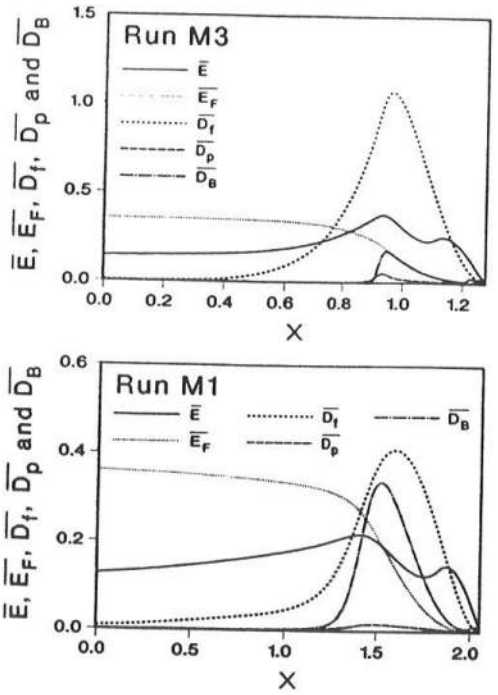

Figure 6. Computed spatial variations of specific energy $\overline{E}$, energy flux $\overline{E_F}$, dissipation rate, $\overline{D_f}$, $\overline{D_p}$ and $\overline{D_B}$ due to bottom friction, permeability and wave breaking, respectively, for runs M3 and M1.

location of the slope for run M3. Correspondingly, large energy dissipation occurs near the still water level on the slope. The energy dissipation due to bottom friction is dominant for run M3 with $\xi = 3.52$, corresponding to collapsing or surging waves (AHRENS and MCCARTNEY, 1975). The energy dissipation due to wave breaking becomes as large as that due to bottom friction for run M1 with $\xi = 1.72$, corresponding to plunging waves. The computed large energy dissipation due to bottom friction is consistent with the analytical and experimental results obtained by MADSEN and WHITE (1976) for surging waves on rough impermeable slopes. The computed energy dissipation due to wave breaking decreases with the increase of ξ for the six runs and is negligible for runs M4, M5 and M6 with $\xi \geq 4.37$. The computed wave energy transmitted and dissipated in the permeable underlayer is small for the six runs with $p = 0.0022$–0.0032 as shown in Table 1. This implies that the thin permeable underlayer is not effective in dissipating wave energy.

Figure 7 shows the computed temporal variations of the armor stability function N_R defined in Eq. 30 during the one wave period $255 \leq t \leq 256$ at $z = -2.06$, -1.28 and -0.10 for run M3. The normalized vertical coordinate, $z = z'/H'$, is used to indicate the location of an armor unit on the slope relative to SWL located at $z = 0$. The stability function N_R becomes small during the wave uprush and downrush as may be seen by comparing the armor stability function shown in Figure 7 with the corresponding flow field shown in Figure 4. The trough of the temporal variation of N_R during the wave downrush is wider and lower than that during the wave uprush. KOBAYASHI and OTTA (1987) defined the critical stability number N_{sc} for initiation of armor movement as the minimum value of N_R with respect to z and t after the periodicity of N_R with respect to t is established. The critical stability number N_{sc} occurs at $z = -1.28$ and at $t = 255.69$ during $255 \leq t \leq 256$ for run M3.

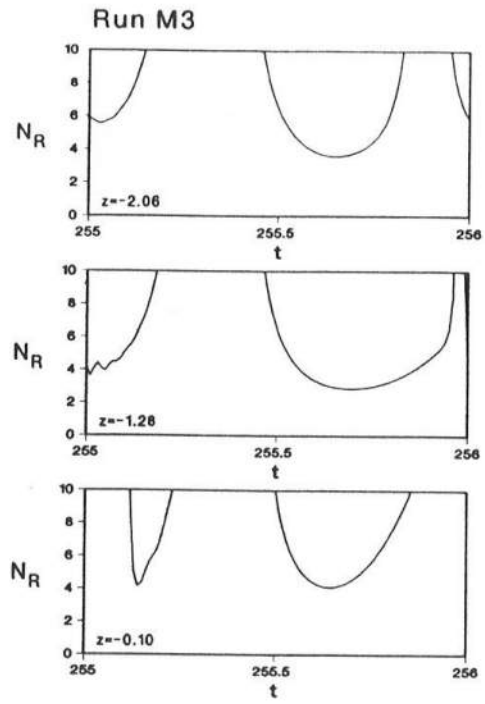

Figure 7. Computed temporal variations of armor stability function N_R during $255 \leq t \leq 256$ at $z = -2.06$, -1.28 and -0.10 for run M3.

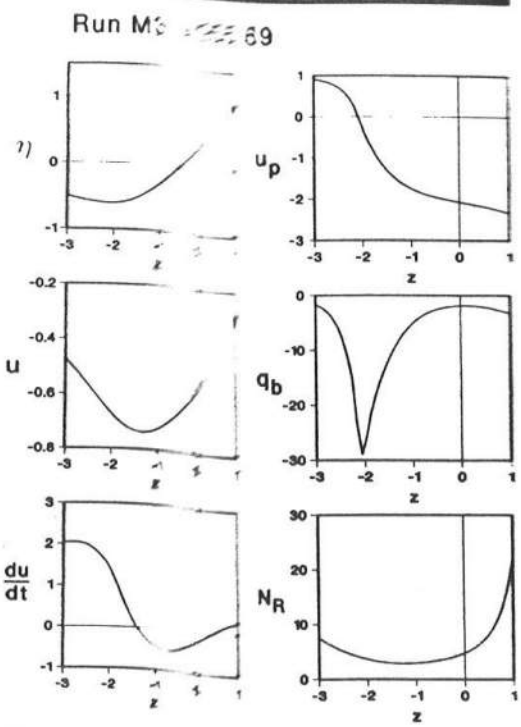

Figure 8. Computed variations of η, u, du/dt, u_p, q_b and N_R with respect to elevation z on slope at t = 255.69 for run M3.

Figure 8 shows the computed variations of η, u, du/dt, u_p, q_b and N_R with respect to the normalized elevation z on the slope at t = 255.69 for run M3 with $\xi = 3.52$. The minimum value of N_R occurring at $z = -1.28$ in Figure 8 corresponds to the critical stability number N_{sc}. The variations of the fluid velocity u, the fluid acceleration du/dt and the armor stability function N_R for run M3 are similar to those plotted by KOBAYASHI and OTTA (1987) for the case of $\xi = 4.0$. The variations of the free surface elevation η shown in Figure 8 and in Figure 4 indicate that the minimum armor stability for run M3 occurs during the wave downrush in the vicinity of the trough of the free surface where the downward velocity is the maximum but the fluid acceleration is relatively small. At the time of the minimum armor stability for run M3, the normalized discharge velocity in the permeable underlayer, u_p, defined in Eq. 11 is mainly downward and the normalized volume flux per unit horizontal area, q_b, defined in Eq. 7 is out of the permeable underlayer. Since $p_u = 0.026$ and $p = 0.026$ for run M3, the magnitudes of the dimensional quantities u'_p and q'_b are much less than the magnitude of the dimensional velocity u'.

The computed results presented in Figures 2–8 indicate that the numerical model yields fairly detailed hydrodynamics and armor response. At present, no data on the detailed hydrodynamics and resulting armor response is available to examine the accuracy of the computed results. In order to examine the permeability effects separately, it would be required to make computation for run M1 to M6 with $p = 0$ and compare the computed results with and without the thin permeable underlayer. KOBAYASHI and WURJANTO (1989b) performed such a comparison for a hypothetical permeable underlayer whose thickness h'_e was roughly the same as the wave height H' and the permeability parameter p was in the range $p = 0.012$–0.026. The comparison indicated that the permeability effects would increase the hydraulic stability of armor units noticeably and decrease wave run-up and reflection

slightly. For the six runs listed in Table 1, $h'_c/H' = 0.20–0.26$ and $p = 0.0022–0.0032$. As a result, the permeability effects for these runs should be smaller than those for the hypothetical cases examined by KOBAYASHI and WURJANTO (1989b). The computed results for run M1 to M6 together with the above considerations suggest that the thin permeable underlayer included in the present computation may have little influence on the overall flow characteristics on the rough permeable slope but may affect the details of the flow characteristics and resulting armor response at the wave front where the outflux from the permeable underlayer may be noticeable.

In the following, the computed wave run-up, run-down and reflection for the six runs are compared with available empirical formulas for regular waves since the data of VAN DER MEER (1988b) is limited to the armor stability. The following comparison is not rigorous and only qualitative since the empirical formulas were developed from different riprap tests.

Figure 9 shows the comparison of the computed normalized wave run-up R for the six runs with the empirical formula, $R = 1.13\,\xi/(1+0.506\xi)$, proposed by AHRENS and MCCARTNEY (1975) on the basis of their large-scale riprap tests. The computed values of R corresponding to the water depth $\delta'_r = 0.1$ and 1 cm are presented in Figure 9 for each run where the value of the surf similarity parameter ξ for each run is listed in Table 1. The computed values of R are not sensitive to δ'_r in the range $0.1 \leq \delta'_r \leq 1$ cm as also discussed in relation to Figure 3. The computed points shown in Figure 9 are within the scatter of data points about the empirical curve presented by AHRENS and MCCARTNEY (1975). The agreement between the computed run-up for the small-scale riprap tests of VAN DER MEER (1988b) and the empirical formula based on the large-scale riprap tests suggests that scale effects on wave runup are small. This is consistent with the findings of VAN DER MEER (1988b) based on the comparison between his large-scale and small-scale tests. This does not imply that viscous effects are negligible in the permeable underlayer. The parameter μ expressing the order of magnitude of the laminar flow resistance as compared to the turbulent flow resistance in Eq. 4 is in the range $\mu = 0.698–0.816$ for the six runs listed in Table 1, whereas the value of μ could be on the order of 0.01 for the large-scale riprap tests (KOBAYASHI and WURJANTO, 1989b). As a result, the permeable underlayer should have little influence on wave run-up on the rough permeable slope as long as the permeable underlayer is thin and located on an impermeable boundary or core.

Figure 10 shows the comparison of the computed normalized wave run-down R_d for the six runs with the empirical formula, $R_d = -6.22[1-\exp(-0.0398\xi)]$, proposed by LOSADA and GIMÉNEZ-CURTO (1981) for the

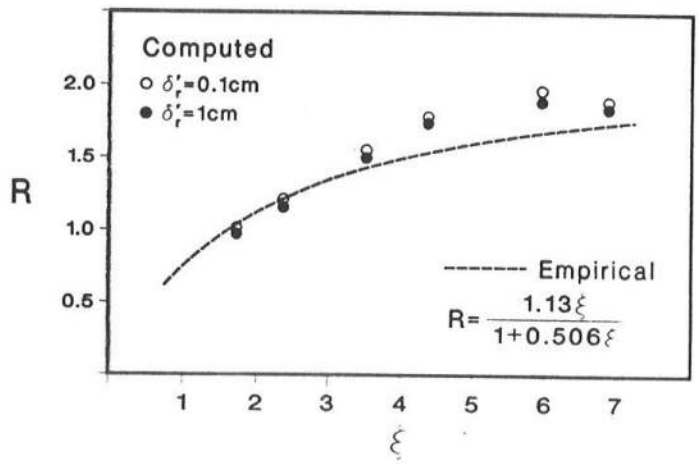

Figure 9. Comparison of computed normalized wave run-up R for six runs with empirical formula.

riprap test data of GUNBAK (1976). The computed values of R_d are sensitive to the water depth δ'_r used to define the location of wave run-down since a thin layer of water remains on the slope during wave downrush as shown in Figure 4. Consequently, visually-observed wave run-down is fairly subjective. Figure 10 is hence intended to show that the numerical model predicts the trend of the decrease of R_d with ξ, although the computed values of R_d with δ'_r = 1 cm are in reasonable agreement with the empirical formula.

Figure 11 shows the comparison of the computed wave reflection coefficient r for the six runs with the empirical formula, $r = 1.35[1-\exp(-0.071\xi)]$, proposed by LOSADA and GIMÉNEZ-CURTO (1981) for the riprap test data of GUNBAK (1976). The agreement shown in Figure 11 may be reasonable considering the difficulties and errors associated with the determination of r from measured free surface oscillations (MADSEN and WHITE, 1976).

Finally, Figure 12 shows the comparison of the computed critical stability number N_{sc} and the actual stability number N_s for each of the six runs. The computed value of N_{sc} for each run is the minimum value of the armor stability function N_R along the slope during one wave period under the periodic action of N = 256 waves of the regular wave train with given wave height H′ and period T′. On the other hand, the stability number N_s given by Eq. 31 for each run corresponds to the damage level S = 2 of the specified primary cover layer under the action of N = 1000 waves of the irregular wave train with given significant wave height H′ and average wave period T′. VAN DER MEER (1988b) indicated that the damage level S = 2 or 3 should correspond to the start of the damage. The value of N_s is not very sensitive to S = 2 or 3 as well as N = 256 or 1000 since $N_s \propto S^{0.2}N^{-0.1}$ based on the empirical formula of VAN DER MEER (1987, 1988a, 1988b). As a result, the critical stability number N_{sc} for the initiation of armor movement should approximately correspond to the stability number N_s with S = 2 and N = 1000. The difference between the values of N_{sc} and N_s plotted in Figure 12 for each run is mostly caused by the regular wave approximation used for the present computation. Since $N_s < N_{sc}$, the stability condition given by Eq. 30 against the sliding or rolling of any armor unit along the slope is well satisfied at any time under the assumed regular wave action.

In order to confirm the above conclusion in a qualitative manner, Figure 12 also shows the empirical curves for $\cot\theta' = 2.5, 3.5$ and 5.0 proposed by LOSADA and GIMÉNEZ-CURTO (1979) for the large-scale riprap tests using regular waves performed by AHRENS and MCCARTNEY (1975). The values of N_s based on the regular wave tests are greater than those based on the random wave tests, although the riprap slopes used in these tests are different. The comparison of the computed values of N_{sc}

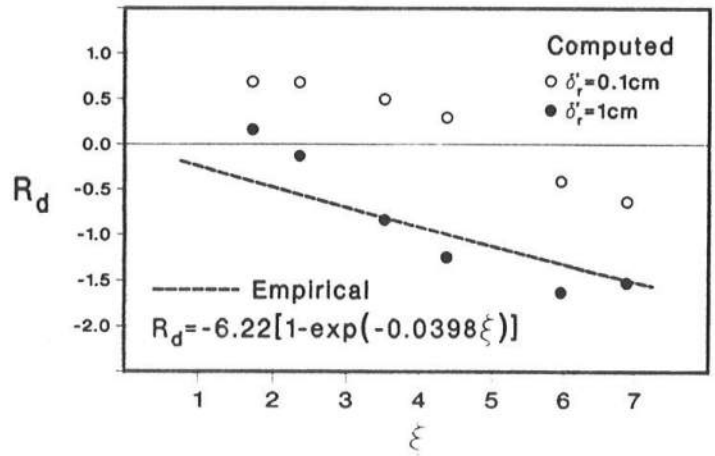

Figure 10. Comparison of computed normalized wave run-down R_d for six runs with empirical formula.

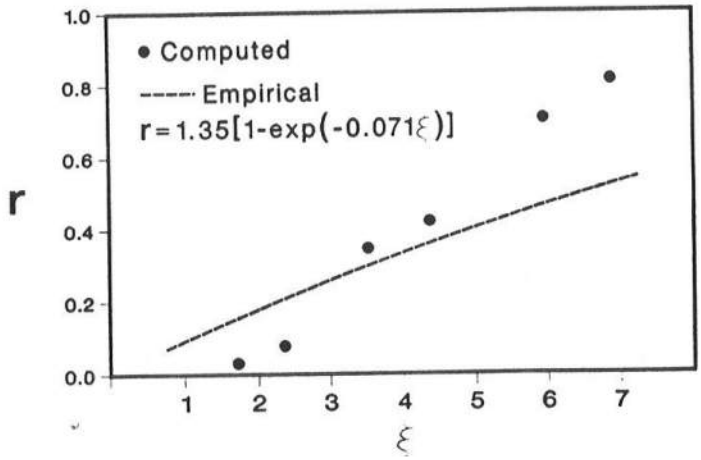

Figure 11. Comparison of computed wave reflection coefficient r for six runs with empirical formula.

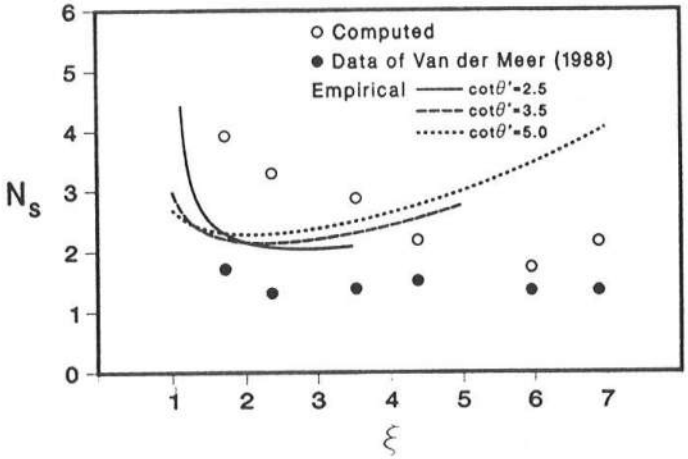

Figure 12. Comparison of computed critical stability number for six runs based on regular wave approximation with random wave data of VAN DER MEER (1988b) and empirical formula based on regular wave data.

and the empirical curves suggests that the armor stability is also sensitive to the specific riprap slope characteristics since the armor stability depends on the detailed hydrodynamics on the slope as discussed in relation to Figures 7 and 8. It is noted that KOBAYASHI and OTTA (1987) obtained good agreement between the numerical model for the rough impermeable slope and the large-scale riprap tests of AHRENS and MCCARTNEY (1975) using C_L = 0.4 for $\cot\theta'$ = 3.5 and 5.0 and C_L = 0.18 for $\cot\theta'$ = 2.5, where C_L changes only the parameter A defined by Eq. 32. Use of C_L = 0.18 for runs M5 and M6 with $\cot\theta'$ = 2.0 would result in N_{sc} = 2.38 and 2.96 for ξ = 5.95 and 6.88 in Figure 12, respectively. Consequently, the change of C_L alone would not explain the difference between the computed values of N_{sc} and the empirical curves in Figure 12. It may hence be concluded that the numerical model needs to simulate the specific riprap slope characteristics as well as the incident random waves for predicting the armor stability in a realistic manner.

CONCLUSIONS

The numerical model developed for the rough permeable slope is shown to yield the fairly detailed flow field and resulting armor response which would be very difficult to measure in experiments. The comparison of the developed numerical model with the random wave data on riprap stability tabulated by VAN DER MEER (1988b) indicates that the conventional regular wave approximation will result in the appreciable overestimation of the riprap stability. The computed regular wave run-up, run-down and reflection coefficients are also shown to be in qualitative agreement with available empirical formulas based on regular wave tests.

In order to make a more realistic comparison of the numerical model with the random wave data, the computation using the incident irregular wave train generated numerically is performed and presented in the accompanying paper of KOBAYASHI *et al.* (1990). Additional improvements of the numerical model will require the modelling of the flow in a permeable core (*e.g.*, SULISZ, 1985) as well as the prediction of the slope profile change with time which are normally measured in experiments. In addition, it is desirable to extend the numerical model to account for the variations of the incident waves and structure geometry along the alignment of a breakwater, although computational efforts will increase considerably.

ACKNOWLEDGMENT

This work is a result of research sponsored by the National Science Foundation, under grant CTS-8900640. The writers would like to thank J. W. VAN DER MEER for providing his thesis.

APPENDIX A. FINITE DIFFERENCE METHOD

Eqs. 9 and 10 are combined and expressed in the following vector form:

$$\frac{\partial \mathbf{U}}{\partial t} + \frac{\partial \mathbf{F}}{\partial x} + \mathbf{G} = 0 \qquad \text{(A.1)}$$

with

$$\mathbf{U} = \begin{bmatrix} m \\ h \end{bmatrix}; \mathbf{F} = \begin{bmatrix} mu + 0.5h^2 \\ m \end{bmatrix} \qquad \text{(A.2)}$$

$$\mathbf{G} = \begin{bmatrix} \theta h + f|u|u + pu_b q_b \\ pq_b \end{bmatrix}$$

where $m = uh$ is the normalized volume flux per unit width. The vectors $\mathbf{F}$ and $\mathbf{G}$ depend on the vector $\mathbf{U}$. The vector $\mathbf{G}$ includes the permeability effects through q_b and u_b.

Eq. (A.1) is discretized using a finite difference grid of constant space size Δx and constant time step Δt based on an explicit dissipative Lax-Wendroff method (e.g., RICHTMEYER and MORTON, 1967). In the following, the known quantities at the node located at $x = (j-1)\Delta x$ $(j = 1,2,\ldots,s)$ and at the time $t = (n-1)\Delta t$ are indicated by the subscript j without a superscript where the integer s indicates the wet node next to the moving waterline at $t = (n-1)\Delta t$. The unknown quantities at the node j and at the time $t = n\Delta t$ are denoted by the subscript j with the superscript * where the asterisk indicates the quantities at the next time level. The values of $\mathbf{U}_1^*$ and $\mathbf{U}_j^*$ for $j \geq (s-1)$ are computed using the seaward and landward boundary conditions, respectively. The values of $\mathbf{U}_j^*$ for $j = 2,3,\ldots,(s-2)$ are computed using the known values of $\mathbf{U}_{j-1}$, $\mathbf{U}_j$ and $\mathbf{U}_{j+1}$ at the time $t = (n-1)\Delta t$

$$\mathbf{U}_j^* = \mathbf{U}_j - \lambda\left[\frac{1}{2}(\mathbf{F}_{j+1} - \mathbf{F}_{j-1}) + \Delta x \mathbf{G}_j\right] + \frac{\lambda^2}{2}(\mathbf{g}_j - \mathbf{g}_{j-1} - \Delta x \mathbf{S}_j) + \mathbf{D}_j - \frac{p}{2}(\Delta t)^2 \mathbf{P}_j \qquad \text{(A.3)}$$

where $\lambda = \Delta t/\Delta x$. The lengthy expressions of $\mathbf{g}_j$, $\mathbf{S}_j$ and $\mathbf{D}_j$ are the same as those given in the paper of KOBAYASHI *et al.* (1987) where the subscript indicating the time level is omitted in this paper for brevity. The vector $\mathbf{g}_j$ contains the permeability effects through the vector $\mathbf{G}_j$, whereas the vectors $\mathbf{S}_j$ and $\mathbf{D}_j$ are independent of the permeability effects. The damping coefficients in the expression $\mathbf{D}_j$ are taken to be unity for the present computation.

The last term in Eq. (A.3) vanishes for the impermeable slope with $p = 0$. The vector $\mathbf{P}$ is defined as

$$\mathbf{P} = \begin{bmatrix} 2fh^{-1}|u|(u - u_b)\, q_b - \theta q_b + \partial(u_b q_b)/\partial t \\ \partial q_b/\partial t \end{bmatrix} \qquad \text{(A.4)}$$

$\mathbf{P}_j$ in Eq. (A.3) is the value of $\mathbf{P}$ at the node j and at the time $t = (n-1)\Delta t$. The computation of $\mathbf{P}_j$ requires the values of $\partial(u_b q_b)/\partial t$ and $\partial q_b/\partial t$ at the node j and at the time $t = (n-1)\Delta t$. In order to avoid iterations, these values are computed using backward-difference schemes based on

the values of u_b and q_b at the time $t=(n-2)\Delta t$ and $t=(n-1)\Delta t$.

The numerical stability criterion for Eq. (A.3) for the case of $p=0$ given by KOBAYASHI *et al.* (1987) is used as a first guideline to estimate the upper limit of $\Delta t/\Delta x$ for numerically stable computation. This criterion requires that the wet node next to the waterline at $t=n\Delta t$ should be located at $j=(s-1)$, s or $(s+1)$. The waterline computation explained in Appendix B is often found to require a smaller value of $\Delta t/\Delta x$ for the numerically stable computation of the waterline movement. For the computed results presented in this paper, the value of Δx is taken to be of the order of 0.01 on the basis of the desirable spatial resolution of 100 grid spacings between the toe and initial waterline on the slope. The value of Δt required for the numerical stability is found to be of the order of 0.0003.

APPENDIX B. PROCEDURE FOR WATERLINE COMPUTATION

The numerical procedure dealing with the moving waterline on the rough permeable slope is given in detail since the moving waterline tends to cause numerical instability. The procedure is somewhat intuitive and could be improved in the future, In the following, the computational waterline is located at $h=\delta$. The subscript j indicates the nodal location, while the superscript * denotes the unknown quantities at the next time level, $t=n\Delta t$.

(1) Compute $h_{s+1}=(2h_s-h_{s-1})$, $u_{s+1}=(2u_s-u_{s-1})$, and $m_{s+1}=h_{s+1}u_{s+1}$ where the integer s indicates the wet node next to the moving waterline at $t=(n-1)\Delta t$.

(2) Compute h_j^* and m_j^* at $t=n\Delta t$ for $j=(s-1)$ and s, using Eq. (A.3) without the damping term D_j since the water depth h can be very small at these nodes.

(3) If $h^*_{s-1}\leq\delta$, the computation is stopped since the waterline should not move more than Δx because of the numerical stability of the adopted explicit method.

(4) If $h_s^*>h^*_{s-1}$, use $h_s^*=(2h^*_{s-1}-h^*_{s-2})$, $u_s^*=(2u^*_{s-1}-u^*_{s-2})$, and $m_s^*=h_s^*u_s^*$ so that the water depth near the waterline decreases landward.

(5) If $h_s^*\leq\delta$, set $s^*=(s-1)$ and return where the interger s^* indicates the wet node next to the waterline at $t=n\Delta t$.

(6) If $h_s^*>\delta$, compute $h^*_{s+1}=(2h_s^*-h^*_{s-1})$, $u^*_{s+1}=(2u_s^*-u^*_{s-1})$, and $m^*_{s+1}=h^*_{s+1}u^*_{s+1}$.

(7) If $h^*_{s+1}\leq\delta$, set $s^*=s$ and return.

(8) If $h^*_{s+1}>\delta$, compute U_s^{**} at the time $t=(n+1)\Delta t$ using Eq. (A.3) without the damping term where U_j^* and U_j in Eq. (A.3) are replaced by U_s^{**} and U_s^*, respectively. Improve the linearly extrapolated values in step 6 using the following finite difference equations based on Eqs. 9 and 10 with $f=0$:

$$m^*_{s+1}=m^*_{s-1}-\frac{\Delta x}{\Delta t}(h_s^{**}-h_s)-2p\Delta x(q_b)^*_s \quad (B.1)$$

$$u^*_{s+1}=u^*_{s-1}-(u^*_s)^{-1}\left[\frac{\Delta x}{\Delta t}(u^{**}_s-u_s)+h^*_{s+1}-h^*_{s-1}+2\Delta x\theta_s\right] \quad (B.2)$$

$$+2p\Delta x(q_b)^*_s(m^*_s)^{-1}[u^*_s-(u_b)^*_s]$$

$$h^*_{s+1}=m^*_{s+1}/u^*_{s+1} \quad (B.3)$$

where $(q_b)^*_s$ and $(u_b)^*_s$ are computed using Eqs. 13, 15 and 16. The upper limit of the absolute values of $(u^*_s)^{-1}$ and $(m^*_s)^{-1}$ in Eq. (B.2) is taken as δ^{-1} to avoid the divisions by the very small values.

(9) If $|u^*_{s+1}|\leq\delta$, set $s^*=s$ and return.

(10) If $h^*_{s+1}\leq h^*_s$ and $h^*_{s+1}\leq\delta$, set $s^*=s$ and return.

(11) If $h^*_{s+1}\leq h^*_s$ and $h^*_{s+1}>\delta$, set $s^*=(s+1)$ and return.

(12) If $h^*_{s+1}>h^*_s$, the linearly extrapolated values in step 6 are adopted instead of those computed in step 8. Furthermore, set $s^*=s$ if $h^*_{s+1}>h^*_s$ and $s^*=(s+1)$ if $h^*_{s+1}\leq h^*_s$ where h^*_{s+1} is the adopted value given by $h^*_{s+1}=(2h^*_s-h^*_{s-1})$.

LITERATURE CITED

AHRENS, J.P. and MCCARTNEY, B.L., 1975. Wave period effect on the stability of riprap. *Proceedings Civil Engineering in Oceans/III, ASCE*, 2, 1019–1034.

GUNBAK, A.R., 1976. The stability of rubble mound breakwaters in relation to wave breaking and rundown characteristics and to $\xi\cdot\tan\alpha\cdot T/\sqrt{H}$ number. Div. Port and Ocean Eng., Norwegian Inst. of Tech., Trondheim, Norway, *Rept. 1-1976*.

JONSSON, I.G., 1980. A new approach to oscillatory rough turbulent boundary layers. *Ocean Engineering*, 7(1), 109–152.

KOBAYASHI, N., 1986. Closure to Riprap stability

under wave action. *Journal Waterway Port Coastal and Ocean Engineering, ASCE,* 112(6), 673–681.

KOBAYASHI, N. and OTTA, A.K., 1987. Hydraulic stability analysis of armor units. *Journal Waterway Port Coastal and Ocean Engineering, ASCE,* 113(2), 171–186.

KOBAYASHI, N.; OTTA, A.K., and ROY, I., 1987. Wave reflection and run-up on rough slopes. *Journal Waterway Port Coastal and Ocean Engineering, ASCE,* 113(3), 282–298.

KOBAYASHI, N. and WURJANTO, A., 1989a. Wave transmission over submerged breakwaters. *Journal Waterway Port Coastal and Ocean Engineering, ASCE,* 115(5), 662–680.

KOBAYASHI, N. and WURJANTO, A., 1989b. Armor stability on rough permeable slopes of marine structures. *Proceedings 23rd IAHR Congress,* Ottawa, Canada, (in press).

KOBAYASHI, N.; WURJANTO, A., and COX, D.T., 1990. Irregular waves on rough permeable slopes. Special Issue on Rational Design of Mound Structures, *Journal Coastal Research,* SI6.

LOSADA, M.A. and GIMÉNEZ-CURTO, L.A., 1979. The joint effect of the wave height and period on the stability of rubble mound breakwaters using Iribarren's number. *Coastal Engineering,* 3, 77–96.

LOSADA, M.A. and GIMÉNEZ-CURTO, L.A., 1981. Flow characteristics on rough, permeable slopes under wave action. *Coastal Engineering,* 4, 187–206.

MADSEN, O.S. and WHITE, S.M., 1975. Reflection and transmission characteristics of porous rubble-mound breakwaters. Department of Civil Engineering, Massachusetts Institute of Technology, Cambridge, MA, *Technical Report No. 207.*

MADSEN, O.S. and WHITE, S.M., 1976. Energy Dissipation on a Rough Slope. Journal Waterways Harbors and Coastal Engineering Division, ASCE, 102 (WW1), 31-48.

RICHTMEYER, R.D. and MORTON, K.W., 1967. *Difference Methods for Initial Value Problems.* New York: Wiley-Interscience, 401p.

SULISZ, W., 1985. Wave reflection and transmission at permeable breakwaters of arbitrary cross-section. *Coastal Engineering,* 9, 371–386.

SYNOLAKIS, C.E., 1989. Discussion on wave reflection and run-up on rough slopes. *Journal Waterway Port Coastal and Ocean Engineering, ASCE,* 115(1), 139–143.

VAN DER MEER, J.W., 1987. Stability of breakwater armour layers—design formulae. *Coastal Engineering,* 11, 219–239.

VAN DER MEER, J.W., 1988a. Deterministic and probabilistic design of breakwater armor layers. *Journal Waterway Port Coastal and Ocean Engineering, ASCE,* 114(1), 66–80.

VAN DER MEER, J.W., 1988b. Rock slopes and gravel beaches under wave attack. Delft University of Technology, Delft, The Netherlands, Doctoral Thesis.

APPENDIX B

IRREGULAR WAVES ON ROUGH PERMEABLE SLOPES

Nobuhisa Kobayashi, Andojo Wurjanto and Daniel T. Cox

Journal of Coastal Research
Special Issue No. 7, pp. 167-184

Spring, 1990

Journal of Coastal Research	SI	7	167–184	Fort Lauderdale, Florida	Spring 1990

Irregular Waves on Rough Permeable Slopes

Nobuhisa Kobayashi, Andojo Wurjanto and Daniel T. Cox

Department of Civil Engineering
University of Delaware
Newark, DE 19716, U.S.A.

ABSTRACT

KOBAYASHI, N.; WURJANTO, A., and COX, D.T., 1990. Irregular waves on rough permeable slopes. *Journal of Coastal Research*, SI#7, 167–184. Fort Lauderdale (Florida). ISSN 0749-0208.

The numerical model presented in the accompanying paper of Kobayashi and Wurjanto (1990) is used to compute the irregular wave motion on a rough permeable slope. The normally-incident irregular wave train characterized by its spectral density at the toe of the slope is generated numerically for the six test runs for which the computed results based on the regular wave approximation have been presented in the accompanying paper. The computed critical stability number for initiation of armor movement under the computed irregular wave motion is shown to be in good agreement with the measured stability number corresponding to the start of the damage. The comparison of the computed armor stability for the incident regular and irregular waves indicates that the armor stability is reduced appreciably and varies less along the slopes under the irregular wave action. On the other hand, the comparison between the computed reflected wave spectrum and the specified incident wave spectrum indicates the reflection of Fourier components with longer periods and the dissipation of Fourier components with shorter periods, while the average reflection coefficient increases with the increase of the surf similarity parameter. The computed waterline oscillations are examined using spectral and time series analyses. The computed spectra of the waterline oscillation show the noticeable low-frequency components similar to low-frequency waves on beaches, which increase with the decrease of the surf similarity parameter. The statistical analysis of individual wave run-up heights indicates that the computed run-up distribution follows the Rayleigh distribution fairly well for some of the six test runs. The computed maximum wave run-up is also shown to be in agreement with the empirical formula based on irregular wave run-up tests.

ADDITIONAL INDEX WORDS: *Irregular waves, reflection, run-up, armor units, breakwaters.*

INTRODUCTION

Design of coastal structures protected with armor units against wind waves needs to account for the randomness of incident waves, although realistic sea states are not defined precisely at present (MANSARD, 1988). It is already standard to perform hydraulic model tests using random waves generated by wave paddles (GODA, 1985). However, the reproduction of the specified sea state in a wave flume requires sophisticated techniques and is not free of difficulties especially in shallow water (MANSARD, 1988). On the other hand, numerical simulation of random waves provides an indispensable tool for studies of random waves and their action on structures (GODA, 1985). The first attempt is made in this paper to compute the irregular wave motion and resulting armor response on a rough permeable slope using the incident irregular wave train generated numerically. This approach bypasses the difficulties associated with the precise control of the wave paddle and the measurements of the detailed hydrodynamics and armor response.

Use is made of the numerical model presented in the accompanying paper of KOBAYASHI and WURJANTO (1990). This numerical model predicts the flow and armor stability on a rough permeable slope as well as the flow in a permeable underlayer for a normally incident wave train. The present numerical model is limited to the rough permeable slope with an impermeable core and with no slope profile change with time. In the accompanying paper, six test runs have been selected from the extensive data of VAN DER MEER (1988). These runs corresponded to the start of the damage to rock slopes under irregular wave action. Computation has been made for the six test runs by approximating the incident irregular wave train characterized by its significant wave height and average period by the regular wave train with the same height and period. The computed results based on the regular wave approximation have been presented and explained in

90036 received June 1989; accepted in revision September 1989.

the accompanying paper where the effects of the permeable underlayer have been examined in detail.

In this paper, the normally-incident irregular wave train characterized by its spectral density at the toe of the rough permeable slope is generated numerically for the same six test runs. In the following, emphasis is placed on the reflected irregular wave train, the irregular waterline oscillation on the slope and the armor stability under the irregular wave action. The flow field on the rough slope and in the permeable underlayer computed for the incident irregular wave train is qualitatively similar to the computed flow field for the incident regular wave train presented in the accompanying paper. The effects of incident random waves on the wave reflection, run-up and armor stability are examined in detail by comparing the computed results for the regular and irregular waves with the measurements on these quantities. The computed critical stability number for initiation of armor movement under the computed irregular wave motion is shown to be in good agreement with the measured stability number corresponding to the start of the damage. This is a significant improvement as compared to the computed critical stability number based on the regular wave approximation which is appreciably greater than the measured stability number. The details of the wave reflection and run-up on the rough permeable slope are also found to be quite different for the incident regular and irregular waves, although the overall trend is similar.

INCIDENT IRREGULAR WAVE TRAINS

The computation performed in this paper is the same as that presented in the accompanying paper of KOBAYASHI and WURJANTO (1990) except for the normalized incident wave train, $\eta_i = \eta_i'/H'$, specified as a function of the normalized time, $t = t'/T'$, at the toe of the rough permeable slope where the prime indicates the dimensional variables. The representative wave height and period denoted by H' and T', respectively, are used for the normalization of the dimensional variables. For the comparison of the numerical model with the data of VAN DER MEER (1988), use has been made of $H' = H_s'$ and $T' = T_m'$ since the significant wave height, H_s', and the average period of zero upcrossings, T_m', were given for each test run. For the regular wave approximation used in the accompanying paper, the normalized incident wave train $\eta_i(t)$ with unit wave height and period for $0 \leq t \leq 256$ has been specified using Stokes second-order wave theory.

The incident random waves for the six test runs selected from the tabulated data of VAN DER MEER (1988) were generated in a wave flume using the Pierson-Moskowitz spectrum (*e.g.*, BOUWS *et al.*, 1985). The normalized Pierson-Moskowitz spectrum used herein is expressed as

$$S_i(f_*) = 5\, m_o\, T_p^{-4}\, f_*^{-5} \exp\left[-\frac{5}{4}(T_p f_*)^{-4}\right] \quad (1)$$

with

$$f_* = f_* T' \;;\; T_p = T_p'/T' \;;\; m_o = \int_0^\infty S_i(f_*)\,df_* \quad (2)$$

where S_i = spectral density of the incident random waves normalized by $T'H'^2$; f_* = normalized frequency; T_p = normalized spectral peak period; and m_o = zeroth moment of $S_i(f_*)$. The normalized frequency in this paper is denoted by f_* since the normalized friction factor is denoted by f in the accompanying paper.

The normalized incident irregular wave train $\eta_i(t)$ for given $S_i(f_*)$ may be simulated using the following random phase scheme (*e.g.*, ELGAR *et al.*, 1985)

$$\eta_i(t) = \sum_{n=1}^{N} C_n \cos(2\pi n \Delta f_* t + \phi_n) \quad \text{for } 0 \leq t \leq t_{max} \quad (3)$$

with

$$\Delta f_* = (t_{max})^{-1} \;;\; C_n = [2\Delta f_*\, S_i(n\Delta f_*)]^{1/2} \quad (4)$$

where t_{max} = normalized duration of the simulation of $\eta_i(t)$; Δf_* = frequency band width; C_n = Fourier amplitudes; ϕ_n = random phase angles distributed uniformly in $[0, 2\pi]$; and N = number of spectral components. Eq. 3 represents a Gaussian sea only in the limit $N \to \infty$. ELGAR *et al.* (1985) compared this random phase scheme with a random coefficient scheme and found no significant differences in wave group statistics for a sufficiently larger number of spectral components. Use is made of $N = 4096$ and $t_{max} = 256$ in the following computation where $t_{max} = 256$ corresponding to 256

individual waves may be sufficient to keep the sampling variability of the wave statistics below an acceptable level (GODA, 1985).

For the spectrum specified by Eq. 1 with given m_o and T_p, the Fourier amplitudes C_n are computed using Eq. 4 and the random phases ϕ_n are produced by a numerical random number generator. An inverse Fast Fourier transform based on Eq. 3 yields the time series $\eta_i(t)$ with the sampling rate $\Delta t = (t_{max}/2N) = 1/32$ for $0 \leq t \leq t_{max} = 256$. The computed irregular wave train $\eta_i(t)$ is then analyzed using a zero upcrossing method (*e.g.*, GODA, 1985) to find the normalized significant wave height, $H_s = H_s'/H'$, and the normalized average period of the zero upcrossings, $T_m = T_m'/T'$. It is required that $H_s = 1$ and $T_m = 1$ since the height H' and the period T' used for the normalization of the dimensional variables are taken as $H' = H_s'$ and $T' = T_m'$. An iteration procedure starting from $H_{m0} = 4\sqrt{m_o} = 1$ and $T_p = 1.25$ is used to satisfy the requirements of $H_s = 1$ and $T_m = 1$ where VAN DER MEER (1988) indicated that $H_{m0} \simeq H_s$ and $T_p \simeq 1.0$–1.5. First, a set of the random phases ϕ_n in Eq. 3 is selected by specifying the seed number for the numerical random number generator. Then, T_p and $H_{m0} = 4\sqrt{m_o}$ are varied until $T_m = 1$ and $H_s = 1$ within the error of 0.001. It should be noted that different sets of the random phases yield different values of H_{m0} and T_p satisfying the requirements of $H_s = 1$ and $T_m = 1$. In theory, there are an infinite number of time series $\eta_i(t)$ with $H_s = 1$ and $T_m = 1$ for a specified spectral form. As a result, the incident irregular wave train specified in the subsequent computation for each test run is not exactly the same as that generated in a wave flume by VAN DER MEER (1988).

Table 1 lists the values of $H' = H_s'$ and $T' = T_m'$ together with the cotangent of the slope angle θ' and the surf similarity parameter, $\xi = T'\tan\theta'(2\pi H'/g)^{-1/2}$, for the six test runs selected from the tabulated data of VAN DER MEER (1988). The computed results based on the incident random wave train computed using Eqs. 1–4 are denoted by run R1 to R6, whereas the corresponding results based on the monochromatic approximation have been denoted by run M1 to M6 in the accompanying paper. The values of $H_{m0} = 4\sqrt{m_o}$ and T_p for each run listed in Table 1 specify the PIERSON-MOSKOWITZ spectrum expressed by Eq. 1. Runs R2a and R2b correspond to run R2 and are intended to examine the effects of the variability of the time series $\eta_i(t)$ with the same significant wave height and average period generated numerically from the PIERSON-MOSKOWITZ spectrum, although a much larger number of the simulated time series are required to perform a statistical analysis of the variability caused by different sets of the random phases ϕ_n in Eq. 3. Table 1 also lists the values of the surf similarity parameter, $\xi_p = \xi T_p/(H_{m0})^{1/2}$, based on the spectral parameters H_{m0} and T_p where $\xi_p \simeq 1.4\,\xi$ since $H_{m0} \simeq 1.05$ and $T_p \simeq 1.4$ as listed in Table 1. The other important dimensionless parameters associated with the numerical model described in the accompanying paper of KOBAYASHI and WURJANTO (1990) remain the same since use has been made of $H' = H_s'$ and $T' = T_m'$ for the computation based on the monochromatic wave approximation. It is noted that $d_t = 7.9$–10.3 for the test runs listed in Table 1 where $d_t = d_t'/H'$ is the normalized water depth below the still water level at the toe of the rough permeable slope. The assumptions of linearity and random phase at the toe of the slope employed in Eqs. 3 and 4 may be reasonable for these runs with $d_t = 7.9$–10.3, although the ocean waves in shallower water depth may show marked departures from the linear simulations (ELGAR *et al.*, 1984).

Table 1. *Six test runs compared with numerical model.*

Run No.	cotθ′	H′ (cm)	T′ (sec)	ξ	H_{mo}	T_p	ξ_p
R1	6	10.09	2.63	1.72	1.035	1.429	2.42
R2a	6	7.75	3.15	2.36	1.048	1.372	3.16
R2b	6	7.75	3.15	2.36	1.053	1.390	3.19
R3	4	8.16	3.22	3.52	1.038	1.398	4.83
R4	3	8.92	3.13	4.37	1.050	1.457	6.21
R5	2	7.98	2.69	5.95	1.050	1.439	8.35
R6	2	7.98	3.11	6.88	1.055	1.417	9.49

Figure 1 shows the incident irregular wave train $\eta_i(t)$ for $0 \leq t \leq 256$ specified at the toe of the rough permeable slope for run R3 where $\overline{\eta_i} = 0$ with the overbar indicating the time averaging for $0 \leq t \leq 256$. In the following, the computed results for run R3 using the incident irregular wave train $\eta_i(t)$ shown in Figure 1 are presented in detail as a typical run and may be compared with those for run M3 presented in the accompanying paper. The numerical model of KOBAYASHI and WURJANTO (1990) predicts the nonlinear irregular wave motion and

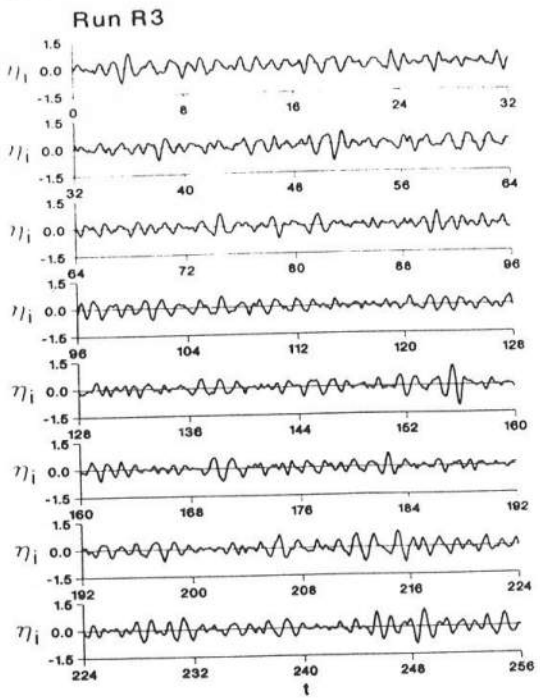

Figure 1. Incident irregular wave train $\eta_i(t)$ for $0 \leq t \leq 256$ specified as input to numerical model for run R3.

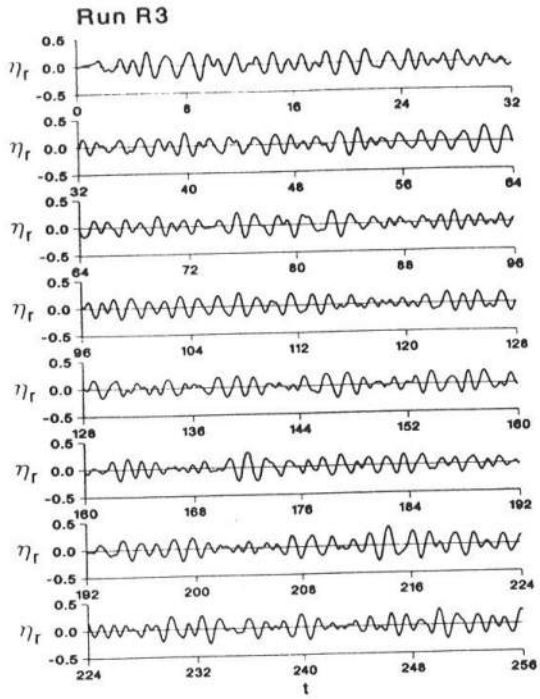

Figure 2. Computed reflected wave train $\eta_r(t)$ for $0 \leq t \leq 256$ at toe of rough permeable slope for run R3.

the hydraulic stability of armor units on the specified rough permeable slope in the time domain. As a result, the numerical model is deterministic for the specified incident wave train $\eta_i(t)$ which can be regular or irregular. The probabilistic nature of the problem arises from the variability of the specified incident wave trains which is considered by runs R2a and R2b only. Furthermore, the irregularities and randomness associated with the rough permeable slope are not considered in this paper.

REFLECTED IRREGULAR WAVE TRAINS

Figure 2 shows the computed reflected wave train $\eta_r(t)$ for $0 \leq t \leq 256$ normalized as $\eta_r = \eta_r'/H'$ at the toe of the rough permeable slope for run R3. The normalized free surface variation $\eta_r(t)$ due to the waves reflected from the rough permeable slope is irregular since the corresponding incident wave train $\eta_i(t)$ shown in Figure 1 is irregular. The reflection coefficient r based on the time series $\eta_r(t)$ and $\eta_i(t)$ is defined as (KOBAYASHI and WURJANTO, 1990)

$$r = \left[\overline{(\eta_r - \overline{\eta_r})^2} \left(\overline{\eta_i^2} \right)^{-1} \right]^{1/2} \qquad (5)$$

where $\overline{\eta_i} = 0$ and $\overline{\eta_r}$ is the difference between the still water level and the mean water level at the toe of the rough permeable slope. The time averaging denoted by the overbar is performed for $0 \leq t \leq 256$ since the transient duration starting from the initial conditions of no wave motion on the rough permeable slope has been found to last only for several wave periods for the computed results based on the monochromatic wave approximation presented in the accompanying paper. The computed values of $\overline{\eta_r}$ are essentially zero for all the runs with large values of d_t listed in Table 1. It may be noted that the wave set-down with $\overline{\eta_r} < 0$ would become noticeable if the value of d_t were much smaller (KOBAYASHI *et al.*, 1989). The computed reflection coefficient using Eq. 5 is r = 0.424 for run R3 with $\xi = 3.52$.

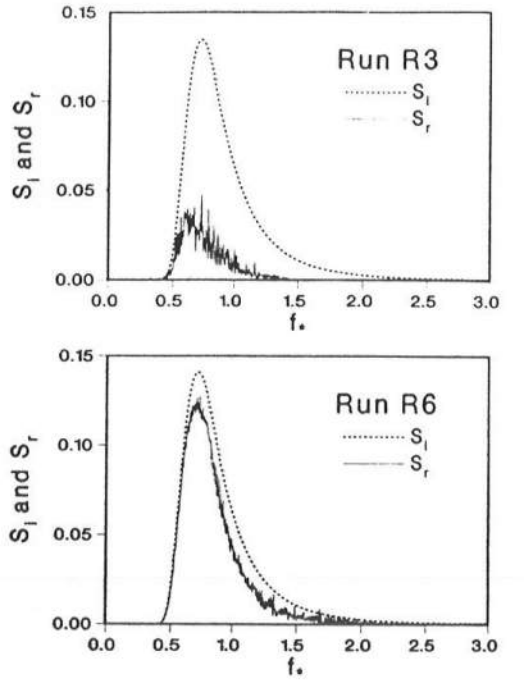

Figure 3. Unsmoothed spectral densities of incident and reflected waves, $S_i(f_\cdot)$ and $S_r(f_\cdot)$, respectively, for run R3 with ξ = 3.52 and run R6 with ξ = 6.88.

Figure 3 shows the unsmoothed spectral densities of the incident and reflected waves denoted by $S_i(f_\cdot)$ and $S_r(f_\cdot)$ with $f_\cdot$ = normalized frequency, respectively, for runs R3 and R6. The incident wave spectrum $S_i(f_\cdot)$ for run R3 is computed using a Fast Fourier transform from the incident wave train $\eta_i(t)$ shown in Figure 1 and is exactly the same as $S_i(f_\cdot)$ given by Eq. 1 with H_{mo} = 1.038 and T_p = 1.398 for run R3 as listed in Table 1. The reflected wave spectrum $S_r(f_\cdot)$ for run R3 with ξ = 3.52 is computed from the reflected wave train $\eta_r(t)$ shown in Figure 2. It is noted that the computed spectra in this paper are not smoothed since the numerical model is deterministic. The spectra $S_i(f_\cdot)$ and $S_r(f_\cdot)$ for run R6 with ξ = 6.88 computed in the same manner are presented to show the effect of the surf similarity parameter ξ on the reflection coefficient function defined by $[S_r(f_\cdot)/S_i(f_\cdot)]^{1/2}$ as a function of the frequency $f_\cdot$. Figure 3 indicates the reflection of Fourier components with longer periods and the dissipation of Fourier components with shorter periods. Figure 3 together with the similar figures plotted for the other runs shows that the reflection coefficient function for given $f_\cdot$ increases with the increase of the surf similarity parameter ξ. The computed variations of the reflection coefficient function with respect to the frequency for different values of ξ are consistent with the observed selective wave reflection and dissipation on natural beaches (*e.g.*, TATAVARTI *et al.*, 1988). It is noted that incoming low-frequency waves are present on natural beaches but are not included in the incident wave spectrum specified by Eq. 1. The computed reflected wave spectra contain low-frequency wave components which become discernible for run R1 with ξ = 1.72. The computed low-frequency waves must be generated on the rough permeable slope and reflected from the slope. On the other hand, the average reflection coefficient may be defined as $[(m_o)_r/m_o]^{1/2}$ where m_o = zeroth moment of $S_i(f_\cdot)$ as defined in Eq. 2; and $(m_o)_r$ = zeroth moment of $S_r(f_\cdot)$. The computed average reflection coefficient is found to be virtually the same as the reflection coefficient r defined by Eq. 5 using the time series $\eta_r(t)$ and $\eta_i(t)$ for each of the test runs listed in Table 1.

Figure 4 shows the computed irregular wave reflection coefficient r as a function of the surf similarity parameter ξ for run R1 to R6 where the value of ξ for each run is given in Table 1. The computed values of r for runs R2a and R2b with ξ = 2.36 turn out to be the same and r = 0.227 for both runs. The computed temporal variations of $\eta_i(t)$ and $\eta_r(t)$ for these two runs appear to be fairly different but the computed reflected wave spectra $S_r(f_\cdot)$ are very similar. Figure 4 also shows the computed reflection coefficient r based on the regular wave approximation together with the empirical formula, $r = 1.35[1-\exp(-0.071\xi)]$, presented in the accompanying paper. Figure 4 suggests that the approximation of the incident irregular wave train by the regular wave train with the height H_s' and the period T_m' may underestimate the reflection coefficient r especially if the surf similarity parameter ξ is small. Use of the spectral peak period instead of the average wave period was suggested by SEELIG (1983) to compare the values of r measured for the regular and irregular waves. However, any regular wave approximation can not account for the selective nature of wave reflection and dissipation discussed in relation to Figure 3.

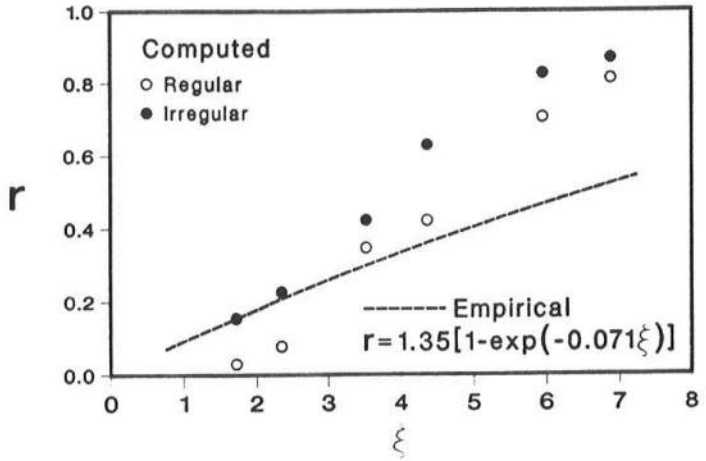

Figure 4. Computed reflection coefficients r for regular and irregular waves for each run with given surf similarity parameter ξ.

IRREGULAR WATERLINE OSCILLATIONS

The computed waterline oscillation on the rough permeable slope is expressed in terms of the normalized waterline elevation, $Z_r = Z_r'/H'$, above the still water level (SWL) where the normalized instantaneous water depth equals δ_r with $\delta_r = \delta_r'/H'$. The variations of Z_r with respect to the normalized time t for $\delta_r' = 0.1, 0.5$ and 1.0 cm are computed to examine the sensitivity of Z_r to the dimensional water depth δ_r' on the rough permeable slope.

Figures 5 and 6 show the computed waterline elevation $Z_r(t)$ for $0 \leq t \leq 256$ corresponding to $\delta_r' = 0.1$ and 1.0 cm, respectively, for run R3. In Figures 5 and 6, $Z_r = 0$ corresponds to SWL. During wave uprush, the water depth near the tip of uprushing water varies rapidly along the slope. During wave downrush, a thin layer of water remains on the slope and the water depth varies slowly along the slope (KOBAYASHI *et al.*, 1989). Consequently, the portions of $Z_r(t)$ increasing with t for $\delta_r' = 0.1$ and 1.0 cm tend to coincide, whereas the portion of $Z_r(t)$ decreasing with t for $\delta_r' = 1.0$ cm decreases faster and lower than the corresponding portion of $Z_r(t)$ for $\delta_r' = 0.1$ cm. The crest elevation of $Z_r(t)$ is not very sensitive to δ_r' in the range $\delta_r' = 0.1$–1.0 cm but the trough elevation of $Z_r(t)$ is very sensitive to δ_r' (KOBAYASHI and WURJANTO, 1990).

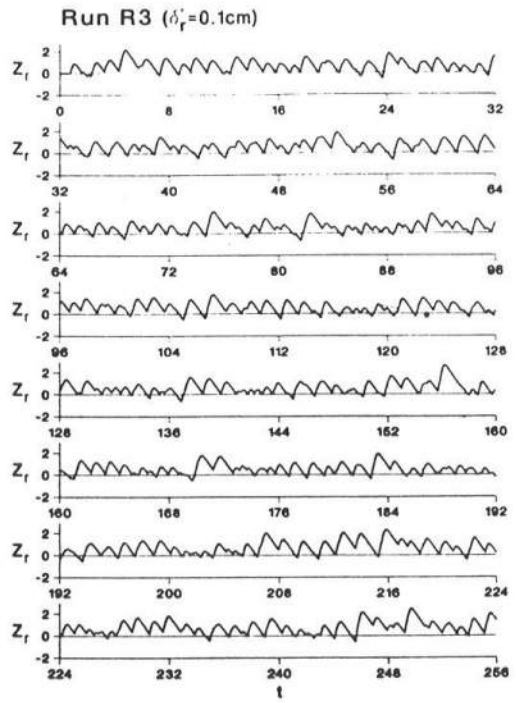

Figure 5. Computed waterline elevation $Z_r(t)$ above SWL of 0.1 cm water depth on rough permeable slope for run R3.

The time averaged value of the normalized waterline elevation $Z_r(t)$ for $0 \leq t \leq 256$ is denoted by $\overline{Z_r}$ which is the normalized wave

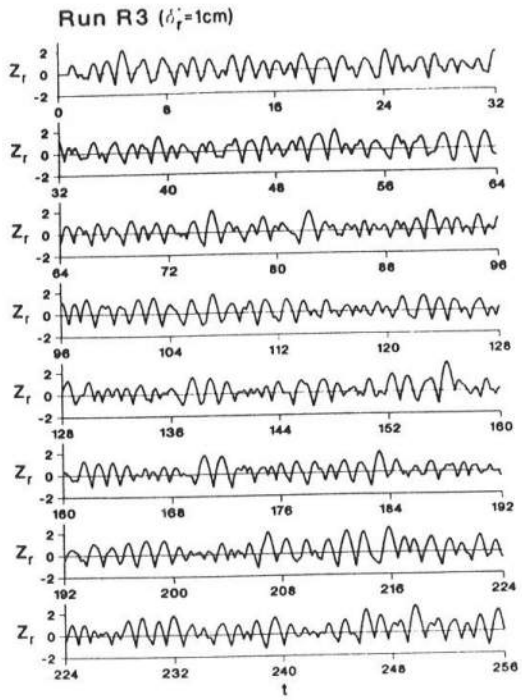

Figure 6. Computed waterline elevation $Z_r(t)$ above SWL of 1.0 cm water depth on rough permeable slope for run R3.

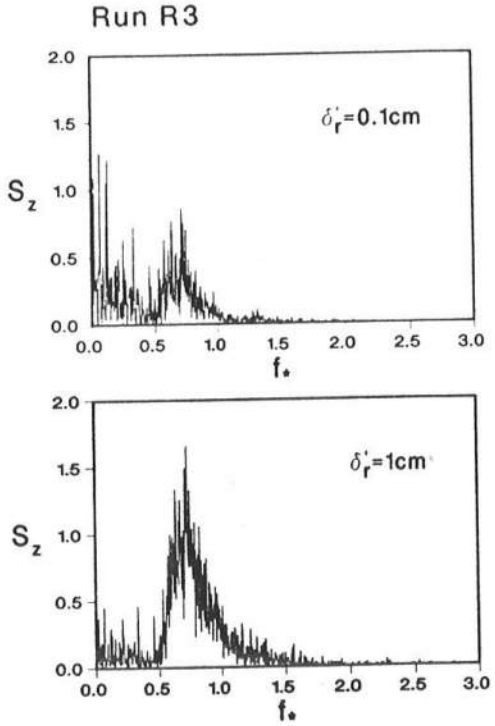

Figure 7. Unsmoothed spectral density $S_z(f_*)$ of waterline oscillation with δ_r' = 0.1 and 1.0 cm for run R3 with ξ = 3.52.

setup on the rough permeable slope. The computed values of $\overline{Z_r}$ for δ_r = 0.1, 0.5 and 1.0 cm together with the corresponding value of ξ are tabulated for each run in Table 2. The values of $\overline{Z_r}$ for runs R2a and R2b are almost the same, although the temporal variations of $Z_r(t)$ appear to be fairly different. The normalized wave setup $\overline{Z_r}$ for given ξ decreases with the increase of δ_r' since the trough elevation of $Z_r(t)$ becomes lower with the increase of δ_r'. The computed values of $\overline{Z_r}$ for given δ_r' remain approximately the same for $1.72 \leq \xi \leq 3.52$ and decrease with the increase of ξ for $\xi \geq 3.52$. This trend is similar to the computed regular wave setup on a smooth slope presented by KOBAYASHI *et al.* (1989). The relatively large wave setup on the rough permeable slope may cause the increase of the mean water level inside a porous breakwater, although the present numerical model is based on the assumption of an impermeable core.

Table 2. *Computed wave setup $\overline{Z_r}$ on rough permeable slope for δ_r' = 0.1, 0.5 and 1.0 cm.*

Run No.	ξ	$\overline{Z_r}$ δ_r' = 0.1cm	δ_r' = 0.5cm	δ_r' = 1.0cm
R1	1.72	0.61	0.45	0.36
R2a	2.36	0.64	0.43	0.33
R2b	2.36	0.66	0.44	0.34
R3	3.52	0.62	0.35	0.26
R4	4.37	0.56	0.28	0.19
R5	5.95	0.40	0.16	0.11
R6	6.88	0.33	0.12	0.08

Figure 7 shows the unsmoothed spectral density, $S_z(f_*)$, computed from the time series $[Z_r(t) - \overline{Z_r}]$ for $0 \leq t \leq 256$ corresponding to δ_r' = 0.1 and 1.0 cm for run R3 with ξ = 3.52. Figure 7 indicates the presence of low-frequency wave components in the waterline oscillation. The low-frequency wave components are larger for δ_r' = 0.1 cm than for δ_r' = 1.0 cm. This is also apparent in Figures 5 and 6 where the degree of grouping of the waterline oscillation appears to be greater for δ_r' = 0.1 cm than for δ_r' = 1.0 cm. In order to show the effect of the surf similarity parameter ξ on the spectral density $S_z(f_*)$ for δ_r' = 0.1 and 1.0 cm, Figure 8 shows the cor-

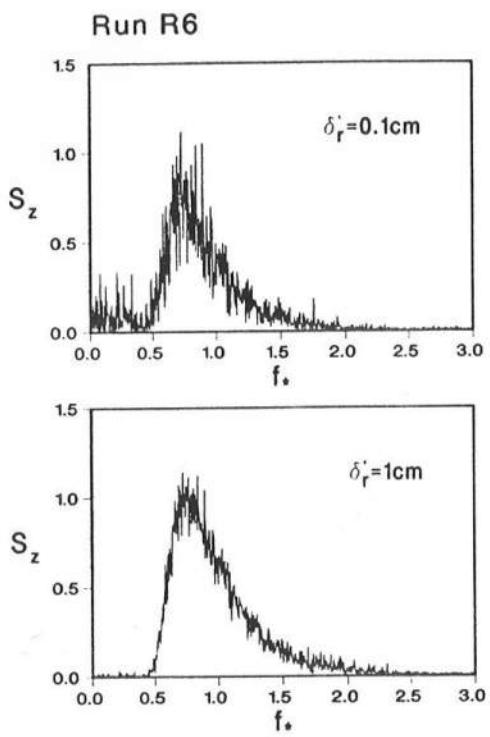

Figure 8. Unsmoothed spectral density $S_z(f_*)$ of waterline oscillation with $\delta_r' = 0.1$ and 1.0 cm for run R6 with $\xi = 6.88$.

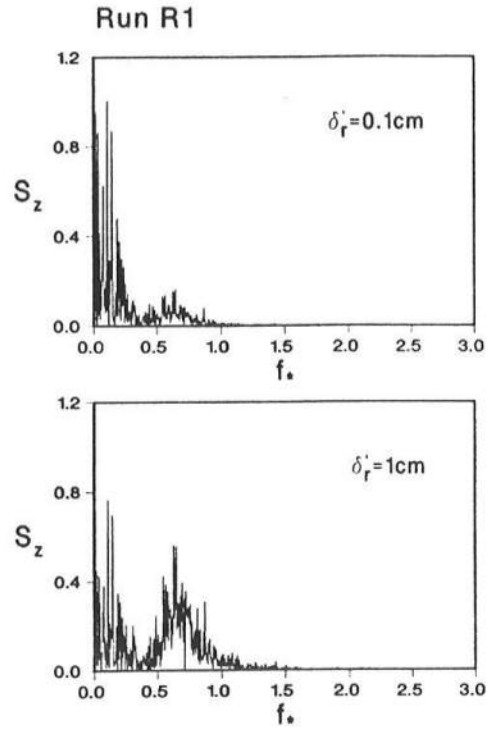

Figure 9. Unsmoothed spectral density $S_z(f_*)$ of waterline oscillation with $\delta_r' = 0.1$ and 1.0 cm for run R1 with $\xi = 1.72$.

responding results for run R6 with $\xi = 6.88$. The incident wave spectral density $S_i(f_*)$ for runs R3 and R6 shown in Figure 3 indicates the frequency band over which the incident wave energy is distributed. Figures 7 and 8 together with the similar figures plotted for the other runs indicate that the low-frequency wave components of the spectral density $S_z(f_*)$ for given δ_r' increase with the decrease of ξ. The low-frequency wave components of the spectral density $S_z(f_*)$ for run R1 with $\xi = 1.72$ are dominant for $\delta_r' = 0.1$ cm and as large as the components associated with the incident wave frequency band for $\delta_r' = 1.0$ cm as shown in Figure 9. The computed spectral densities $S_z(f_*)$ for runs R2a and R2b with $\xi = 2.36$ are similar. This suggests that the variability caused by the different sets of the random phases ϕ_n in Eq. 3 may be smaller than the variability due to the different values of ξ. The computed low-frequency wave oscillations on the rough permeable slope appear to be related to the low-frequency swash oscillations on beaches (*e.g.*, HOLMAN and SALLENGER, 1985; KOBAYASHI *et al.*, 1988). In order to elucidate the generation and reflection processes of the low-frequency wave components, the variations of the incident-frequency and low-frequency wave motions along the slope will need to be examined in detail. For example, the low-frequency wave components of the reflected wave spectra $S_r(f_*)$ shown in Figure 3 are much smaller than those associated with $S_z(f_*)$ shown in Figures 7 and 8.

The computed time series $[Z_r(t) - \overline{Z_r}]$ for $0 \leq t \leq 256$ are also analyzed using the zero upcrossing method which is normally used for the time series analysis of the free surface oscillation (*e.g.*, GODA, 1985). Since wave run-down is sensitive to δ_r' and hard to define quantitatively, the following analysis is limited to wave run-up. The maximum value of $Z_r(t)$ between the two adjacent zero upcrossings in the time series $[Z_r(t) - \overline{Z_r}]$ for $0 \leq t \leq 256$ is denoted by R_j with $j = 1, 2, \ldots, N_0$ where $(N_0 + 1)$ is the number of the zero upcrossings. The average period $\overline{t_r}$ of the two adjacent zero upcrossings is

Table 3. *Computed average period $\overline{t_r}$ of zero upcrossings in time series $[Z_r(t) - \overline{Z_r}]$ with $\delta_r' = 0.1$, 0.5 and 1.0 cm.*

Run No.	ξ	$\overline{t_r}$ $\delta_r' = 0.1$cm	$\delta_r' = 0.5$cm	$\delta_r' = 1.0$cm
R1	1.72	2.23	1.51	1.33
R2a	2.36	1.66	1.23	1.15
R2b	2.36	1.73	1.29	1.23
R3	3.52	1.38	1.15	1.12
R4	4.37	1.19	1.06	1.04
R5	5.95	1.02	0.95	0.96
R6	6.88	0.95	0.93	0.94

given by $\overline{t_r} = 256/N_0$. The individual run-up heights R_j above SWL are ranked in the descending order. The maximum run-up R_{max} is defined as the run-up height corresponding to the first rank. The significant run-up R_s is defined as the average of the highest one-third run-up heights. The exceedance probability P corresponding to the run-up height R_p of the n-th rank is estimated by $P = n/(N_0 + 1)$. If the probability distribution of run-up heights follows the Rayleigh distribution (BATTJES, 1971; LOSADA and GIMÉNEZ-CURTO, 1981), the exceedance probability P associated with R_p is given by

$$P = \exp[-2(R_p/R_s)^2] \quad (6)$$

which yields $P = 1$ for $R_p = 0$. On the other hand, $R_p > \overline{Z_r}$ because of the definition of the run-up height R_j adopted in this paper. For the analysis of extreme value statistics for wave run-up on a natural beach, HOLMAN (1986) defined the run-up as a local maximum of the measured instantaneous shoreline elevation. This definition could include secondary crests between the zero upcrossings as wave run-up, although his definition diagram did not indicate them. For the present definition of R_j, the Rayleigh distribution expressed by Eq. 6 will not fit the computed run-up distribution in the vicinity of $P = 1$ if the wave set-up $\overline{Z_r}$ is not negligible.

Table 3 shows the computed average period $\overline{t_r}$ of the two adjacent zero upcrossings in the time series $[Z_r(t) - \overline{Z_r}]$ with $\delta_r' = 0.1$, 0.5 and 1.0 cm for each run. It is noted that the normalized unit time corresponds to the average period of the time series $\eta_i(t)$. The average period $\overline{t_r}$ increases with the decrease of ξ and δ_r'. This trend appears to be correlated to the increase of the low-frequency wave components of $S_z(f)$ with the decrease of ξ and δ_r'.

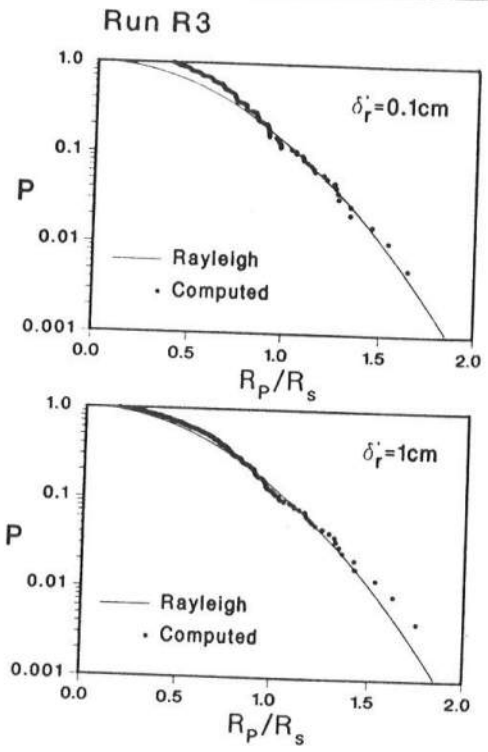

Figure 10. Computed exceedance probability P for run R3 of wave run-up R_p normalized by significant run-up R_s for $\delta_r' = 0.1$ and 1.0 cm as compared with Rayleigh distribution.

Figure 10 shows the computed exceedance probability P as a function of R_p/R_s together with the Rayleigh distribution given by Eq. 6 for the time series $[Z_r(t) - \overline{Z_r}]$ with $\delta_r' = 0.1$ and 1.0 cm for run R3. The computed run-up distribution follows the Rayleigh distribution fairly well for run R3. The agreement is also good for run R6. The agreement appears to be the worst for run R2a as shown in Figure 11. The difference between the computed exceedance probabilities for runs R2a and R2b becomes noticeable for the computed points corresponding to the rank n = 1, 2, and 3. Extreme wave run-up is expected to be affected by different sets of the random phases ϕ_n as well as the simulation duration t_{max} in Eq. 3. Comment may be made on the hypothesis of equivalency which was used by BATTJES (1971) to derive the Rayleigh run-up distribution for waves breaking on slopes. This hypothesis assumes that the irreg-

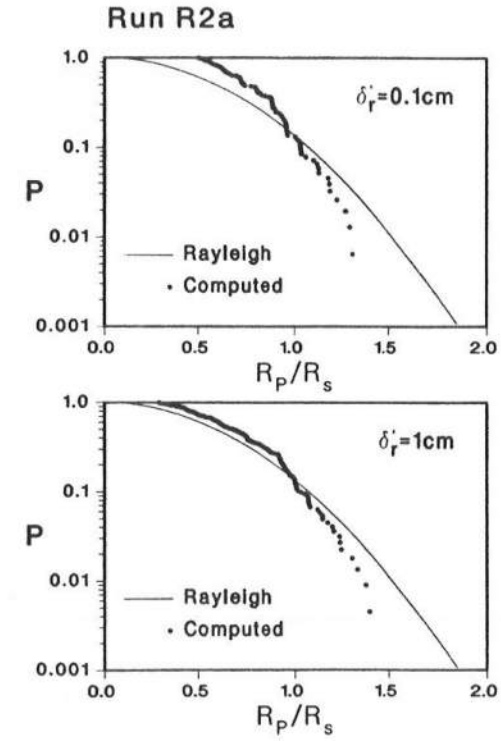

Figure 11. Computed exceedance probability P for run R2a of normalized wave run-up R_p/R_s for $\delta_r' = 0.1$ and 1.0 cm as compared with Rayleigh distribution.

ular wave run-up distribution can be found by assigning to each individual wave the run-up value of a regular wave train of corresponding height and period. This hypothesis does not account for the low-frequency wave components as shown in Figures 7–9 and is more applicable to surging waves on slopes with large values of ξ. The comparisons made for the runs with $1.72 \leq \xi \leq 6.88$ computed herein suggest that the Rayleigh distribution might be used for a preliminary prediction of the run-up distribution on a rough permeable uniform slope because of its simplicity rather than its accuracy.

In order to apply the Rayleigh distribution given by Eq. 6, the significant run-up R_s defined as the average of the highest one-third run-up heights needs to be predicted. Figure 12 shows the computed significant run-up R_s with $\delta_r' = 1.0$ cm as a function of the surf similarity parameter ξ for the runs listed in Table 1. Figure 12 also shows the computed run-up based on the regular wave approximation for each run presented in the accompanying paper as well as the empirical formula, $R_s = 1.13\,\xi/(1 + 0.506\xi)$, which was originally proposed by AHRENS and MCCARTNEY (1975) for regular wave run-up on riprap slopes. In Figure 12, $R_s = 1.17$ and 1.22 for runs R2a and R2b, respectively, whereas the corresponding regular wave run-up is 1.16. The significant run-up and regular wave run-up are also essentially the same for the computed points with $\xi = 3.52$. Figure 12 indicates that the significant run-up R_s normalized by the significant wave height H_s' may be expressed empirically as a function of the surf similarity parameter ξ based on the significant wave height and the average period T_m' of the incident irregular wave train. Furthermore, the run-up computed for the regular wave train with the height H_s' and the period T_m' is in reasonable agreement with the corresponding significant run-up. However, a different empirical formula may also be used to predict R_s. Figure 13 shows the computed significant run-up R_s with $\delta_r' = 0.1$ and 1.0 cm as compared with the empirical formula, $R_s = 1.13\,\xi_p/(1 + 0.506\xi_p)$, where ξ_p is the surf similarity parameter based on the spectral parameters H_{m0} and T_p listed in Table 1. Figure 13 shows that R_s is not sensitive to δ_r' in the range $\delta_r' = 0.1$–1.0 cm.

Figure 14 shows the computed maximum run-up R_{max} defined as the maximum elevation of the waterline elevation $Z_r(t)$ with $\delta_r' = 0.1$ and 1.0 cm for the computation duration $0 \leq t \leq 256$ as compared with the empirical formula based on the spectral parameters, $R_{max}/H_{m0} = 1.022\,\xi_p/(1 + 0.247\,\xi_p)$, which was proposed by AHRENS and HEIMBAUGH (1988) on the basis of small-scale tests on irregular wave run-up on riprap revetments. The maximum run-up in these tests was based on a 256 sec test observation, where an experienced observer measured the extreme excursion of green water. The spectral peak periods for these tests were in the range $T_p' = 1.02$–4.74 sec. The test durations are hence not too different from the computation duration. The riprap revetments used in these tests appear to be similar to the test structures with the impermeable core used by VAN DER MEER (1988) for which the present computation is made. The computed results presented in the accompanying paper have indicated that wave run-up on a rough permeable slope with an impermeable core is not very sensitive to the detailed slope characteristics. As a

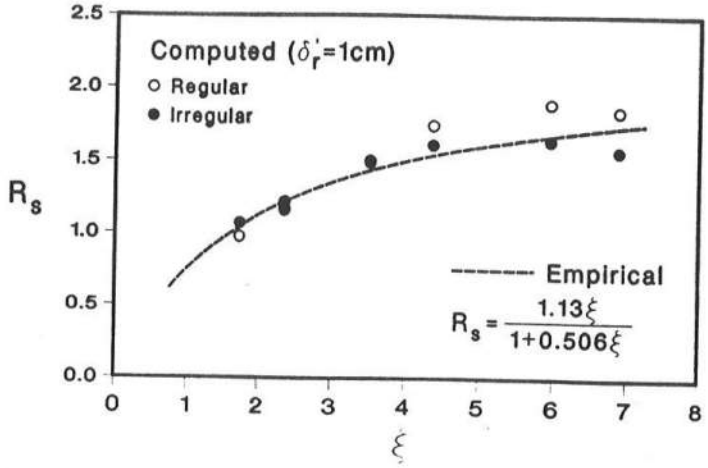

Figure 12. Computed significant run-up R_s with δ_r' = 1.0 cm and corresponding regular wave run-up for each run as compared with an empirical formula based on ξ.

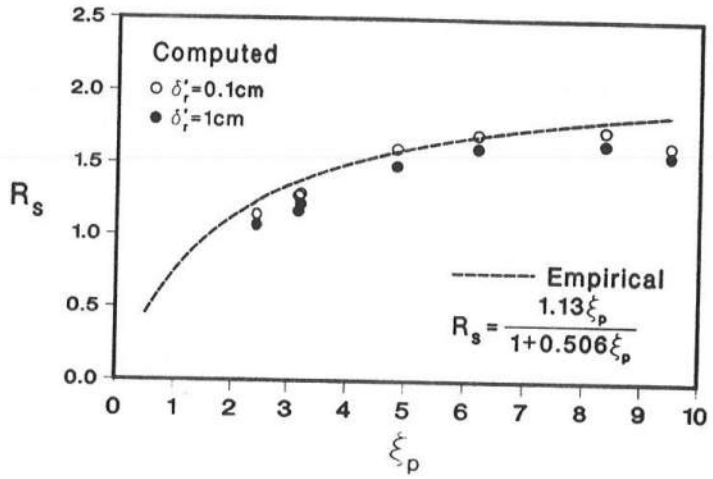

Figure 13. Computed significant run-up R_s with δ_r' = 0.1 and 1.0 cm for each run as compared with an empirical formula based on ξ_p.

result, the comparison of the computed maximum run-up R_{max} with this empirical formula is justified except that the incident random wave spectra used in the tests were not specified. The computed maximum run-up is not sensitive to the physical water depth δ_r' used to define the run-up, indicating that the maximum run-up observed visually should be sufficiently accurate. The computed points shown in Figure 14 appear to be within the scattered data points presented by AHRENS and HEIMBAUGH (1988). The difference between the computed points for run R2a with ξ_p = 3.16 and run R2b with ξ_p = 3.19 implies the variability of R_{max} caused by the different sets of the random phases ϕ_n in Eq. 3, although a much larger number of the computed values will be required for a statistical analysis of the variability. Alternatively, it may be suggested that the accurate deterministic prediction of the maxi-

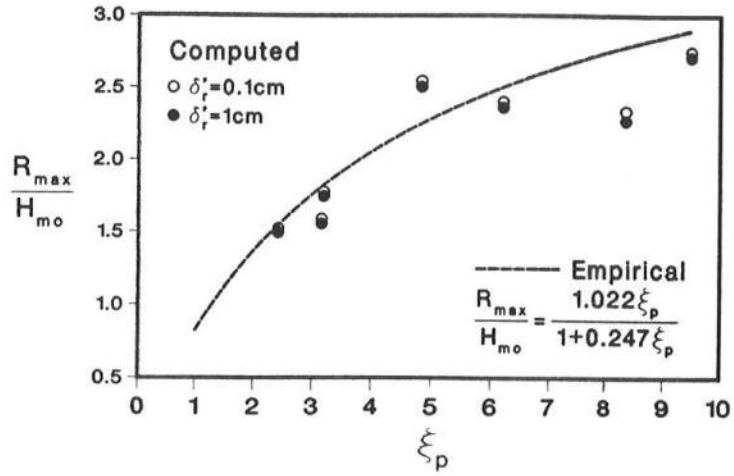

Figure 14. Computed maximum run-up R_{max} with δ_r' = 0.1 and 1.0 cm for each run as compared with the empirical formula of Ahrens and Heimbaugh (1988).

mum wave run-up will require the information on the phase angles ϕ_n which are deterministic for each run.

ARMOR STABILITY UNDER IRREGULAR WAVE ACTION

In the accompanying paper of KOBAYASHI and WURJANTO (1990), the hydraulic stability condition against sliding or rolling of an armor unit has been expressed as

$$N_s = H' (s-1)^{-1} \left(\frac{W'}{\rho s}\right)^{-1/3} \leq N_R(t,z) \qquad (7)$$

where N_s = stability number, H' = incident significant wave height; s = specific density of the armor unit; ρ = fluid density; W' = median mass of the armor units; and N_R = armor stability function varying with the normalized time t and the normalized elevation, $z = z'/H'$, indicating the location of the armor unit along the uniform slope. The dimensional vertical coordinate z' has been taken to be positive upward with $z' = 0$ at SWL. The normalized vertical coordinate z instead of the normalized horizontal coordinate x is used in the following to indicate the location of the armor unit on the slope relative to SWL. The expression of N_R as a function of the normalized fluid velocity and acceleration has been given in the accompanying paper where the input parameters for the computation of the armor stability have been specified.

For each of the runs listed in Table 1, the armor stability function N_R is computed as a function of t for $8 \leq t \leq 256$ and as a function of z from the toe of the slope to the point above the maximum run-up. The duration $0 \leq t < 8$ is excluded partly because the transient wave motion during $0 \leq t < 8$ might cause the minimum stability of armor units and partly because the computed temporal variation of N_R at given z is analyzed in the time domain only, eliminating the requirement that the number of data points should be a power of 2 for an efficient Fast Fourier transform (*e.g.*, GODA, 1985).

Figures 15, 16 and 17 show the computed temporal variation of the armor stability function $N_R(t,z)$ for $8 \leq t \leq 256$ at $z = -3.24$, -1.67 and -0.10, respectively, for run R3. The stability number for run R3 is $N_s = 1.39$. The movement of the armor unit located at given z will occur when $N_R(t,z)$ becomes smaller than N_s. Comparing the temporal variations of N_R with the incident irregular wave train $\eta_i(t)$ for run R3 shown in Figure 1, it is possible to quantify the response of armor units under various incident wave sequences. The various sequences of waves which may cause severe conditions on a breakwater were

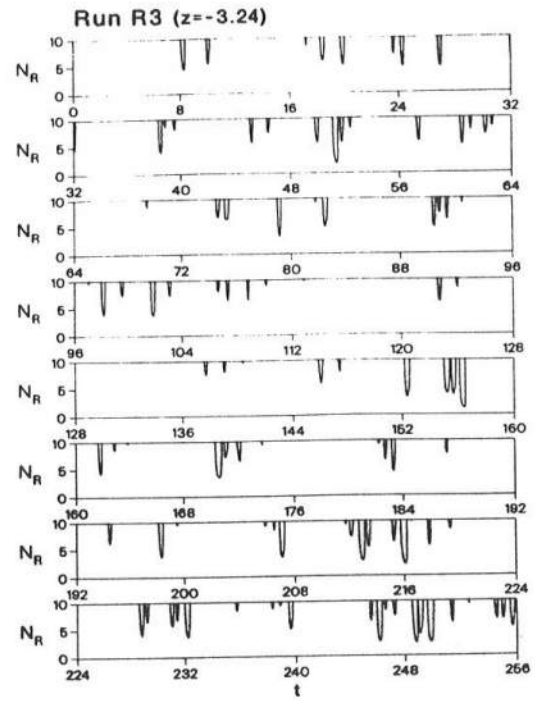

Figure 15. Computed temporal variation of armor stability function $N_R(t,z)$ for $8 \leq t \leq 256$ at $z = -3.24$ for run R3.

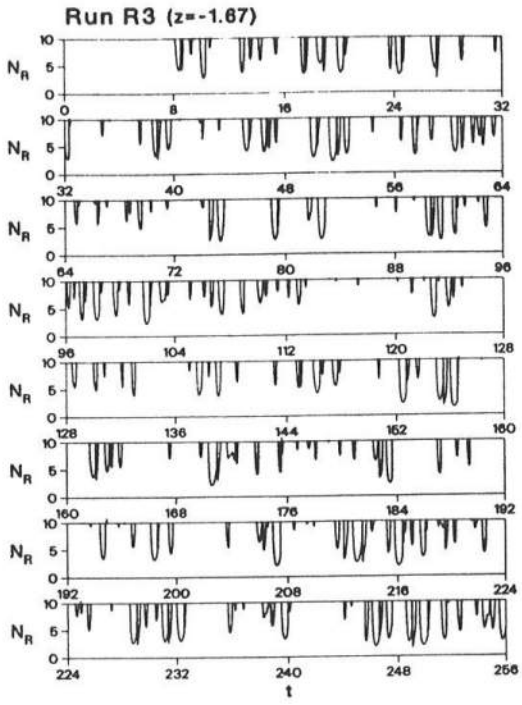

Figure 16. Computed temporal variation of armor stability function $N_R(t,z)$ for $8 \leq t \leq 256$ at $z = -1.67$ for run R3.

described qualitatively by GUNBAK and BRUUN (1979). The armor stability function N_R at $z = -3.24$, -1.67 and -0.10 below SWL becomes the minimum at $t = 156.38$, 156.35 and 155.69, respectively, as may be read from Figures 15–17. This indicates that the minimum stability of armor units at these locations is caused by the downrushing water on the slope resulted from the same sequence of waves. Correspondingly, the incident irregular wave train $\eta_i(t)$ shown in Figure 1 exhibits the high crest followed by the deep trough in the vicinity of $t = 156$ where the wave travel time from the toe of the slope is relatively small for run R3 as may be inferred by comparing the temporal variations of $\eta_i(t)$ and $Z_r(t)$ shown in Figures 1, 5 and 6. A careful examination of Figures 15–17 in light of Figure 1 suggests that it is not always easy to identify the incident wave group or sequence corresponding to the small values of N_R. The figures similar to Figures 15–17 are plotted for the other runs and compared with the corresponding incident irregular wave trains. The comparisons made for the other runs indicate that the incident wave group or sequence causing the minimum value of N_R at given z is variable. This variability may partly be resulted from the presence of the low-frequency wave components on the rough permeable slope since the low-frequency waves may respond to a larger group of incident waves.

Figure 18 shows the spatial variation of the local stability number $N_{sx}(z)$ for run R3 where $N_{sx}(z)$ is defined as the minimum value of $N_R(t,z)$ at given z during $8 \leq t \leq 256$. Figure 18 also shows the corresponding spatial variation of $N_{sx}(z)$ based on the regular wave approximation. The spatial variation of $N_{sx}(z)$ computed for the irregular and regular waves for the other runs are similar to those shown in Figure 18. As a result, the approximation of the incident irregular wave train by the regular wave train whose height and period are taken as the significant wave height and average period results in the overestimation of the armor stability especially in the regions $z \lesssim -2$ and $z \gtrsim 0$. The weak variation of N_{sx} along the slope for the incident irregular wave train may

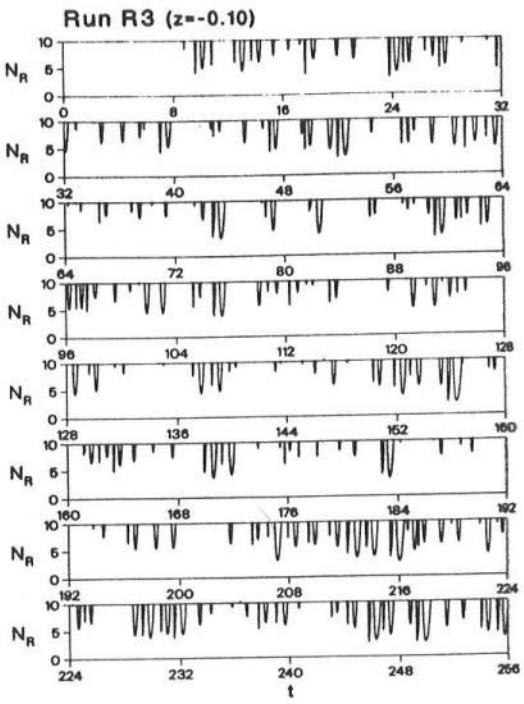

Figure 17. Computed temporal variation of armor stability function $N_R(t,z)$ for $8 \leq t \leq 256$ at $z = -0.10$ for run R3.

not be surprising since the location of the small armor stability moves along the slope under the irregular wave action.

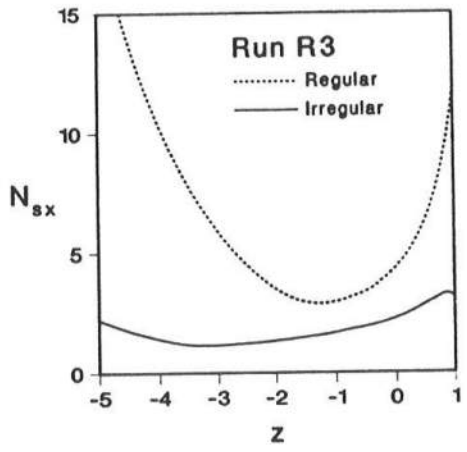

Figure 18. Computed spatial variations of local stability number $N_{sx}(z)$ under irregular and regular wave action for run R3.

The local stability number N_{sx} may be used to estimate whether the armor unit at given location will move or not under the specified irregular wave action. After the initiation of armor movement occurs, the local stability number N_{sx} alone will not indicate the intensity, frequency and duration of the armor movement. For example, the minimum value of N_{sx} in Figure 18 is $N_{sx} = 1.15$ occurring at $z = -3.24$, whereas $N_{sx} = 1.43$ and 2.18 at $z = -1.67$ and -0.10, respectively. On the other hand, $N_s = 1.39$ for run R3. In Figure 18, $N_{sx} < N_s$ for $-3.97 < z < -1.80$. Comparison of Figures 15, 16 and 17 indicates that the armor unit at $z = -1.67$ is exposed to the severe wave action more frequently than those located at $z = -3.24$ and -0.10. This suggests that the movement of armor units for run R3 will occur in the region $-3.97 < z < -1.80$ and will be more frequent in the region $-3.24 < z < -1.80$ than at the location $z = -3.24$ of the minimum stability. The simplified model for the sliding motion of individual armor units along the slope proposed by KOBAYASHI and OTTA (1987) could be used to predict the displacement of armor units. However, this model does not predict the slope profile change with time which was measured by VAN DER MEER (1988).

Finally, the computed critical stability number N_{sc} defined as the minimum value of the local stability number $N_{sx}(z)$ varying along the slope is compared with the stability number N_s for the six runs selected from the extensive data of VAN DER MEER (1988). These runs corresponded to the start of the damage to the specified primary cover layer under the action of 1000 waves of the incident irregular wave train as discussed in the accompanying paper. Since $N_{sx}(z)$ does not vary much over the wide region along the slope as shown in Figure 18, the critical stability number N_{sc} may be used as a criterion for the initiation of armor movement. Furthermore, the computed value of N_{sc} may be assumed to correspond to the stability number N_s for the start of the damage since the present stability analysis does not account for armor units placed in unstable positions at the completion of the tested riprap slope. The difference between the value of N_{sc} computed for $8 \leq t \leq 256$ and that for $8 \leq t \leq 1008$ is expected to be small on the basis of the empirical formula of VAN DER MEER (1988) as well as the sampling duration recommended by GODA (1985)

to reduce the sampling variability of the wave statistics.

Figure 19 shows the measured stability number N_s as a function of the surf similarity parameter ξ for the six runs listed in Table 1. Figure 19 also shows the computed critical stability number N_{sc} for the incident irregular wave train with given H_s' and T_m' generated numerically using Eqs. 1–4 as well as for the incident regular wave train with the height H_s' and the period T_m'. The regular wave approximation results in the appreciable overestimation of the armor stability especially for the runs with smaller values of ξ. The computed critical stability number N_{sc} for the incident irregular wave train is in good agreement with the measured stability number N_s whose variation with respect to ξ is smaller than that associated with the regular wave data of AHRENS and MCCARTNEY (1975). This is probably because the irregular wave motion on the slope varies with time and along the slope much more than the corresponding regular wave motion. The differences between the measured value of N_s and the computed value of N_{sc} for the irregular wave are caused partly by the inherent differences of these two stability numbers as discussed above and partly by the fact that the incident irregular wave train used for the computation is not exactly the same as that generated in a wave flume for each test. The latter difference is related to the variability resulting from different sets of the random phases ϕ_n in Eq. 3. In Figure 19, $N_{sc} = 1.75$ and 1.63 for runs R2a and R2b with $\xi = 2.36$. This small difference in the computed values of N_{sc} indicates that the simulation duration $8 \leq t \leq 256$ may be sufficient to keep the variability of the computed critical stability number below an acceptable level. However, the examination of the detailed response of the armor stability function N_R to the incident irregular wave train for runs R2a and R2b reveals that the sequences of the incident waves causing the critical stability number N_{sc} for runs R2a and R2b are fairly different. Consequently, the detailed response of the armor units will be different for different incident random waves with the same significant wave height and average period.

The agreement between the computed critical stability number N_{sc} and the measured stability number N_s shown in Figure 19 is very encouraging in light of considerable efforts made by VAN DER MEER (1988) to develop his empirical formula. Figure 20 shows the comparison of his empirical formula with the data used to develop the formula. The data points shown in Figure 20 are plotted from those listed in Appendix I of his thesis, excluding the tests with a 1:30 foreshore slope. Comparison of Figures 19 and 20 suggest that the numerical model predicts the hydraulic stability of armor units well, although no calibration of the empirical parameters included in the numeri-

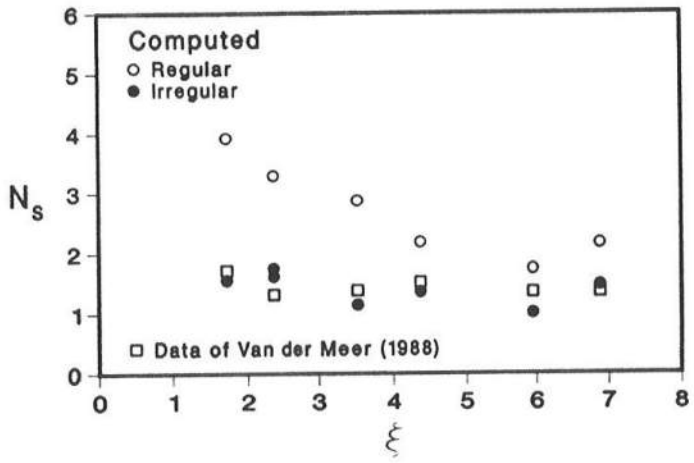

Figure 19. Comparison of measured stability number with critical stability number computed for incident irregular and regular wave trains.

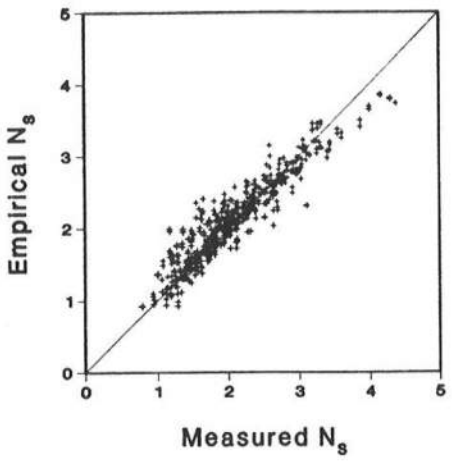

Figure 20. Comparison between measured and empirical stability number N_s for empirical formula of van der Meer (1988).

cal model is made in the present computation. However, it should be cautioned that it appears to be much easier to predict the stability number N_s than the amount of the slope profile change. Figure 21 shows the comparison of the measured and empirical values of the dimensionless damage level S based on the eroded area of the slope. The empirical values of S are calculated from the empirical formula of VAN DER MEER (1988) using the measured values of N_s. The large scatter shown in Figure 21 suggests that it will be difficult to predict the eroded area for given wave, slope and armor characteristics.

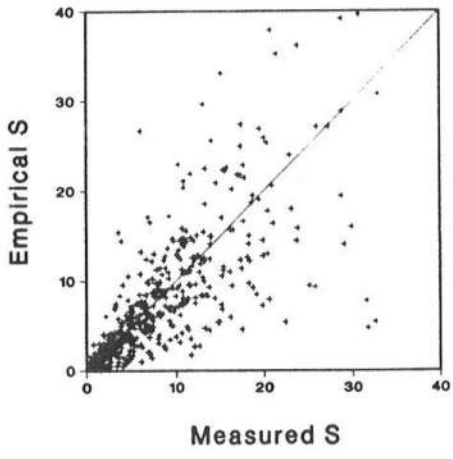

Figure 21. Comparison between measured and empirical damage level S for empirical formula of van der Meer (1988).

CONCLUSIONS

The numerical model for predicting the wave motion and resulting armor stability on a rough permeable slope proposed by KOBAYASHI and WURJANTO (1990) is coupled with the standard numerical method for simulating incident irregular wave trains for given spectral density (GODA, 1985; MANSARD, 1988). The Pierson-Moskowitz spectrum for fully developed wind waves in deep water is used herein since this spectrum was used for most of the extensive tests performed by VAN DER MEER (1988) who also examined the effects of the spectral shape and the wave shoaling on the beach in front of the test structure. For the application of the present numerical model, it is more general to use the TMA spectrum in finite water depth proposed by BOUWS *et al.* (1985), although additional input parameters are required to describe the TMA spectrum. Furthermore, the standard numerical method for simulating incident random wave trains for given spectral density may not reproduce wave group statistics in very shallow water (ELGAR *et al.*, 1984). In that case, the incident irregular wave train measured at the site or simulated using a nonlinear model needs to be specified as input to the numerical model of KOBAYASHI and WURJANTO (1990).

The coupled numerical model for the irregular wave motion and resulting armor stability on a rough permeable slope is compared with the six test runs corresponding to the start of the damage to the riprap slope with an impermeable core tested by VAN DER MEER (1988). The computed critical stability number for the initiation of armor movement is shown to yield good agreement with the measured stability number for these runs. The difference caused by the variability of incident irregular wave trains with the same significant wave height and average period is found to be small for the limited computation made herein. The numerical model is also shown to predict the fairly detailed response of armor units which varies along the slope as the incident irregular wave train propagates on the slope. The accuracy of the predicted armor response can not be assessed since measurements on the detailed

armor response and corresponding flow field are not available at present. The numerical model needs to be expanded to predict the slope profile change with time which was measured by VAN DER MEER (1988). The accurate prediction of the slope profile change appears to be much more difficult in view of the results shown in Figure 21.

The reflected wave trains and waterline oscillations computed for the six test runs are examined using spectral and time series analysis methods. The computed reflected wave spectra indicate the selective wave reflection and dissipation processes similar to those observed on natural beaches except that the reflection of the low frequency waves generated on the rough permeable slope appears to be small. The average irregular wave reflection coefficient increases with the increase of the surf similarity parameter in the manner similar to the regular wave reflection coefficient. On the other hand, the computed spectral densities of the waterline oscillations indicate the appreciable low-frequency wave components for the runs with small values of the surf similarity parameter. The generation and reflection processes of the low-frequency waves on the slope need to be examined in detail to evaluate their influence on irregular wave run-up. The time series analysis of the waterline oscillations is shown to yield the run-up distribution, significant run-up and maximum run-up which are basically consistent with the limited available data on irregular wave run-up. Detailed and accurate measurements on the irregular wave reflection and run-up on a rough permeable slope are required in order to evaluate the accuracy of the predicted irregular wave reflection and waterline oscillation.

In conclusion, a hybrid approach based on empirical formulas, numerical models and hydraulic model tests will improve our quantitative understanding of the complicated interaction between incident irregular waves and coastal structures protected with armor units. The improved understanding will then lead to more efficient and reliable design procedures.

ACKNOWLEDGEMENT

This work is a result of research sponsored by the National Science Foundation, under grant CTS-8900640. The writers would like to thank J. W. van der Meer for providing his thesis.

LITERATURE CITED

AHRENS, J.P. and MCCARTNEY, B.L., 1975. Wave period effect on the stability of riprap. *Proceedings Civil Engineering in Oceans/III,* ASCE, 2, 1019–1034.

AHRENS, J.P. and HEIMBAUGH, M.S., 1988. Irregular wave runup on riprap revetments. *Journal Waterway Port Coastal and Ocean Engineering,* ASCE, 114(4), 524–530.

BATTJES, J.A., 1971. Run-up distributions of waves breaking on slopes. *Journal Waterways Harbors and Coastal Engineering Division,* ASCE, 97(WW1), 91–114.

BOUWS, E.; GUNTHER, H.; ROSENTHAL, W., and VINCENT, C.L., 1985. Similarity of the wind wave spectrum in finite depth water. 1. spectral form. *Journal Geophysical Research,* 90(C1), 975–986.

ELGAR, S.; GUZA, R.T., and SEYMOUR, R.J., 1984. Groups of waves in shallow water. *Journal Geophysical Research,* 89(C3), 3623–3634.

ELGAR, S.; GUZA, R.T., and SEYMOUR, R.J., 1985. Wave group statistics from numerical simulations of a random sea. *Applied Ocean Research,* 7(2), 93–114.

GODA, Y., 1985. *Random Seas and Design of Maritime Structures.* University of Tokyo Press, Tokyo, 323p.

GUNBAK, A.R. and BRUUN, P.M., 1979. Wave mechanics principles on the design of rubble-mound breakwaters. *Proceedings Port and Ocean Engineering Under Arctic Conditions,* Norwegian Inst. of Tech., Trondheim, Norway, pp. 1301–1318.

HOLMAN, R.A. and SALLENGER, A.H., 1985. Setup and swash on a natural beach. *Journal Geophysical Research,* 90(C1), 945–953.

HOLMAN, R.A., 1986. Extreme value statistics for wave run-up on a natural beach. *Coastal Engineering,* 9, 527–544.

KOBAYASHI, N. and OTTA, A.K., 1987. Hydraulic stability analysis of armor units. *Journal Waterway Port Coastal and Ocean Engineering,* ASCE, 113(2), 171–186.

KOBAYASHI, N.; STRZELECKI, M.S., and WURJANTO, A., 1988. Swash oscillation and resulting sediment movement. *Proceedings 21st Coastal Engineering Conference,* ASCE, 2, 1167–1181.

KOBAYASHI, N.; DESILVA, G.S., and WATSON, K.D., 1989. Wave transformation and swash oscillation on gentle and steep slopes. *Journal Geophysical Research,* 94(C1), 951–966.

KOBAYASHI, N. and WURJANTO, A., 1990. Numerical model for waves on rough permeable slopes. Special Issue on Rational Design of Mound Structures, *Journal Coastal Research,* SI6.

LOSADA, M.A. and GIMÉNEZ-CURTO, L.A., 1981. Flow characteristics on rough, permeable slopes under wave action. *Coastal Engineering,* 4, 187–206.

MANSARD, E.P.D., 1988. Towards a better simula-

tion of sea states for modelling of coastal structures. *Proceedings Berm Breakwaters,* ASCE, 1–21.
SEELIG, W.N., 1983. Wave reflection from coastal structures. *Proceedings Coastal Structures '83,* ASCE, 961–973.
TATAVARTI, R.V.S.N.; HUNTLEY, D.A., and BOWEM, A.J., 1988. Incoming and outgoing wave interactions on beaches. *Proceedings 21st Coastal Engineering Conference,* ASCE, 1, 136–150.
VAN DER MEER, J.W., 1988. Rock slopes and gravel beaches under wave attack. Delft University of Technology, Delft, The Netherlands, Doctoral Thesis.